Distribution Agreement

In presenting this thesis or dissertation as a partial fulfillment of the requirements for an advanced degree from Emory University, I hereby grant to Emory University and its agents the non-exclusive license to archive, make accessible, and display my thesis or dissertation in whole or in part in all forms of media, now or hereafter known, including display on the world wide web. I understand that I may select some access restrictions as part of the online submission of this thesis or dissertation. I retain all ownership rights to the copyright of the thesis or dissertation. I also retain the right to use in future works (such as articles or books) all or part of this thesis or dissertation.

Signature:

_____ _____

Alexandra V. Goodnight Date

Chromatin Accessibility and Transcription Dynamics During *In Vitro* Astrocyte Differentiation of Huntington's Disease Monkey Pluripotent Stem Cells

By

Alexandra V. Goodnight
Doctor of Philosophy

Graduate Division of Biological and Biomedical Sciences
Genetics and Molecular Biology

_____
Anthony W.S. Chan, DVM, Ph.D.
Advisor

_____
Andrew Escayg, Ph.D.
Committee Member

_____
David Katz, Ph.D.
Committee Member

_____
Kenneth H. Moberg, Ph.D.
Committee Member

_____
Carlos S. Moreno, Ph.D.
Committee Member

Accepted:

_____
Lisa A. Tedesco, Ph.D.
Dean of the James T. Laney School of Graduate Studies

_____
Date

Chromatin Accessibility and Transcription Dynamics During *In Vitro* Astrocyte Differentiation of Huntington's Disease Monkey Pluripotent Stem Cells

By

Alexandra V. Goodnight
B.S., Oglethorpe University, 2010

Advisor: Anthony W.S. Chan, DVM, Ph.D.

An abstract of
A dissertation submitted to the Faculty of the
James T. Laney School of Graduate Studies of Emory University
in partial fulfillment of the requirements for the degree of
Doctor of Philosophy
in Genetics and Molecular Biology
2018

Abstract

Chromatin Accessibility and Transcription Dynamics During *In Vitro* Astrocyte Differentiation of Huntington's Disease Monkey Pluripotent Stem Cells

By

Alexandra V. Goodnight

Huntington's disease (HD) is a neurodegenerative disorder caused by a CAG repeat expansion, producing a mutant huntingtin (mHTT) protein with an extended polyglutamine tract. Evidence exists showing transcriptional dysregulation across neurodevelopment contributes to HD pathogenesis by disrupting many cellular processes. Additionally, aberrant epigenomic profiles have been reported in HD, but their impact on transcription remains unclear. Most HD research has focused on understanding the mechanisms of neuron degeneration, but neurons require astrocytes for normal development, function and survival. Recent evidence suggests that astrocytes not only contribute to, but are sufficient to trigger, neuronal dysfunction and HD pathogenesis, highlighting their pathogenic role, as well as potential therapeutic value in HD. However, transcriptional and epigenomic dysregulation in HD astrocytes has not been fully examined. Using pluripotent stem cells (PSCs) from transgenic HD non-human primates (NHP), we characterized global transcription and chromatin accessibility dynamics during *in vitro* astrocyte differentiation. We show genomic alterations in accessibility and transcription at all stages; however, trends observed throughout differentiation are established in neural progenitor cells (NPCs), after commitment to a neural lineage. Promoter-proximal accessibility is not associated with transcriptional changes. Differential distal accessibility, including a subset of NHP putative brain enhancers, show trends across astrogenesis. We also found p53 signaling and cell cycle dysregulation across HD differentiation, with observed down regulation of cell cycle genes in NPCs and aberrant cell cycle reentry and apoptosis in astrocytes. Interestingly, E2F target genes (ETGs) show this inverse expression between HD NPCs and astrocytes. While this coincides with differential E2F motif enrichment at promoters genome-wide, ETG promoter accessibility did not reflect differential expression patterns. Closer examination revealed that ETG expression shows stronger association with accessibility at nearby putative enhancers, suggesting interactions between regulatory elements, possibly enhancers, and promoters may drive aberrant transcription profiles across HD differentiation, highlighting the complex interplay of epigenetic mechanisms contributing to the HD transcriptome. Taken together, these results show altered chromatin accessibility and transcription throughout *in vitro* HD astrocyte differentiation and suggest E2F dysregulation may cause alterations in cell cycle and apoptosis pathways as HD NPCs differentiate towards astrocytes.

Chromatin Accessibility and Transcription Dynamics During *In Vitro* Astrocyte Differentiation of Huntington's Disease Monkey Pluripotent Stem Cells

By

Alexandra V. Goodnight

B.S., Oglethorpe University, 2010

Advisor: Anthony W.S. Chan, DVM, Ph.D.

A dissertation submitted to the Faculty of the
James T. Laney School of Graduate Studies of Emory University
in partial fulfillment of the requirements for the degree of
Doctor of Philosophy
in Genetics and Molecular Biology
2018

Acknowledgments

First and foremost, I would like to thank Dr. Anthony Chan his for endless support, patience and mentorship. From my first moment in graduate school, you recognized my potential and have provided me with invaluable skills, guidance and autonomy that have laid the foundation for my success as a scientist. Truly, I am forever grateful. I would also like to thank all the past and present members of our lab for laying the groundwork for my research, being willing to help, providing feedback, and above all else, being a supportive family. I would like to give special thanks to Dr. In Ki Cho and Jin-Jing Yang for all your time, assistance, and mentoring, and to Sujittra Khampang for all your help, feedback, giggles and endless food supply that has provided the fuel for this research. I would also like to express ineffable gratitude to Cari Hunter for all the early mornings, assistance, bringing me medicine when I was sick and writing grants, hours of insightful dialogues about science, our walks in the woods, ongoing motivation and always being willing to lend a sympathetic ear to my frustrations.

I would also like to thank my committee members, Drs. Andrew Escayg, David Katz, Kenneth Moberg, and Carlos S. Moreno, as well as Dr. Anita Corbett, for your guidance and unwavering support through difficult times. Additionally, special thanks are given to our collaborators from Dr. Victor Corces's lab, particularly Dr. Yoonhee Jung, who trained me on the ATAC-seq protocol and Dr. Isaac J. Kremsky, who performed most of the bioinformatic analysis and provided input in the development of chapter 2 of this dissertation. I would also like to thank Dr. James M. Billingsley and the Yerkes Non-Human Primate Genomic Core for their assistance in RNA-seq library preparation and data analysis. Likewise, I would like to thank my previous mentor, Dr. Paula Vertino, who provided me with invaluable experiences and pushed me to access my full potential. Additionally, I would like to give special thanks to the Vertino lab members;

specifically, Dr. Joshua Bell and Elizabeth Zoeller for all the things, I would seriously not be where I am without you both, and Doris Powell and Dr. Priya Kapoor for the technical training and assistance. I also want to express gratitude to Emory University, Laney Graduate School, and the Genetics and Molecular Biology program. This work was supported by the National Institutes of Health [NIH; 5F31CA196181] to Alexandra Goodnight, and the Transgenic Huntington's Disease Monkey Resource [THDMR; OD010930] sponsored by the Office of Research and Infrastructure Programs (ORIP) at the NIH, to Anthony Chan. Without this funding, none of this work would be possible.

Finally, I would like to thank my tribe of friends and family that have supported me and given endless patience during the past 7 and a half years. Michele and Frank, without your financial support and childcare assistance, I would have not been able to pursue this degree. You have taught me to strive for excellence but more importantly, you have always believed in me. Additionally, Michele, so much gratitude for going out of your way to help take care of me in the last months of my degree. While there are more than I can mention, I also want to give thanks to Carmen, Jen, Ann and Dug. A special thanks to my favorite forever, Drago; you are there by myside every day, good or bad, with nothing but love and belief in me. Last but most importantly, I want to give inexpressible gratitude to my son Bodhi. You are incredible, patient, supportive, and have helped me so much more than anyone else. All 10 years of your life, I have spent a majority of my time focused on completing this degree and you have never complained, although I know all you want is my time. My hope is one day you look back at this and take away two things: 1. no matter what anyone says or where you have been, with hard work and dedication, you can do anything you set your mind, and 2. I have truly done this all for you. Thank you, Bodhi.

Table of Contents

Index of Figures and Tables

Figures

Table

List of Abbreviations

5-hmC: 5-hydroxymethylcytosine

ANOVA: analysis of variance

AP-1: activator protein 1

APOE: apolipoprotein E

ATAC-seq: assay for transposase-accessible chromatin using sequencing

AZA-C: azacitidine

BBB: blood–brain barrier

BDNF: brain-derived neurotrophic factor

BMP2: bone morphogenetic protein 2

CBP: CREB binding protein

CCL5/RANTES: chemokine (C-C motif) ligand 5/regulated on activation normal T cell expressed and secreted

CDK1: cyclin dependent kinase 1

CDKN2A ($p14^{ARF}$): cyclin dependent kinase inhibitor 2A

ChIP-seq: chromatin immunoprecipitation with sequencing

CPM: counts per million

CNS: central nervous system

CX3CR1: C-X3-C motif chemokine receptor 1

DE: differentially expressed

DNMT: DNA methyltransferase

E2F: E2F transcription factor

ECM: extracellular matrix

EMT: epithelial to mesenchymal transition

ESC: embryonic stem cell

ESET: ERG-associated protein with SET domain

ETG: E2F target gene

EZH2: enhancer of zeste 2

FDR: false discovery rate

FGF: fibroblast growth factor

FOSL2: FOS like 2, AP-1 transcription factor subunit

FOXO4: forkhead box O4

FPKM: fragments per kilobase of transcript per million mapped reads

GABA: $\boldsymbol{\gamma}$-aminobutyric acid

GAD: glutamate decarboxylase 1

GAPDH: glyceraldehyde-3-phosphate dehydrogenase

GFAP: glial fibrillary acidic protein

GFP: green fluorescent protein

GLAST: solute carrier family 1 (glial high affinity glutamate transporter), member 3

GLT1: solute carrier family 1 (glial high affinity glutamate transporter), member 2

GO: gene ontology

GRM1: glutamate metabotropic receptor 1

GSEA: gene set enrichment analysis

GWAS: genome-wide association study

H3K27ac: histone H3 lysine 27 acetylation

H3K27me3: histone H3 lysine 27 trimethylation

H3K4me3: histone H3 lysine 4 trimethylation

H3K9me3: histone H3 lysine 9 trimethylation

H4R3me2s: symmetric dimethylation of arginine 3 on histones H4

HAT: histone acetyltransferase

HD: Huntington's disease

HDACi: histone deacetylase inhibitor

HMGN3: high mobility group nucleosomal binding domain 3

HTT: huntingtin

iPSC: induced pluripotent stem cells

JARID: jumonji/ARID domain-containing demethylase family

JMJD6: jumonji C domain-containing protein 6

JUN: Jun proto-oncogene, AP-1 transcription factor subunit

K+: potassium ion

KCNJ10: potassium voltage-gated channel subfamily J member 10 (Kir4.1)

KEGG: Kyoto encyclopedia of genes and genomes

KLF5: kruppel like factor 5

LCN2: lipocalin 2

LIF: leukemia inhibitory factor

MAP2: microtubule-associated protein 2

MAPK: mitogen-activated protein kinase

MCM: minichromosome maintenance protein complex

MDM2: MDM2 proto-oncogene

MFF: mouse fetal fibroblast

mHTT: mutant huntingtin protein

MSI1: musashi-1

MsigDB: molecular signature database

MSN: medium spiny neuron

NES: nestin

NF-κB: nuclear factor kappa B

NHP: non-human primate

NIH: National Institute of Health

NMDAR: *N*-methyl-D-aspartate receptor

NPC: neural progenitor cell

OCT4: POU class 5 homeobox 1 (POU5F1)

ORIP: Office of Research and Infrastructure Programs

p53: tumor protein p53

PABE: putative active brain enhancer

PAX6: paired box gene 6

PCA: principal component analysis

polyQ: poly-glutamine

PPAR: peroxisome proliferator-activated receptor

PRC2: polycomb repressive complex 2

PRMT5: protein arginine methyltransferase 5

PSC: pluripotent stem cell

RB: retinoblastoma

RFX: regulatory factor X transcription factor

RNAP II: RNA polymerase II

RNA-seq: RNA sequencing

RRM2B: ribonucleotide reductase regulatory TP53 inducible subunit M2B

qRT-PCR: quantitative reverse transcription PCR

shRNA: short-hairpin RNA

SOX2: SRY (sex determining region Y)-box 2

SP1: specificity protein 1

TF: transcription factor

TH: tyrosine hydroxylase

THDMR: Transgenic Huntington's Disease Monkey Resource

THSS: Tn5 hypersensitive site

TNR: trinucleotide repeat

TP53I3: tumor protein P53 inducible protein 3

TSA: trichostatin A

TSS: transcription start site

TUBB3: tubulin beta 3 class III

UBC: polyubiquitin-C

UHRF1: ubiquitin like with PHD and Ring Finger Domains 1

WNT: Wingless/Integrated

WT: wild-type

Chapter 1: General Introduction

1.1 Huntington's disease

Huntington's disease (HD) is a fatal, autosomal dominant neurodegenerative disease currently affecting about 30,000 symptomatic Americans (NINDS, 2018). HD is characterized by progressive brain atrophy, initiating in the striatum and subsequently extending to other brain regions, along with cognitive decline, psychiatric disturbances and motor dysfunction (e.g., chorea, dystonia), with a typical onset of symptoms at 35-55 years old (Zuccato et al., 2010). Despite the fact that HD is the most common inherited neurodegenerative disorder (Landles et al., 2004), there are currently no cures or therapies available to slow or reverse disease progression; however, several potential therapeutic strategies have been identified (Gagnon et al., 2010; Hu et al., 2009; Watts et al., 2012; Yu et al., 2012). HD is caused by a CAG trinucleotide repeat (TNR) expansion in exon 1 of the huntingtin gene, *HTT* (Macdonald et al., 1993). HD is one of over 20 human diseases caused by TNR instability. TNRs, such as CAG, are among the most variable loci in the human genome due to their high mutation rate (Payseur et al., 2011). While healthy individuals have < 36 CAG repeats, HD is characterized by ≥ 40 repeats, and the repeat size is inversely correlated with disease onset and severity (Gil et al., 2008; Goldberg et al., 1994; Langbehn et al., 2010; Li et al., 2006; Snell et al., 1993). Furthermore, HD and other TNR diseases are characterized by genetic "anticipation", where an increase in repeat length occurs through successive generations and leads to earlier onset and greater severity of symptoms (McMurray, 2010; Orr et al., 2007).

In HD, the CAG expansion produces an extended polyglutamine (polyQ) tract at the N-terminus of the HTT protein, resulting in a mutant HTT protein (mHTT) (Davies et al., 1997; DiFiglia et al., 1997; Sieradzan et al., 1999). Cleavage of mHTT by proteases generates protein fragments containing the abnormal polyQ tract (Scherzinger et al., 1997). These fragments can

aberrantly interact with various critical proteins within neural cells and interrupt a myriad of cellular processes including cell cycle regulation, mitochondrial activity, synapse function, vesicular transport, signaling, and transcription (Cattaneo et al., 2005; Crook et al., 2013; Li et al., 2006; Lopes et al., 2016; Ross et al., 2011; Saudou et al., 1998; Seredenina et al., 2012; Valor, 2015; Zuccato et al., 2010). Moreover, mHTT fragments can form aggregates and nuclear inclusions, which are a hallmark cellular pathology of HD (Cattaneo et al., 2005; DiFiglia et al., 1997; Sieradzan et al., 1999). These aggregates also aberrantly bind to and sequester transcription factor (TFs), epigenetic enzymes, and other critical proteins, causing the disruption of necessary cellular functions through transcriptional dysregulation (Davies et al., 1997; Crook et al., 2013; Labbadia et al., 2013; Li et al., 2006). For example, a study using neuronal cultures from transgenic HD mice showed that mHTT binds to and sequesters p53, causing repression of select p53-target genes (Steffan et al., 2000). In contrast, another study also demonstrated the mHTT-p53 interaction *in vitro*, but reported this aberrant interaction resulted in increased p53 transcriptional activity (Bae et al., 2005). p53 is involved in many diverse and tightly regulated processes, including cell cycle, apoptosis, DNA repair, metabolism and mitochondrial function, which show deficits associated with HD-mediated p53 dysfunction (Bae et al., 2005; Illuzi et al., 2011; Lu et al., 2015; Marcel et al., 2018; Reynolds et al., 2018; Szlachcic et al. 2015; Vaseva et al., 2009). Increased p53 expression in the HD brain (Bae et al., 2005; Reynolds et al., 2018) and peripheral tissues (Ehrnhoefer et al., 2014) have also been reported. However, the downstream transcriptome consequences of aberrant mHTT interactions with TFs, such as p53, are not well defined. Nevertheless, it is clear that despite the monogenic nature of HD, many complex cellular networks and processes are impacted by the presence of mHTT in neural cells.

HTT is a large, ubiquitously expressed protein, with highest expression reported in the adult brain and testes (Li et al., 1993; Sharp et al., 1995; Strong et al., 1993). Interestingly, HD patients show similar distribution and expression of HTT and mHTT (Cattaneo et al., 2001). HTT has widespread subcellular localization and interacts with over 350 other proteins, making defining its role and function in specific cellular processes difficult (Goehler et al., 2004; Harjes et al., 2003; Marco et al., 2013; Sauduo et al., 2016). Studies in mice have demonstrated that homozygous knock-out of *HTT* results in embryonic lethality, suggesting that HTT is essential for embryonic development (Nasir et al., 1995; Zeitlin et al., 1995). Work performed in various mouse models has also demonstrated that sufficient expression of HTT is required for successful neurogenesis and for the differentiation of embryonic stem cells (ESCs) into neural progenitor cells (NPCs), but not pancreatic or cardiac progenitor cells, providing evidence that HTT plays a role in neurodevelopment specifically (White et al., 1997; Wiatr et al., 2018; Yu et al., 2017). Additionally, a plethora of other studies have demonstrated roles for HTT in transcription regulation (e.g. brain-derived neurotrophic factor (*BDNF*)), facilitating vesicular transport, synaptic transmission, cytoskeleton dynamics, regulating ciliogenesis and negatively regulating apoptosis (Cattaneo et al., 2005; Harjes et al., 2003; Sauduo et al., 2016). It is likely that HTT serves as a scaffold to multiple complexes responsible for coordinating cellular processes that are temporally and spatially regulated based on external signals and cell types (Cattaneo et al., 2005; Sauduo et al., 2016). *In vivo* and *in vitro* experiments have established HTTs involvement in many cellular processes, but the key molecular mechanisms of mHTT and its pathogenic roles in HD remain to be fully understood.

Evidence has suggested that the polyQ expansion in HD has both gain-of-function and a loss-of-function activity in cells (Cattaneo et al., 2001; Cattaneo et al., 2005; Sauduo et al., 2016).

The original hypothesis was that HD pathology resulted from gain-of-function activity of mHTT (Cattaneo et al., 2001; Cattaneo et al., 2005; Ross et al., 2011; Sauduo et al., 2016; White et al., 1997). The earliest evidence for this came from the observation that HD follows a dominant inheritance pattern (Ross et al., 2011). Similarly, the deletion of one *HTT* allele does not lead to the development of HD, which indicates that the CAG expansion is necessary in one allele to cause HD (Housman, 1995). This idea is further supported by the fact that HD individuals with homozygous expansions do not have a more severe disease pathology, thus, the presence of a normal allele in heterozygotes has no impact on disease phenotype (Durr et al., 1999; Wexler et al., 1987). Additional evidence for a gain-of-function phenotype in HD is that the expanded CAG repeat itself is toxic. Evidence from mouse studies, demonstrated that ectopic expression of CAG repeats alone, outside an HD context, or with exon 1 of *HTT* causes a neurological phenotype and cell death, suggesting mHTT takes on a new toxic activity (Mangiarini et al.,1996; Ordway et al., 1997; Shao et al., 2007). On a molecular level, mHTT aggregates aberrantly interact with various critical proteins, interfering with their activity and disrupting various cellular processes (Zuccato et al., 2010). However, HD pathology is complex and cannot simply be explained by mHTT gain-of-function mechanisms.

Through examination of HTT function, it has become evident that loss-of-function is also involved in disease pathology. Conditional inactivation of HTT in the brains of mice resulted in a progressive neurodegeneration, providing evidence that loss of HTT is sufficient for an HD-like neurodegenerative phenotype (Dragatsis et al., 2000). Similarly, studies examining the effects of reduced HTT levels in mice found that heterozygous *HTT* knockout impaired cognitive and motor abilities, and lead to neurodegeneration (Nasir et al., 1995; O'Kusky et al., 1999). Molecular studies have established that the loss of HTT function, specifically in regulating the transcription

and transport of an important neurotrophic signaling factor, brain-derived neurotrophic factor (BDNF), contributes to HD pathology (Crook et al., 2013; Drouet et al., 2014; Gil et al., 2008; Xie et al., 2010; Zuccato et al., 2007; Zuccato et al., 2009). Moreover, HTT downregulation in wild-type (WT) neurons caused a reduction in *BDNF* transport to the same extent as observed in HD cells (Gauthier et al., 2004). These studies provide evidence of a loss-of-function mechanism in that the expansion of the CAG repeat in one allele produces a protein that is unavailable to perform the normal molecular activities of HTT. Taken together, these studies illustrate the diverse consequences of the polyQ expansion on HTT function and support the hypothesis that HD pathology results from combined gain and loss of function effects (Cattaneo et al., 2001; Zuccato et al., 2010).

Although most HD pathology is attributed to neuronal dysfunction (Ross et al., 2011), HTT is ubiquitously expressed in all cells, including the brain and peripheral tissues, and pathology and clinical features have been reported outside the central nervous system (CNS) (e.g. weight loss, metabolic and immune disturbances, testicular atrophy) (Bjorkqvist et al., 2008; van der Burg et al., 2009; Wild et al., 2008). Within the HD brain, atrophy of the striatum and cortex is evident prior to clinical symptoms, and reductions in the thalamus and other brain regions occurs subsequently as the disease progresses (Aylward et al., 2011; Aylward et al., 2012; Hadzi et al., 2012; Rosas et al., 2008; Sapp et al., 1997; Tabrizi et al., 2013; Vonsattel et al., 1985; Waldvogel et al., 2015; Wu et al., 2017). Although all neural cell types are affected, the γ-aminobutyric acid (GABA)-ergic medium spiny neurons (MSNs) of the striatum are particularly susceptible to mHTT-induced toxicity and death (Deng et al., 2004; Halliday et al., 1998; Sapp et al., 1997; Vonsattel et al., 1985; Waldvogel et al., 2015). Many studies have been performed to identify the factors that make MSNs vulnerable. Loss of *BDNF* is well documented in HD mice and HD

patients (Baquet et al. 2004; Crook et al., 2013; Drouet et al., 2014; Gil et al., 2008; Xie et al., 2010; Zuccato et al., 2007; Zuccato et al., 2009), and overexpression of *BDNF* can rescue certain HD phenotypes in neuronal cells (Gharami et al., 2008; Lynch et al., 2007). Evidence suggests that BDNF is necessary for striatal neuron survival, and its depletion in HD contributes to striatal degeneration (Baquet et al., 2004; Strand et al., 2007). Another major contributor to MSN vulnerability in HD is *N*-methyl-D-aspartate receptor (NMDAR)-mediated toxicity (Ross et al., 2011; Zeron et al., 2002). NMDARs are a type of ionotropic glutamate receptor and are critical for excitatory synaptic plasticity and neuronal survival (Raymond et al., 2011). However, in HD neurons, dysregulated NMDAR expression and altered endocytic trafficking results in excessive NMDAR activity, glutamatergic excitotoxicity and selective degeneration of MSNs (Hardingham et al., 2010; Labbadia et al., 2013; Marco et al., 2013; Milnerwood et al., 2010; Okamoto et al., 2009; Zeron et al., 2002). Suppression of NMDAR activity rescues the excitotoxicity phenotype associated with mHTT (Marco et al., 2013). Although mHTT impacts many molecular processes, it is clear that altered BDNF regulation and glutamate transmission are major contributors to the selective striatal vulnerability reported in HD.

Until recently, most studies have focused on the mechanisms of HD pathogenesis in striatal and cortical neurons. However, it is becoming evident that HD affects the whole brain, not just certain neuronal populations. In fact, the growth, homeostasis and survival of all neurons requires the activity of support cells called glia (astrocytes, oligodendrocytes, and microglial cells), which make up about 90% of the human brain and are critical to the formation and function of neural circuits (Allen et al., 2009; Barres, 2008; Belanger et al., 2011; Clarke et al., 2013). Currently, only a paucity of data is available on the impact of mHTT on glia function and their contribution to HD pathogenesis. Considering their integral role in CNS viability and function, understanding

how mHTT affects glial cells and their ability to support neurons and neural circuits will be instrumental in better understanding HD pathogenesis and in identifying therapeutic strategies that restore CNS homeostasis and the synergy of glia and neurons.

Astrocytes, a type of glial cell, are the most abundant cells in the brain and have many critical roles in the CNS including, development, metabolic support of neurons, synaptic formation and regulation, tissue repair, blood–brain barrier (BBB) maintenance, protection against oxidative stress, and the homeostasis of glutamate, ions and water (Belanger et al., 2009; Belanger et al., 2011; Phatnani et al., 2015; Volterra et al., 2005). Unexpectedly, recent studies have identified additional roles for astrocytes in complex brain functions and behaviors, such as sleep homeostasis, memory, and regulation of breathing, further emphasizing their importance to a properly functioning brain (Gibbs et al., 2008; Gourine et al., 2010; Halassa et al., 2009). Astrocytes have unique phenotypic features and structural organization that allude to their extensive dedication to neuronal support. Each astrocyte has a cell body, thick vascular-associated processes known as "endfeet", and thin perisynaptic processes that ensheath synapses and establish connections to many neurons and neural circuits (Belanger et al., 2011; Khakh et al., 2017; Sica, 2015). A wide range of neurotransmitter receptors, growth factors and membrane transport proteins are localized in the perisynaptic processes of astrocytes (Belanger et al., 2011; Sica, 2015). Astrocytes are territorial; an astrocyte and its processes occupy their own anatomical domain with minimal overlap between neighboring astrocytes (Belanger et al., 2011; Oberheim et al., 2009). Therefore, within an astrocytic domain, a single astrocyte will make contact with up to two million synapses, and support and maintain the associated neuron population (Belanger et al., 2011; Oberheim et al., 2009; Sica, 2015). Considering their extensive involvement in neuronal function, it is not surprising that astrocyte dysfunction results in inadequate support for domains of neurons and

compromised regions of neural circuits, contributing to pathology in neurodegenerative diseases such as HD (Barres, 2008; Lobsiger et al., 2007; Maragakis et al., 2006; Phatnani et al., 2015; Sica, 2015).

Only recently have studies begun to characterize the impact of astrocyte function on HD pathogenesis, despite the fact that intracellular mHTT aggregates were observed in the astrocytes of HD mice and patients (Jansen et al., 2017; Khakh et al., 2017; Shin et al., 2005; Tong et al., 2014). Transgenic HD mice selectively expressing mHTT in astrocytes below the endogenous level, showed several HD phenotypes, including, loss of body weight, motor deficits and premature death, demonstrating that low mHTT expression in only astrocytes is sufficient to lead to clinical features similar to that of HD (Bradford et al., 2009). *In vivo* and *in vitro* astrocyte models expressing mHTT demonstrated a significant reduction in the levels of two glutamate transporters, solute carrier family 1 (glial high affinity glutamate transporter), member 2 (*GLT1*) and solute carrier family 1 (glial high affinity glutamate transporter), member 3 (*GLAST*), along with impaired glutamate transport and uptake, which are both well documented contributors to HD pathogenesis (Bradford et al., 2009; Faideau et al., 2010; Shin et al., 2005). Additional molecular studies uncovered that decreased GLT1 expression results from the direct binding of mHTT to the transcription factor, specificity protein 1 (SP1), which prevents its association with the *GLT1* promoter in astrocytes and causes glutamatergic excitotoxicity in HD (Bradford et al., 2009). Interestingly, when cocultured with WT astrocytes, HD neurons had higher levels of microtubule-associated protein 2 (MAP2), a neuronal marker, than when cultured alone, suggesting functional astrocytes can protect against HD-mediated neurotoxicity (Shin et al., 2005). Alternatively, when cocultured with HD astrocytes, WT neurons displayed substantial decreases in MAP2, indicating early neuronal dysfunction in the presence of diseased astrocytes (Shin et al., 2005). In the latter

experiment, drug inhibition of glutamate receptors restored MAP2 levels, providing direct evidence that mHTT expression in astrocytes impairs glutamate uptake and promotes glutamate excitotoxicity, even in WT neurons (Shin et al., 2005). Additionally, astrocytes from transgenic HD mice show reduced expression of the Kir4.1 potassium ion (K+) channel, which caused elevated extracellular K+ concentrations and thus, MSN excitability (Tong et al., 2014). Of note, Kir4.1 over-expression in these astrocytes rescued deficits in K+ signaling and resulted in increased *GLT1* expression (Tong et al., 2014). Taken together, these studies demonstrate that multiple mechanisms, such as glutamate and K+ signaling, collaborate to orchestrate astrocyte, and thus neuronal, homeostasis.

Further evidence for astrocyte dysregulation in HD comes from RNA sequencing (RNA-seq) experiments, which reported that glial fibrillary acidic protein (*GFAP*), a marker for astrogliosis or reactive astrocytes, was the second most significantly overexpressed gene in the prefrontal cortex of HD patient (Labadorf et al., 2015). Astrogliosis refers to the activation of and increase in astrocytes in response to CNS trauma, neuroinflammation or disease (Sofroniew, 2009). Multiple studies in HD human, monkey and mouse models have also observed increased *GFAP* across disease progression, as well as colocalization of mHTT and GFAP in HD astrocytes prior to any neuronal damage (Faideau et al., 2010; Hedreen et al., 1995; Kocerha et al., 2014; Lin et al., 2001; Shin et al., 2005; Vonsattel et al., 1985). Evidence from these studies has supported the use of astrogliosis, specifically *GFAP* expression, as an early marker of CNS damage in HD. Astrocyte dysfunction in HD can arise from aberrant regulation of other trophic factors as well. mHTT-mediated repression of *BDNF* transcription, a well-established signature of HD pathology, also occurs in astrocytes (Wang et al., 2012), which is consistent with previous results in HD animal models. Selective expression of *BDNF* in striatal astrocytes led to delayed onset of motor

phenotypes in transgenic HD mice (Arregui et al., 2011). Additionally, molecular evidence from a transgenic HD mouse model revealed that mHTT inhibits both the transcription and secretion of another tropic factor, chemokine (C-C motif) ligand 5/regulated on activation normal T cell expressed and secreted (*CCL5/RANTES*), reducing the availability of astrocytic CCL5/RANTES to neurons and contributing to neuronal dysfunction in HD (Chou et al., 2008). Other studies examining the contributions of astrocytes to HD pathogenesis specifically reported reduced cholesterol biosynthesis, impaired production and secretion of apolipoprotein E (ApoE), prolonged inflammatory responses via NF-κB activation, compromised regulation of glutamate-GABA-glutamine cycling, and mitochondrial dysfunction (Hsiao et al., 2013; Oliveira, 2010; Skotte et al., 2018; Valenza et al., 2010).

Over the past few years, studies investigating the dysfunction of astrocytes in HD have provided evidence that many complex cellular pathways are impacted and altered in different cell types by mHTT (Figure 1-1). It is clear that neuronal disturbances alone cannot account for all the pathological features of HD; not only is selective expression of mHTT in astrocytes sufficient for neurological deficits, but WT astrocytes can protect HD neurons from neurotoxicity and degeneration (Bradford et al., 2009; Shin et al., 2005). It is clear that mHTT affects the function of both neurons and astrocytes, and that astrocyte and neuron synergy is necessary for normal CNS development and function. To fully uncover the mechanisms of HD pathology and identify possible therapeutic targets, future studies need to focus on the pathological contributions of astrocytes to neuron function and survival, as well as the non-cell autonomous mechanisms of striatal neurodegeneration in HD. Recognition of the non-cell-autonomous mechanisms of HD is critical for the development of therapies; rather than attempting to replace lost neurons, targeting mechanisms of astrocyte dysfunction, such as loss of Kir4.1, or supplementing with WT astrocytes,

would reduce the toxicity of HD astrocytes, and provide healthy support and protection for remaining neuron populations (Tong et al., 2014).

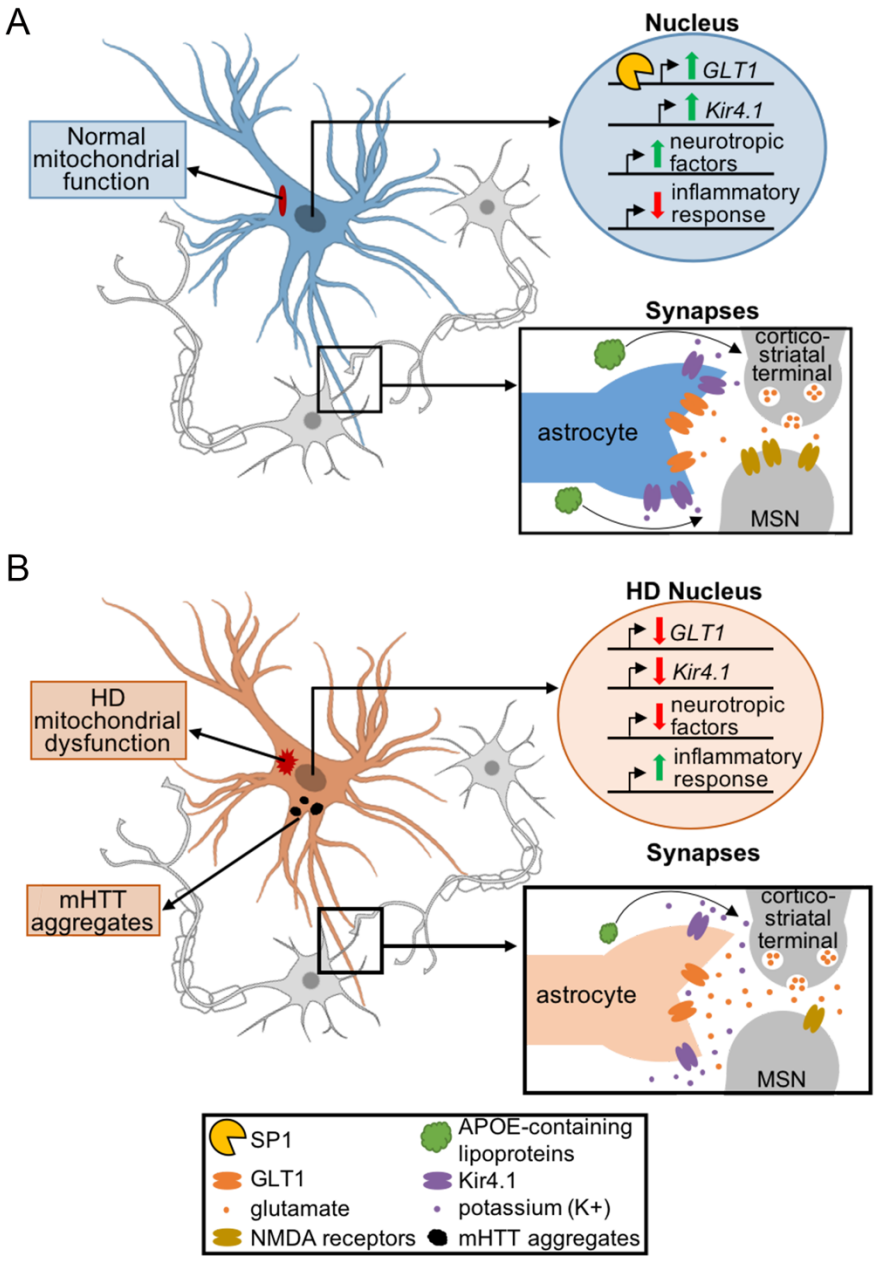
A
Nucleus
GLT1
Kir4.1
neurotropic factors
inflammatory response
Normal mitochondrial function
Synapses
cortico-striatal terminal
astrocyte
MSN
B
HD Nucleus
GLT1
Kir4.1
neurotropic factors
inflammatory response
HD mitochondrial dysfunction
mHTT aggregates
Synapses
cortico-striatal terminal
astrocyte
MSN
SP1
APOE-containing lipoproteins
GLT1
Kir4.1
glutamate
potassium (K+)
NMDA receptors
mHTT aggregates

Figure 1-1. Astrocyte function is disrupted in HD. (A) In a healthy brain, astrocytes provide neuronal homeostasis and prevent toxicity via the expression of the glutamate transporter, *GLT1*, and the potassium channel, Kir4.1, which regulate extracellular K+ and glutamate near synapses. Wild-type (WT) astrocytes also produce neurotrophic factors necessary for neuronal survival. Furthermore, astrocytes are completely responsible for the cholesterol biosynthesis of mature neurons, facilitating major neuronal functions such as signal transduction and synaptogenesis, via the secretion of APOE-containing lipoproteins. (B) In the HD brain, reduced *GLT1* and Kir4.1 expression impact glutamate uptake at synapses and leads to excitotoxity in HD neurons. Additionally, mHTT expression in astrocytes causes decreased expression of neurotropic factors, activation of inflammatory genes, and mitochondrial dysregulation, further contributing to neuronal dysfunction and degeneration. Defects in APOE-meditated cholesterol transport from astrocytes to neurons also occur in HD and impacts neural cell synergy.

1.2 Neurodevelopmental dysregulation in Huntington's disease

In the previous section, the vast impact of mHTT expression on molecular and cellular processes leading to neurodegeneration in HD brains was detailed. Different *in vivo* and *in vitro* models of HD have established multiple roles for HTT and mHTT that may vary between cell types. The progressive pathology of HD is characterized by neuronal dysfunction, neurotoxicity, brain atrophy and death, making it a textbook example of a neurodegenerative disease. However, more recent evidence has highlighted an important neurodevelopmental role for HTT, suggesting that disease pathology may initiate early in development, impact neurogenesis and alter adult neuronal homeostasis, producing chronic vulnerability to environmental signals and stressors (Godin et al., 2010; HD iPSC Consortium, 2012; Lopes et al., 2016; Molero et al., 2009, 2016; Ruzo et al., 2018; Wiatr et al., 2018; Yu et al., 2017). Clinical studies using neuroimaging to identify prodromal signatures of HD have provided macro-level observations of abnormal neurodevelopment in HD patients decades before symptoms appear (Aylward et al., 2013; Gómez-Tortosa et al., 2001; Lee et al., 2012; Nopoulos et al., 2007; Paulsen et al., 2014; Schippling et al., 2009). Subtle cognitive and behavioral deficits in pre-diagnosed HD individuals have also been reported (Duff et al., 2007; Hinton et al., 2007; Solomon et al., 2007). Furthermore, neurodevelopmental genes and pathways are known to be dysregulated in human and mice models of HD (Fossale et al., 2011; HD iPSC Consortium, 2017; Jin et al., 2012; Labadorf et al., 2015; Milnerwood et al., 2006; Ng et al., 2013). While these findings indicate that premanifest HD individuals develop various, subtle mHTT-mediated changes that may prime the brain for neurodegeneration, they did not address whether aberrant neurodevelopment caused these prodromal symptoms.

Since mHTT acts through both gain and loss of function mechanisms, the finding that HTT

is important for embryonic survival only hinted that HD pathogenesis may be established during neurodevelopment (Nasir et al., 1995; Zeitlin et al., 1995). The first support for this idea came from investigations of heterozygous *HTT* knock-out mice, which exhibited increased motor activity, cognitive deficits, and regional neuronal loss, although no aberrant brain atrophy was observed, suggesting sufficient expression of HTT (> 50%) is necessary for proper neurodevelopment and loss of a normal allele, such as in HD, had neurogenic consequences (Nasir et al., 1995; O'Kusky et al., 1999). Moreover, selective inactivation of *HTT* in the forebrain of mice before birth resulted in neuronal degeneration, motor deficits and premature lethality (Dragatsis et al., 2000). These findings were further substantiated by heterozygous transgenic mice with hypomorphic expression of one *HTT* allele selectively during development. These mice demonstrated early neuronal loss and dysregulated neurodevelopment during embryogenesis, as well as motor deficits, astrogliosis, and neurodegeneration in adult animal (Arteaga-Bracho et al., 2016). Taken together, these data illustrate that loss of normal HTT function causes neurodevelopmental abnormalities, which prime neural cells for dysregulation and degeneration similar to HD pathology. However, they do not directly address the consequences of mHTT gain-of-function activity and its impact on development.

To this end, experiments in transgenic knock-in mice showed that mHTT homozygotes displayed embryonic brain malformation and perinatal lethality (Auerbach et al., 2001; White et al., 1997). Examination of the embryos of mHTT heterozygous mice revealed impaired striatal architecture, cell cycling deficits, and aberrant expression of pluripotency and neurogenesis markers prior to birth, demonstrating that inappropriate molecular signals in the HD embryo may drive aberrant neurodevelopmental programs that produce dysfunctional neurons (Molero et al., 2009). To better understand how mHTT affects neurodevelopment specifically, researchers

selectively expressed mHTT only during neurodevelopment in mice and surprisingly found that as adults, these mice exhibit neurodegeneration, glutamate excitotoxicity, motor deficit, and abnormal electrophysiology (Molero et al., 2016). This finding suggests that selective exposure to mHTT during development is sufficient to recapitulate many phenotypes observed in HD mice constitutively expressing mHTT. Taken together, it is undeniable that both mHTT and reduced HTT expression results in developmental abnormalities at very early stages that lay the foundation for HD pathogenesis.

In vitro studies examining HD induced pluripotent stem cells (iPSCs) and NPCs have also reported early dysregulation in the presence of mHTT, further supporting the idea that HD pathogenesis begins prior to the production of mature neural cell lineages. For example, in mouse and human HD iPSCs, aberrant mitogen-activated protein kinase (MAPK), tumor protein p53 (p53) and Wingless/Integrated (WNT) signaling has been observed along with activation of oxidative stress genes, illustrating that multiple molecular alterations observed in HD are already dysregulated in undifferentiated pluripotent stem cells (PSCs) (Szlachcic et al., 2015). NPCs derived from the fetal brains of mHTT homozygous and heterozygous mice have also replicated multiple disease phenotypes (Ritch et al., 2012; Wiatr et al., 2018). HD NPCs exhibited reduced propensity for neuronal differentiation, which was accompanied by increased cell death compared to control NPCs (Conforti et al., 2013; Wiatr et al., 2018; Yu et al., 2017). One of these studies further expanded on these findings in an experiment comparing the neuronal differentiation capacity of WT, *HTT*-null and HD NPCs derived from mice (Conforti et al., 2013). Interestingly, when induced to differentiate into neurons, HD NPCs showed significantly less capacity and massive cell death compared to WT NPCs (Conforti et al., 2013). HTT knock-out NPCs not only produced less neurons than HD NPCs, but also demonstrated a dramatic increase in astrogliosis,

with over 3-fold change in *GFAP* expression (Conforti et al., 2013). Notably, changes in GFAP levels where evident early on, prior to apparent cell death, which highlights that not only does mHTT differentially impact developmental events, it is likely these early HD-associated aberrancies create unknown vulnerabilities in non-neuronal cell populations, such as astrocytes, that later contribute to neurodegeneration (Conforti et al., 2013). Thus, an understanding of the impact of mHTT on astrocytes both in the adult brain and in a developmental context is essential.

Additional studies in human and animal models have shown that HD NPCs display abnormal cell cycle progression that could be rescued by silencing mHTT and has been previously linked to cell fate specification in *HTT*-null NPCs (Godin et al., 2010; Lopes et al., 2016). Furthermore, chromosomal instability during neurogenesis was also reported in *HTT*-null and HD human ESCs, illustrating signs of early HTT loss-of-function occurs in primates as well (Ruzo et al., 2018). mHTT expression in NPCs also causes differential deregulation of the Notch signaling pathway, causing an aberrant developmental cascade impacting neural lineage specification (Nguyen et al., 2013). Finally, the HD iPSC Consortium (2017) performed RNA-seq on heterogeneous neural cultures, containing NPCs, neurons and astrocytes, derived from HD-patient iPSCs. One third of the genes differentially expressed between HD and control cultures were in neuronal development and maturation, as well as adult neurogenesis pathways (HD iPSC Consortium, 2017; Wiatr et al., 2018).

It is a growing consensus that neurodevelopmental defects occur very early in HD cells, setting the stage for disease pathogenesis and neurodegeneration in adult life. It has also been established that mHTT causes molecular dysregulation that can be detected early both *in vivo* and *in vitro,* prior to the establishment of differentiated neuronal cells. All neural cell types, not just neurons, arise from these precursor NPCs exhibiting early HD phenotypes, so it is undeniable that

most, if not all, neural cells experience the impact of mHTT prior to neuronal differentiation. However, all HD neurodevelopmental studies have focused on neuronal cell types or heterogenous brain populations, with very limited work on astrogenesis specifically. Future studies should focus on characterizing early signatures of HD pathogenesis during the development of astrocytic lineages. A broad understanding on the impact of mHTT on the development of all neural lineages is essential to developing effective neuroprotective therapies for the progressively degenerating brain in HD prior to symptom appearance.

1.3 Epigenetics of Huntington's disease

Transcriptional dysregulation has been widely reported across HD *in vivo* and *in vitro* models and is an important contributor to HD pathogenesis (Becanovic et al., 2010; HD iPSC Consortium, 2017; Hodges et al., 2006; Labadorf et al., 2015; Langfelder et al., 2016; Luthi-Carter et al., 2000). These studies revealed dysregulated gene expression occurs early in development, with functional signatures that vary between different brain regions and cell types (HD iPSC Consortium, 2017; Hodges et al., 2006; Seredenina et al., 2012). Several mechanisms by which mHTT impacts the transcriptome have been proposed, including the aberrant interaction of mHTT with various transcription factors, causing inhibition of their regulatory functions leading to widespread transcriptional consequences (Bradford et al., 2009; Seredenina et al., 2012; Zuccato et al., 2010). Transcription is also known to be regulated by the coordination of various epigenetic mechanisms, such as histone modifications and chromatin accessibility. Chromatin accessibility defines the activity status of genomic regulatory elements, such as promoters and enhancers, by regulating the binding of TF and epigenetic complexes and has been suggested to be associated with various post-translational histone modifications (Shlyueva et al., 2014). Although the impact of HD on chromatin accessibility dynamics specifically remains unknown, recent studies have

begun to provide evidence that epigenetic and chromatin modifying factors play a major role in HD transcriptional dysregulation. It is clear that the etiologic mechanisms of aberrant transcription in HD are complex and context-dependent, making them difficult but necessary to fully understand both across neurodevelopment and in different neural cell types.

A growing body of research has demonstrated that aberrant epigenetic modifications, including DNA methylation and post-translational histone modifications, occur globally in HD and influence the transcriptome and disease development. Genomic investigation of DNA methylation in mouse cells expressing mHTT demonstrated global changes in methylation (Ng et al., 2013). Genes with differentially methylated promoters also showed corresponding changes in expression, suggesting dysregulated patterns of methylation directly impacts gene expression in HD (Ng et al., 2013). Increased DNA methylation in HD patients' brains lead to region specific, accelerated aging of the cortex tissues, but not the striatum (Horvath et al., 2016). While these regional differences may be due to the massive death that occurs in striatal neurons, the differential impact of mHTT on DNA methylation in different cell populations has not been fully examined. Furthermore, the transcriptional effects of the accelerated aging in HD brains remains unknown, but it is likely that investigations will reveal age-dependent alterations in the transcriptome as a result of this aberrant epigenetic aging effect. An epigenetic drug screen in HD neurons found DNA methyltransferase (DNMT) inhibitors provided effective neuroprotection against mHTT-induced toxicity and lead to restored expression of *BDNF* and other key genes (Pan et al., 2016). The findings from this *in vitro* screen were replicated in a HD mouse model (Pan et al., 2016). Additionally, 5-hydroxymethylcytosine (5-hmC) is globally decreased in HD mice brains, with differentially hydroxymethylated regions associated with genes involved in neuronal development and differentiation (Wang et al., 2013). Taken together these studies provide proof of global

dysregulation of DNA methylation in the context of HD, and that genes associated with differential methylation play key roles in neurodevelopment.

Post-translational histone modifications, such as histone methylation and acetylation, have also been shown to be impacted by mHTT (Francelle et al., 2017; Lee et al., 2013a; Lee et al., 2013b). Trimethylation of histone H3 lysine 9 (H3K9me3) is a well-established mechanism of transcriptional repression that is facilitated by several methyltransferases, including, ERG-associated protein with SET domain (ESET). Both H3K9me3 and ESET are observed at higher levels in HD human and mice striatum tissues compared to controls (Lee et al., 2013b; Ryu et al., 2006). Pharmacological inhibition of ESET led to reduced H3K9me3, rescued neuropathological phenotypes and increased survival of HD mice (Ryu et al., 2006). There is also evidence that mHTT alters transcription by aberrantly interacting with histone-modifying enzymes and modulating their activity (Giralt et al., 2012; Jiang et al., 2006; Ratovitski et al., 2015; Seong et al., 2010; Valor et al., 2013). For example, data from primary neuron cultures demonstrated that HTT interacts with protein arginine methyltransferase 5 (PRMT5) to mediate symmetrical dimethylation of arginine 3 on histones H4 (H4R3me2s) (Ratovitski et al., 2015). However, mHTT binds PRMT5 and inhibits its activity, resulting in reduced R3me2s at transcriptionally repressed promoters in HD neurons (Ratovitski et al., 2015). Silencing of jumonji C domain-containing protein 6 (*JMJD6*), the only known R3me3s demethylase, rescues mHTT phenotypes in this neuronal model (Ratovitski et al., 2015).

Global decreases in histone H3 acetylation have also been widely reported in HD models (Giralt et al., 2012; Lee et al., 2013b; McFarland et al., 2012; Sadri-Vakili et al., 2007). Reduced histone H3 lysine 27 acetylation (H3K27ac) at gene promoters in HD mice brains was accompanied by decreased enrichment of RNA polymerase II (RNAP II) and reduced gene

expression, providing support for the direct transcriptional consequences of the abnormal HD epigenome (Achour et al., 2015). Significant changes in H3K27ac were also observed at enhancers, with HD-associated loss of H3K27ac seen at enhancers known to regulate striatal cell identity (Achour et al., 2015). CREB binding protein (CBP) interacts with many different proteins to coordinate a variety of cellular processes but is also a known histone acetyltransferase (HAT), specifically mediating H3K27ac (Chan et al., 2001; Marmorstein et al., 2014; Valor et al., 2013). Early studies demonstrated that mHTT aberrantly sequesters CBP in its aggregates, and also causes reduced CBP expression through undefined mechanisms (Giralt et al., 2012; Jiang et al., 2006; Nucifora et al., 2001; Steffan et al., 2000). There is extensive evidence that the inhibitory interaction of mHTT with CBP leads to global decreases in H3 acetylation in the brain and selective silencing of CBP target genes (Giralt et al., 2012; Jiang et al., 2006; Valor et al., 2013). In HD mice, treatment with a histone deacetylase inhibitor (HDACi) not only rescued overt disease phenotypes and H3 acetylation levels, but it also restored expression of CBP-target and other aberrantly expressed genes, providing evidence that the loss of CBP-mediated H3 acetylation directly impacts the HD transcriptome (Giralt et al., 2012; Jia et al., 2012; Thomas et al., 2008). Other studies examining HDACi treatment in HD have provided further support that the epigenetic dysregulation that underlies disease pathology also serves as a potential therapeutic target. For example, in response to HDACi treatment, both WT and HD male mice showed increased DNA methylation at the promoter of the Y chromosome-linked, histone H3 lysine 4 demethylase, Jumonji/ARID domain-Containing Protein 1D (*JARID1D*) (Jia et al., 2014). Interestingly, only the male progeny of male HD HDACi-treated mice displayed an improved disease phenotype, along with increased *JARID1D* expression and reduced levels of CNS histone H3 lysine 4 trimethylation (H3K4me3), compared to that of WT and non-treated HD mice (Jia et al., 2014). Studies such as

these have provided a myriad of important findings. First, they provide evidence for the potential value of epigenetic therapies for HD. Moreover, they highlight the complexity of HD pathogenesis and the epigenetic mechanisms underlying it. HDACi treatment restoring aberrant histone acetylation *in vivo,* also produced changes in DNA methylation and transgenerationally impacted multiple epigenetic modifications, such as H3K4me3, which demonstrates the dynamic and context-dependent characteristic of epigenetic dysregulation in HD and reinforces the need for deeper investigation of the HD epigenome of all neural populations across development.

H3K4me3 is an active epigenetic mark that is reported to be globally reduced in HD. In the brains of HD mice, H3K4me3 was decreased at the promoter of *BDNF* and other genes known to be down-regulated in HD, prior to the appearance of symptoms (Vashishtha et al., 2013). RNA-seq experiments in these HD mice revealed up-regulation of two H3K4me3 demethylases, Jumonji/ARID Domain-Containing Protein 1 B (*JARID1B*) and C (*JARID1C*), compared to controls (Vashishtha et al., 2013). Moreover, *JARID1C* knock-down in HD mice restored the expression of key HD-dysregulated genes (Vashishtha et al., 2013). A genome-wide investigation of HD related changes in H3K4me3 and transcription in the human brain also detected global differential H3K4me3 enrichment, with more than half of these regions being lost in HD-patient brains, replicating the findings from the HD mouse model (Dong et al., 2015; Vashishtha et al., 2013). In contrast to the mouse model however, this study did not observe corresponding changes in H3K4me3 with differential gene expression. However, it did report a significant correlation between promoter H3K4me3 enrichment and gene expression levels (Dong et al., 2015). This difference in findings is likely due to the fact that Dong et al. (2015) performed H3K4me3 chromatin immunoprecipitation with sequencing (ChIP-seq) in sorted neurons from HD patient brains, while RNA-seq was performed on brain tissue homogenate; therefore, H3K4me3 profiles

only represented a portion of the transcriptome findings reported. It may also be true that while HD-mediated alterations in H3K4me3 influence gene expression, evidence exists that other epigenetic mechanisms are also impacted by HD and directly influence H3K4me3 dynamics (Jia et al., 2014). A global view of the aberrant epigenome across neurodevelopment will be required to fully explain the transcriptional dysregulation that characterizes HD pathology.

To that end, a study of H3K4me3 and transcriptionally repressive histone H3 lysine 27 trimethylation (H3K27me3) dynamics during differentiation of HD mouse ESC into NPCs demonstrated a developmental stage-specific, abnormal chromatin landscapes in HD (Biagioli et al., 2015). In HD ESCs, differential enrichment of H3K4me3 and H3K27me3 were observed globally compared to WT ESCs (Biagioli et al., 2015). However, when differentiated into NPCs, HD cells had a significant global reduction in H3K4me3 levels that corresponded with decreased gene expression, while H3K27me3 enrichment became more similar to that of WT NPCs (Biagioli et al., 2015). This unique developmental study provides further evidence that mHTT expression impacts epigenetic mechanisms differentially during neurodevelopment, generating HD NPCs with altered potential that give rise to dysfunctional neural cell types. In contrast, a study in HD murine embryoid bodies observed elevated H3K27me3 level in the presence of mHTT (Seong et al., 2010). It has been demonstrated that HTT directly interacts with H3K27 methyltransferase, enhancer of zeste 2 (EZH2) and facilitates its activity in the polycomb repressive complex 2 (PRC2), which mediates H3K27me3 and is essential to the regulation of differentiation into various cell types, including the transition from ESC to NPCs (Jepsen et al., 2007 ; Orlando, 2003; Seong et al., 2010). Interestingly, the transcriptional profiles of mHTT striatal cells and PRC2 knockout cells are very similar (von Schimmelmann et al., 2016). However, the direct impact of mHTT on PRC2 function remains unclear.

In summary, these studies of HD epigenetic dysregulation, whether through direct interactions with mHTT or as an indirect consequence of other disease-related changes, highlight its significant role in disease pathology and demonstrate the therapeutic potential of targeting epigenetic mechanisms in HD. It is clear that the HD expansions impacts epigenetic mechanisms globally very early in development, leading to altered transcription profiles that forecasts increased susceptibility to the neurotoxic effects of mHTT (Figure 1-2). Furthermore, many of these epigenomic abnormalities are observed as early as the pluripotent stage and impact important factors that regulate development and neural differentiation. It is also evident that neuron-specific epigenetic changes show associations with, but cannot account for all, the global transcriptome dysregulation reported in the context of heterogeneous HD brain tissue. Still, very little is known about the differential mechanisms and sensitivities of all neural cell types to mHTT. Future studies aimed at interrogating HD-mediated epigenomic differences and transcriptional consequences, in non-neuron cell types, such as astrocytes, will be essential to both our understanding of HD and of neurodevelopmental and neurodegenerative processes in general.

A

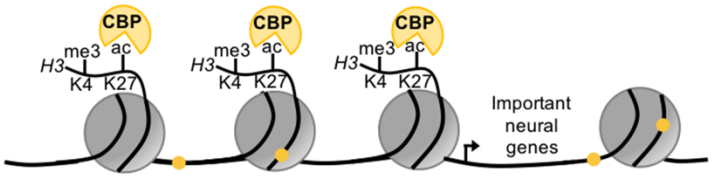
CBP
me3
ac
H3
K4
K27
Important
neural
genes

B

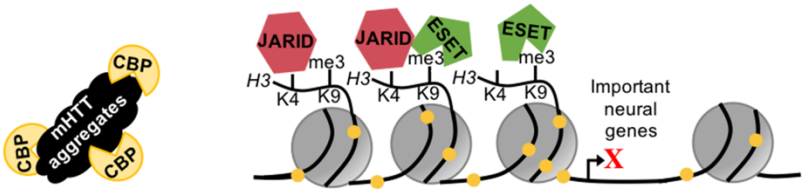
CBP
mHTT
aggregates
JARID
ESET
me3
H3
K4
K9
Important
neural
genes
X

Figure 1-2. Summary of abnormal epigenomic profile in HD. (A) Wild-type neural populations possess active epigenetic signatures at neural promoters, such as CBP-mediated H3K27ac, H3K4me3, and DNA hypomethylation, leading to functional neural populations in the healthy adult brain. (B) In HD, increased expression of *JARID* proteins, known to demethylate H3K4me3, and *ESET*, a H3K9me3 methyltransferase, cause a global loss of active chromatin modifications, the establishment of an aberrant epigenomic profile, and a dysregulated transcriptome. Additionally, mHTT directly binds and sequesters CBP in its aggregates, preventing CBP-mediated H3K27 acetylation and further contributing to the global transcriptional dysregulation driving HD pathology.

1.4 Study Proposal

Despite extensive characterization of HD neuropathology and molecular dysregulation, HD remains an untreatable and devastating disease. A majority of research has focused on the impact of mHTT on striatal MSNs, as this population of cells exhibit significant susceptibility to disease-associated toxicity. However, the various cell types comprising the CNS act in symphony, constantly and continually communicating and supporting one another. While there is limited understanding of the role of glia in HD pathogenesis, it is clear mHTT expression in astrocytes causes dysregulation of astrocytic processes, which is sufficient to trigger a cascade of neurodegenerative effects on both healthy and diseased neuron populations. Additionally, it has recently been recognized that early developmental abnormalities set the stage for later HD vulnerabilities, and that epigenetic dysregulation underlies the aberrant transcriptional signatures reported across neurodevelopment in HD. Although, research is lacking, an emerging theme arises: the aberrant establishment of lineage-specific chromatin and transcriptional signatures occurs as early as PSCs and NPCs in HD cells, giving rise to various neural cell types predisposed to mHTT-mediated toxicity, altered homeostasis and impacted viability over time. Characterization of the epigenome and transcriptome in different HD neural cell populations across development will provide a powerful resource for the assessment of mHTTs impact on neurodevelopment, HD pathogenesis and the identification of targets for therapeutic intervention prior to disease onset.

This dissertation will focus on characterizing the dynamics of chromatin accessibility and transcription during *in vitro* astrocyte differentiation of transgenic HD non-human primate (NHP) PSCs. Given the obvious similarities in anatomy, neurodevelopment, and behavior, NHP models provide a reliable and translatable resource for understanding neurological disease pathogenesis and developing effective therapeutic strategies. Our laboratory has generated the first transgenic

HD rhesus macaques (Yang et al., 2008), from which we have successfully established HD NHP iPSCs (Chan et al., 2010). Our transgenic HD iPSCs carry exon 1 of the human *HTT* gene with 65 CAG repeats, along with green fluorescent protein (*GFP*), driven by the human polyubiquitin-C (*UBC*) promoter (Chan et al., 2010). These HD iPSCs were used to derive NPCs for long term culture, which are capable of differentiating into both neurons and astrocytes that recapitulate classic HD phenotypes (Carter et al., 2014; *unpublished data*). Furthermore, shRNA-mediated silencing of HTT could reverse HD phenotypes in both HD NHP neurons and astrocytes (Carter et al., 2014; *unpublished data*). The following chapter will describe the impact of mHTT on chromatin accessibility and gene expression during *in vitro* astrocyte differentiation from HD NHP PSCs. This study will provide insight into altered chromatin accessibility and transcriptional dysregulation that specifically impacts astrocyte differentiation in HD NHP cells.

Chapter 2: Chromatin Accessibility and Transcription Dynamics During *In Vitro* Astrocyte Differentiation of Huntington's Disease Monkey Pluripotent Stem Cells.

This chapter is also a manuscript currently in preparation for submission.

2.1 Author's Contribution and Acknowledgement of Reproduction

Alexandra Goodnight, Dr. Anthony Chan, and Dr. Victor Corces conceived and coordinated this study and designed the experiments. Alexandra Goodnight wrote the paper and Dr. Isaac J. Kremsky helped with editing. Alexandra Goodnight performed all the experiments, with the assistance and guidance of Dr. In Ki Cho and Dr. Yoonhee Jung. Sujittra Khampang cultured PSCs for this study. Dr. Isaac J. Kremsky performed all the ATAC-seq analysis and most of the RNA-seq analysis. Dr. James M. Billingsley performed the remaining RNA-seq analysis, specifically for Figure s2-3 and gene set enrichment analyses (GSEA). The Yerkes Non-Human Primate Genomic Core performed RNA library preparation and sequencing. All authors reviewed the results and approved the final versions of the manuscripts.

2.2 Abstract

Huntington's disease (HD) is a fatal, neurodegenerative disorder caused by a CAG repeat expansion, resulting in a mutant huntingtin protein. While it is now clear that astrocytes are affected by HD and significantly contribute to neuronal dysfunction and pathogenesis, the aberrant transcription and epigenetic profiles in HD astrocytes have yet to be characterized. Here, we examined global transcription and chromatin accessibility dynamics during *in vitro* astrocyte differentiation in a transgenic non-human primate (NHP) model of HD. We found global changes in accessibility and transcription across HD differentiation, with differential trends first observed in neural progenitor cells (NPCs), once cells have committed to a neural lineage. Transcription of p53 signaling and cell cycle pathway genes was highly impacted during differentiation, with depletion in HD NPCs and upregulation in HD astrocytes. E2F target genes (ETGs) also displayed this inverse expression pattern, and strong associations between ETG expression and accessibility at nearby, putative enhancers were observed. All together, we demonstrate chromatin accessibility and transcription are altered throughout *in vitro* HD astrocyte differentiation and provide evidence that E2F dysregulation contributes to aberrant cell cycle reentry and apoptosis as NPCs differentiate into astrocytes.

2.3 Introduction

Huntington's disease (HD) is an autosomal dominant, neurodegenerative disease characterized by progressive brain atrophy, along with cognitive and motor dysfunction, and affecting adults between 35-55 years of age (Zuccato et al., 2010). Although several potential therapeutic strategies have been identified, no cure or therapies exist to prevent or reverse disease progression (Gagnon et al., 2010; Hu et al., 2009; Watts et al., 2012; Yu et al., 2012). HD results from an expansion of more than 40 CAG repeats in exon 1 of the huntingtin gene, *HTT*, which gives rise to a mutant huntingtin protein (mHTT) with an extended polyglutamine (polyQ) tract at the N-terminus (Davies et al., 1997; DiFiglia et al., 1997; Goldberg et al., 1994; Macdonald et al., 1993; Sieradzan et al., 1999; Snell et al., 1993). mHTT can form aggregates and nuclear inclusions, a signature characteristic of HD (Cattaneo et al., 2005; DiFiglia et al., 1997; Sieradzan et al., 1999), and can be cleaved to create polyQ-containing protein fragments (Scherzinger et al., 1997).

The disruption of many cellular processes, including neurodevelopment, cell cycle, apoptosis, mitochondrial function, inflammation, and synapse formation and activity by mHTT in neurons is well documented but incompletely understood (HD iPSC Consortium, 2012; Labadorf et al., 2015; Lopes et al., 2016; Molero et al., 2009, 2016; Seredenina et al., 2012). However, transcriptional dysregulation is thought to play an important role in driving these pathogenic mechanisms (HD iPSC Consortium, 2012; Lopes et al., 2016; Molero et al., 2009, 2016; Seredenina et al., 2012). Altered transcriptional profiles are evident very early in HD and impact neurogenesis, setting the stage for dysfunctional homeostasis and degeneration in the adult brain (HD iPSC Consortium, 2012; Lopes et al., 2016; Molero et al., 2009, 2016; Ruzo et al., 2018; Wiatr et al., 2018). Furthermore, the impact of mHTT on transcription varies between neural populations in the central nervous system (CNS), as well as across development (Becanovic et al.,

2010; HD iPSC Consortium, 2017; Hodges et al., 2006; Labadorf et al., 2015; Langfelder et al., 2016; Luthi-Carter et al., 2000; Seredenina et al., 2012). It has been demonstrated that mHTT aberrantly interacts with and sequesters critical proteins, such as transcription factors (TFs) and epigenetic enzymes, causing widespread transcriptional dysregulation and disruption of important cellular processes in the brain (Crook et al., 2013; Davies et al., 1997; Giralt et al., 2012; Labbadia et al., 2013; Li et al., 2006; Ratovitski et al., 2015; Ross et al., 2011; Saudou et al., 1998; Seong et al., 2010; Valor, 2015; Zuccato et al., 2010). For example, mHTT binds to p53 and causes downstream alterations in the transcriptional activity of select p53-target genes (Bae et al., 2005; Steffan et al., 2000). p53 regulates many diverse and specific cellular processes, including cell cycle, apoptosis, DNA repair, metabolism and mitochondrial function (Marcel et al., 2018; Vaseva et al., 2009). However, the downstream transcriptional consequences of aberrant mHTT interactions with TFs, such as p53, are not well understood.

The transcriptome is largely regulated by epigenetic mechanisms, such as histone modifications, DNA methylation, and binding of TFs and architectural proteins. The accessibility (relatively high DNase-seq or ATAC-seq signal) of genomic regulatory elements, such as promoters and enhancers, dictates the binding of TFs and architectural proteins, and thus indicates regions regulating the activation and repression of transcription (Shlyueva et al., 2014). Chromatin accessibility is highly specific between cell types, developmental time points, and pathological conditions (Shlyueva et al., 2014; Vermut et al., 2016). Further, post-translational histone modifications are used to classify the activity status of promoters and enhancers (Shlyueva et al., 2014). For example, active marks, like histone H3 lysine 27 acetylation (H3K27ac), are associated with accessible chromatin at active promoters and enhancers specifically, while repressive modifications indicate inactive promoters and enhancers, which display a less accessible

chromatin structure. While this association has been well documented, the specificity and directionality of this association is complex and not fully understood. Although there have been no investigations of chromatin accessibility dynamics in HD, there is growing support that epigenetic mechanisms contribute to HD transcriptional dysregulation and pathology. For example, acetylation of histone H3 in general, but also specifically H3K27ac, is globally reduced in HD (Giralt et al., 2012; Lee et al., 2013a; McFarland et al., 2012; Sadri-Vakili et al., 2007). CBP acts as a histone acetyltransferase (HAT), specifically mediating H3K27ac (Chan et al., 2001; Marmorstein et al., 2014; Valor et al., 2013). Studies have demonstrated that mHTT aggregates sequester CBP and inhibit its HAT activity, leading to genomic loss of H3 acetylation and repressed transcription in HD brains (Giralt et al., 2012; Jiang et al., 2006; Nucifora et al., 2001; Steffan et al., 2001; Valor et al., 2013). In addition, histone deacetylase inhibitor (HDACi) treatment in HD mouse models both rescued disease phenotypes, and restored transcription and histone H3 acetylation profiles (Giralt et al., 2012; Jia et al., 2012; Thomas et al., 2008). An *in vivo* study in HD mice found that HDACi treatment restored histone H3 acetylation and also produced changes in DNA methylation (Jia et al., 2014), highlighting the dynamic and context-dependent characteristic of epigenetic regulation and reinforcing the need for a better understanding of the altered epigenome across development in in HD.

To that end, one study differentiated HD mouse embryonic stem cells (ESCs) into neural progenitor cells (NPCs) and examined histone H3 lysine 4 trimethylation (H3K4me3) and histone H3 lysine 27 trimethylation (H3K27me3) dynamics (Biagioli et al., 2015). While HD ESCs showed global differences in H3K4me3 and H3K27me3, HD NPCs demonstrated a reduction in H3K4me3 only, with corresponding decreased transcription, compared to wild type (WT) cells (Biagioli et al., 2015). Overall, these findings indicate that during development, stage-specific

chromatin landscapes are differentially dysregulated in HD, giving rise to alterations in all neural cell types (Biagioli et al., 2015). Thus, studies exploring accessibility at specific developmental stages and in specific cell types, along with its relationship to transcriptional changes, have the potential to contribute greatly to our understanding of the pathological mechanisms underlying HD, as well as in the discovery of therapies for HD. Additional epigenetic studies have reported loss of active modifications and reduced transcription in HD (Biagioli et al., 2015; Giralt et al., 2012; Jiang et al., 2006; Nucifora et al., 2001; Steffan et al., 2001; Thomas et al., 2008; Valor et al., 2013), which is in contrast to findings from transcriptome studies in the prefrontal cortex of HD patients, which report both up and down regulation of global transcription, but more differentially expressed (DE) genes are overexpressed in HD (Labadorf et al., 2015). It is clear that transcription and the epigenome are dynamically altered during HD progression. However, the impact of epigenetic mechanisms on transcription are complex and highly context dependent, making it difficult but important to fully characterize across neurodevelopment and in different neural cell types in HD.

Most studies of transcriptional and epigenetic dysregulation in HD pathogenesis have focused on neuronal models and heterogenous brain tissues. However, neurons require glia cells, which comprise 90% of the human CNS cell population, for normal function, homeostasis, and the establishment and healthy activity of neural circuits (Allen & Barres, 2009; Belanger et al., 2009; Belanger et al., 2011; Clarke et al., 2013). Given its ubiquitous expression and vast impact on cellular processes, it is undeniable that mHTT affects all neural cell types, not just certain neuron populations, yet little is known about the impact of HD on glial development and function. Astrocytes are the most abundant type of glial cell and are critical CNS regulators, with roles in neurodevelopment, neuronal metabolic support, synaptic formation and function, tissue repair,

neuroprotection, ion signaling homeostasis, and complex brain functions such as sleep, memory and breathing (Belanger et al., 2009; Belanger et al., 2011; Gibbs et al., 2008; Gourine et al., 2010; Halassa et al., 2009; Phatnani et al., 2015; Volterra et al., 2005). Both mHTT expression and aggregate formation have been reported in HD astrocytes (Jansen et al., 2017; Khakh et al., 2017; Shin et al., 2005; Tong et al., 2014). Increased expression of glial fibrillary acidic protein (*GFAP*), a marker for astrogliosis, is a well-documented indicator of early neural damage in HD. (Faideau et al., 2010; Hedreen et al., 1995; Kocerha et al., 2014; Labadorf et al., 2015; Lin et al., 2001; Shin et al., 2005; Vonsattel et al., 1985). In fact, RNA sequencing (RNA-seq) performed on HD patient brains found *GFAP* to be the second most significantly overexpressed gene compared to control tissues (Labadorf et al., 2015).

A growing body of evidence suggests a role for astrocytes in HD pathology (Arregui et al. 2011; Bradford et al. 2009; Chou et al. 2008; Faideau et al., 2010; Hsiao et al., 2013; Oliveira, 2010; Shin et al., 2005; Skotte et al., 2018; Tong et al., 2014; Valenza et al., 2010; Wang et al. 2012). Selective expression of mHTT in the astrocytes of transgenic mice was sufficient to produce neuropathology resembling HD and premature death (Bradford et al. 2009). *In vivo* and *in vitro* HD astrocyte models have also shown impaired glutamate transport, resulting from reduced expression of key glutamate transporters and ion channels, such as *GLT1* and *GLAST*, and the Kir4.1 potassium ion (K+) channel (Bradford et al. 2009; Faideau et al., 2010; Shin et al., 2005; Tong et al., 2014). Additionally, aberrant transcription of important trophic factors, including *BDNF*, reduced cholesterol biosynthesis, increased NF-*κ*B-mediated inflammatory response, dysregulated glutamate-GABA-glutamine cycling, and mitochondrial dysfunction, are reported in HD astrocyte models (Hsiao et al., 2013; Oliveira, 2010; Skotte et al., 2018; Valenza et al., 2010; Wang et al. 2012). Surprisingly, a study found that when co-cultured with WT astrocytes, HD

neurons had improved molecular phenotypes, demonstrating that functional astrocytes can protect against HD-mediated neurotoxicity (Shin et al., 2005). In contrast, WT neurons co-cultured with HD astrocytes showed markers of early neurodegeneration, which could be reversed through chemical inhibition of astrocytic glutamate receptors, suggesting that HD astrocytes cause intercellular dysregulation that may contribute to HD pathogenesis and serve as a potential therapeutic target for HD treatment (Arregui et al. 2011; Shin et al., 2005).

Astrocyte dysfunction is gaining growing recognition for its role in HD pathogenesis and potential value as a therapeutic target, as normal astrocyte and neuron synergy is necessary for CNS development and function (Bradford et al. 2009; Shin et al., 2005). Most studies examining astrocytes in HD have used rodent models. However, it has been established that primate and rodent astrocytes have morphological and functional differences (Colombo et al., 1995; Colombo et al., 2004; Oberheim et al., 2009). For example, not only are human astrocytes more structurally complex and phenotypically diverse than that of rodents, certain types of astrocytes (interlaminar and varicose projection astrocytes) are specific to primate species (Colombo et al., 1995; Colombo et al., 2004; Oberheim et al., 2009). Additionally, primate astrocytes exhibit faster Ca2+ signaling compared to rodent astrocytes (Oberheim et al., 2009). These findings demonstrate the limitations of rodent models when studying astrocytes in human disease and highlight the need for a primate model of HD astrocytes.

Here, we examined the impact of mHTT on chromatin accessibility and transcription during *in vitro* astrocyte differentiation in a transgenic non-human primate (NHP) model of HD (Yang et al., 2008). Given similarities in CNS anatomy, neurodevelopment, and behavior, NHPs may offer a more translatable model for investigating neurological disease pathology and identifying efficient therapies. We used induced pluripotent stem cells (iPSCs) derived from

transgenic HD NHPs to establish stable NPC lines, which are able to differentiate into functional neurons and astrocytes that recapitulate HD phenotypes (Carter et al., 2014; Chan et al., 2010; Laowtammathron et al., 2010; *unpublished data*). HD NPCs were further differentiated *in vitro* to generate astrocytes. RNA-seq and assay for transposase-accessible chromatin using sequencing (ATAC-seq) experiments were performed in parallel, in HD and WT NHP cell lines to characterize chromatin accessibility dynamics and transcriptome profiles during HD astrocyte differentiation. This discovery-based approach revealed genome wide alterations in chromatin accessibility and transcription across differentiation, with observable trends occurring once cells have committed to a neural lineage (NPCs through astrocytes). Although alterations of accessible promoters were evident in HD cells across differentiation, most differences in accessibility occurred distal to promoters. At a subset of putatively active rhesus macaque brain enhancers, the altered chromatin accessibility observed in HD astrocytes appeared to be established in the NPC stage. Additionally, an integrated analysis of RNA-seq and ATAC-seq data revealed consistent deficits in various cell cycle-related pathways, such as p53 signaling and E2F target genes, as well as a striking correlation between changes in gene expression and TF occupancy at putative enhancers. Taken together, these results suggest a pathogenic mechanism during HD astrogenesis: dysregulation of several interacting pathways causes expression signatures indicating delayed cell cycle progression in HD NPCs and aberrant cell-cycle reentry and apoptosis, possibly through an E2F TF dependent mechanism, in HD astrocytes.

2.4 Methods

2.4.1 NHP PSC cultures

WT NHP ESCs and transgenic NHP HD iPSCs were previously established (Chan et al., 2010). Transgenic HD iPSCs expressed both exon 1 of the human *HTT* gene with 65 CAG repeats and *GFP* under the control of the human polyubiquitin-C (*UBC*) promoter (Yang et al., 2008; Chan et al., 2010). NHP PSCs were cultured on mouse fetal fibroblast (MFF) feeder cells in ESC culture media [Knockout-Dulbecco's modified Eagle's medium (KO-DMEM; Invitrogen) with 20% Knock-out Serum Replacement (KSR; Invitrogen), 1 mM glutamine, 1 nonessential amino acids (NEAA), and 4 ng/mL of human basic fibroblast growth factor (bFGF; Chemicon, Inc., Tumecula, CA)]. Additionally, NHP PSC cultures were expanded by mechanical passaging. Since these NHP PSC lines were previously used to derive stable NPC cultures (Carter et al., 2014), PSCs were collected for experimental analysis, but not further differentiated into NPCs in this study.

2.4.2 NHP NPC culture maintenance

NPCs were maintained and expanded as previously described (Carter et al., 2014). Briefly, P/L-coated [20 µg/mL poly-L-ornithine (Sigma) and 1 µg/cm2 laminin (Sigma)] cell culture dishes were used to culture cells in neural proliferation medium [Neurobasal-A medium (Life Technologies) with 1x penicillin/streptomycin (Invitrogen), 2 mM of L-glutamine, 1x B27 (Life Technologies), 20 ug/mL of bFGF (R&D), and 10 ng/mL of mLIF (Millipore)]. Cells were maintained at 37°C and 5% CO_2 and media was changed every two days. Upon reaching confluence, cells were passed at a 1:1.5 ratio.

2.4.3 In vitro astrocyte differentiation

The astrocyte differentiation protocol used in this study was based on a previously published protocol (Majumder et al., 2013). For in vitro differentiation of NPCs into astrocytes, NHP NPCs were seeded with the seeding density of 2x105 cells/cm2 on P/L-coated culture plates. Neural proliferation media was replaced with astrocyte differentiation media [Neurobasal-A medium (Life Technologies) with 1x penicillin/streptomycin (Invitrogen), 2 mM of L-glutamine, 500 nM of azacytidine (Aza-C; Sigma), 20 nM of trichostatin (TSA; Sigma), 20 ng/mL of bone morphogenetic protein 2 (BMP2; R&D), and 1x B27 (Life Technologies)]. After 2 days, the Aza-C and TSA were removed, and cells were cultured in the astrocyte differentiation media for an additional 28 days.

2.4.4 Quantitative reverse transcription PCR (qRT-PCR)

Total RNA was prepared from cell samples using TRIzol® (Life Technologies), followed by DNA digestion using Turbo DNA-freeTM kit (Invitrogen) according to the manufacturer's instructions. RNA samples (500 ng) was used to synthesize cDNA using a High-Capacity cDNA Reverse Transcription Kit (Applied Biosystems). qRT-PCR was performed on CFX96 Real-Time Detection System (Bio-Rad) using either IQTM SYBR® Green Supermix (Bio-Rad) or TaqMan™ Gene Expression Master Mix (Applied Biosystems) depending on the primers used. qRT-PCR primer sequences are listed in Table s2-1. PCR conditions for SYBR Green primers: Initial 95°C activation step for 30 sec followed by amplification cycles 95°C for 10 sec and 55°C for 30 sec for 50 cycles. Reaction conditions for TaqMan® gene expression primers: Initial 95°C activation step for 10 min followed by amplification cycles 95°C for 15 sec and 60°C for 60 sec for 40 cycles. Unless otherwise mentioned, one-way analysis of variance (ANOVA) was used for statistical

comparison of qRT-PCR data. Statistical tests were performed using SPSS 23 (IBM) and graphs were prepared using GraphPad Prism 6 (GaphPad Software, Inc.). Bar graphs reflect the mean ± standard error of the mean (SEM) values for each sample. Statistical significance was established $P < 0.05$.

2.4.5 RNA-seq experiments

Cell cultures were harvested and counted. Five hundred thousand cells were pelleted and homogenized in 350 µL TRIzol® (Life Technologies). Cell homogenates were briefly vortexed and stored at -80°C. The RNA was extracted using Qiagen' s miRNeasy Mini Kit with DNase digestion. The RNA quantity and quality were validated using Nanodrop 2000 Spectrophotometer and Agilent's 4200 Bioanalyzer Capillary electrophoresis. 10ng of total RNA was used as an input for mRNA amplifications using Clontech Smarter V4 chemistry according to manufactures instruction. Amplified mRNA was fragmented, and barcodes were added using Illumina's Nextera XT kits. Amplified Libraries were validated by Agilent 4200 Tapestation and quantified using a Qubit fluorimeter. Libraries were normalized, pooled and clustered on an Illumina HiSeq 3000/4000 Flowcell using the Illumina cBOT. The libraries were sequenced on an Illumina HiSeq 3000 system in 101-base single-read reactions with multiplexing to achieve approximately 20 million reads per sample. RNA-seq experiments were performed in three different replicates.

2.4.6 Assay for transposase-accessible chromatin using sequencing (ATAC-seq)

ATAC-seq was performed using the Omni-ATAC protocol (Corces et al., 2017). Cell cultures were harvested, washed in cold 1x PBS, and counted. One hundred thousand cells were resuspended in 50 µL cold resuspension buffer (RSB; 10 mM Tris-HCl pH 7.4, 10 mM NaCl, and

3 mM $MgCl_2$) containing 0.1% NP-40 (Sigma), 0.1% Tween-20 (Sigma), and 0.01% digitonin (Abcam ab141501) and incubated for 3 min on ice. Following lysis, 1 mL RSB with 0.01% Tween-20 was added to the samples. Samples were centrifuged for 10 min at 4°C/500 x g and the supernatant was carefully removed. Nuclei were then resuspended in the transposase reaction mix (25 µL 2x TD buffer, 2.5 µL Tn5 transposase, 0.5 µL 10% Tween-20, 2.5 µL 1% digitonin [0.05% final concentration], and 19.5 µL water) and incubated at 37°C for 30 min in a thermomixer with shaking at 600 r.p.m. Following the reaction, samples were treated with Proteinase K (Fisher 25530015) at 55°C for 2 hr and genomic DNA was isolated via phenol:chloroform:isoamyl alcohol extraction and ethanol precipitation. Library preparation was performed using 2x KAPA HiFi mix (KAPA BIOSYSTEMS INC #kk4604) and 1 mM indexed primers under the following PCR conditions: 72°C for 5 min; 98°C for 30 sec; and 8-12 cycles at 98°C for 10 sec, 63°C for 30 sec, and 72°C for 1 min. ATAC-seq experiments were performed on two replicates, which combine to at least 50 million reads after all the quality control steps.

2.4.7 Analysis of RNA-seq and ATAC-seq data

RNA-seq and ATAC-seq data were analyzed as follows for all subsequent analysis except the ANOVA. All data were aligned to "MacaM_Rhesus_Genome_Annotation_v7.8.2" (Zimin et al., 2014). RNA-seq data were aligned using Tophat2 v2.1.0 (Kim et al., 2013) with the flags, "--no-mixed --no-discordant", and differentially expressed genes were called using cuffdiff v2.1.1 (Trapnell et al., 2012) using default parameters and a cutoff of $q < .01$. ATAC-seq reads were first trimmed using pyadapter_trim.py and then aligned using bowtie version 2 2.2.6 with the flag, "-X 2000", then duplicates were removed from ATAC-seq samples using picard-tools-2.1.7 MarkDuplicates (Langmead et al., 2012). To adjust for fragment size, we aligned all reads as +

strands offset by +4 bp and – strands offset by -5 bp (Buenrostro et al., 2013). Non-nucleosomal ATAC-seq fragments (length < 125 bp) were then separated out for subsequent analysis.

Peaks of non-nucleosomal ATAC-seq reads were called on each replicate of each sample separately using MACS2 version 2.1.0.20151222 (Zhang et al., 2008) in BAMPE mode with default parameters. Peaks from separate replicates were then merged using bedtools merge to get a single set of THSSs (Tn5 hypersensitive sites) for each sample. These were then input into MAnorm3 to call differential peaks (HD vs. WT) at each stage (Shao et al., 2012). We required that differential peaks had a logCPM (Counts per Million), averaged over HD and WT samples, > 1, as reported by MAnorm3. In addition, we required that they either had $q < .01$ or a logFC (HD/WT) magnitude > 3 and $p < .01$.

2.4.8 Differential Heatmaps

To generate the differential heatmaps presented in this paper, fragments per kilobase per million mapped reads (FPKM) values were calculated in each sample separately using pooled replicates. Then log ratios were calculated as log((FKM_HD+.0001)/(FKM_WT+.0001)) to avoid division by zero errors. In cases were FPKM_HD < 1 and FPKM_WT < 1, the value of the log ratio was set equal to 0. The base of the log for these calculations was 2.

2.4.9 ANOVA

For ANOVAs, reads were aligned to the rhesus macaque (*Macaca mulatta*) assembly (MacaM_Rhesus_Genome_v7.fasta; Zimin et al., 2014) using STAR software (v2.5.2b; Dobin et al., 2013). Transcripts were annotated using the UNMC rhesus annotation v 7.6.8 and unsorted

bam files were sorted and indexed using samtools and converted to HTSeq-count format. Estimates of gene-wise and isoform-wise expression levels for individual genes were performed using the R package DESeq2 with R version 3.5.0 (Love et al., 2014).

2.4.10 Motif Analysis

Peaks were called for each sample with replicates pooled, using the same method described above for individual replicates. Then FIMO, from MEME version 4.11.2, was used to scan for motif occurrences within 200 bp of the summit of each peak in each sample, separately (Grant et al., 2011). For cases where multiple motifs were called for the same peak, only the most statistically significant motif was kept. To determine motif enrichment in the HD samples, we constructed a 2X2 contingency matrix for each motif separately, as follows. For example, for motif X, the matrix

N11 N12

N21 N22,

was constructed, where N11=# of times motif X overlaps an HD-up differential peak, N12=# the number of times all other motifs besides X overlap an HD-up differential peak, N21=# of times motif X overlaps any HD peak, and N22=# of times all motifs except X overlap any HD peak. Fisher's exact test was then used to test the null hypothesis N11/(N11+N12) = N21/(N21+N22), i.e. that the proportion of times that motif X occurs in HD-up differential peaks is the same as the proportion amongst all HD peaks (i.e. what would be expected if a random sample of HD peaks were selected). Those motifs with low p-values, therefore, have a much higher proportion of motif X occurring in HD-up samples than would be expected by chance.

This procedure was performed separately for proximal-promoter peaks (TSS +/- 500 bp) and for distal peaks (> 500 bp from any TSS). The same procedure was conducted for each motif using WT-up differential peaks and WT peaks to determine the significance of motif enrichment in WT samples. In that case, the same matrix as above was constructed, except with N11=# of times the motif X overlaps a WT-up differential peak, N12=# the number of times all other motifs besides X overlap a WT-up differential peak, N21=# of times motif X overlaps any WT peak, and N22=# of times all motifs except X overlap any WT peak.

p-values from this test were used to determine the size of circles in the motif enrichment plots as in Fig. 1F,G, etc. No multiple test corrections were used in this case because the high degree of degeneracy of motifs for different transcription factors means that the p-values for numerous pairs of motifs are strongly dependent on one another, whereas multiple test-corrections such as q-value require that all p-values have at most a weak degree of dependence (Storey et al., 2003). A weak correlation amongst p-values is hypothesized in genome-wide differential expression analyses from RNA-seq (Storey et al., 2003), for example, but in the case of a list of TF motifs, the relatively small number of TFs combined with the high degree of correlation of p-values amongst related TFs mean that this dependency amongst p-values is stronger than that for p-values from a genome-wide differential expression analysis.

2.4.11 Gene set enrichment analysis (GSEA)

To identify pathways differentially modulated between WT and HD samples and different differentiation stages, GSEA (Subramanian et al., 2005) was performed as follows. For each contrast, transcripts were ranked by differential expression using the Signal2Noise metric. GSEA

was performed using the desktop module available from the Broad Institute (www.broadinstitute.org/gsea/). GSEA was performed on the ranked transcript lists using 1,000 gene set permutations, collapse of duplicates to Max probe, and random seeding. Gene sets used included the (H) Hallmark and (C5) GO_BP gene sets (MSigDB v6.2; Liberzon et al., 2011).

2.5 Results

2.5.1 In vitro astrocyte differentiation of HD and WT NHP cells

Stable NPC lines were previously established from HD and WT NHP pluripotent stem cells (PSCs) (Carter et al., 2014). HD cell lines carried a construct for exon 1 of the human *HTT* gene with 65 CAG repeats, along with an additional *GFP* vector, both under the regulation of the human polyubiquitin-C (*UBC*) promoter (Yang et al., 2008). NPC cell cultures were induced to differentiate into astrocytes using a previously established 30-day protocol (Majumder et al., 2013) (Figure s2-1A). Quantitative reverse transcription PCR (qRT-PCR) analysis of both cell lines across astrocyte differentiation shows increased expression of exon 1 *HTT* transcripts relative to exon 26 *HTT* transcripts in HD cells compared to WT cells (Figure s2-1B), demonstrating expression of the CAG expanded transgene in our HD cells. Additionally, both HD and WT cell lines exhibit cell type-specific expression of canonical markers over the course of differentiation, such as *OCT4* and *SOX2* in PSCs (Figure s2-1C, D); *SOX2*, *MSI1*, and *NES* in NPCs (Figure s2-1C, D); and *GFAP*, *APOE*, and *LCN2* in astrocytes (Figure s2-1E, F). Neuronal (*MAP2*, *TH*, *GAD*), microglial (*CX3CR1*), and oligodendrocyte (*FOXO4*) markers were largely down regulated following astrocyte differentiation (Figure s2-1G, H).

2.5.2 Aberrant transcriptional profiles are present during in vitro HD astrocyte differentiation

We performed RNA-seq in HD and WT NHP cells at four time points across astrocyte differentiation: PSCs, NPCs, day 3, and astrocytes (day 30) (Figure s2-2). RNA-seq data for markers of PSCs and NPCs (Figure s2-2A, B), astrocytes (Figure s2-2C, D), and other neural cell types (Figure s2-2E, F), generally reflected the trends observed by qRT-PCR (Figure s2-1C-H). Some minor inconsistencies are observed, but this is to be expected due to the high degree of noise inherent in RNA-seq data. Interestingly, the inclusion of day 3 expression data in RNA-seq

experiments revealed that HD cells showed early expression of astrocyte markers (*GFAP, APOE, LCN2*) compared to WT cells (Figure s2-2C, D). These findings are in agreement with results from a recent study, which reported that heterogeneous neural cultures (NPCs, astrocytes, and neurons) derived from human HD iPSCs show expression profiles of premature initiation and incomplete terminal differentiation compared to WT cells (HD iPSC Consortium, 2017).

Principal component analysis (PCA) of log2 transformed, normalized RNA-seq data demonstrated the least variability between HD and WT cells was at the PSC stage, with progressive divergence at each stage of differentiation and the greatest variability at the astrocyte stage (Figure s2-3A). Additionally, global log2-transformed, normalized read counts illustrate the distinct expression patterns of HD and WT cell lines that become progressively dissimilar as cells progress towards the astrocyte stage (Figure s2-3B). Overall, RNA-seq libraries segregated by cell type (HD vs. WT) and stage (PSCs, NPCs, day 3, astrocytes), with low variability between replicates. This demonstrates that the observed variance is a result of mHTT expression and stage of astrocyte differentiation. Cuffdiff (Trapnell et al., 2012) analysis of the RNA-seq data uncovered 5,643 differentially expressed (DE) genes between HD and WT cells in at least one time point ($q < 0.01$), with 2,218 DE genes in PSCs, 1,344 in NPCs, 3,118 at day 3, and 1,316 in astrocytes (Figure 2-1A; Table 2-1; Table s2-2). Of these, 63 genes were differentially expressed across all 4 stages (Figure 2-1A; Table s2-3). Figure 2-1B shows an example DE gene, *KCNJ10*, that has decreased expression in HD astrocytes compared to WT astrocytes, with differences observed as early as the NPC stage. *KCNJ10*, which encodes the Kir4.1 potassium ion channel, has been previously demonstrated to be downregulated in HD mouse astrocytes (Tong et al., 2014). Thus, these data provide further support for that finding, as well as for the ability of our NHP astrocytes to recapitulate reported HD phenotypes. Hierarchical clustering of all DE genes showed associations

between NPC, day 3 and astrocyte samples, whereas PSCs showed a unique DE profile (Figure 2-1C).

We next compared the DE genes identified by our RNA-seq analysis to those identified to be DE in heterogeneous neural cultures derived from human HD iPSCs (HD iPSC Consortium, 2017). Only DE genes annotated in both species' genomes were counted. This comparison yielded 824 overlapping genes, which is more than their reported overlap with a HD mouse data set (Figure s2-3C; HD iPSC Consortium, 2017). Moreover, comparison of our DE gene list to a list of 3,853 DE genes in HD human brain tissues that were also annotated in the MacaM genome, demonstrated 1,323 genes shared between the two data sets (Figure s2-3D; Labadorf et al., 2015). It is not surprising that many DE genes found by these studies in human HD models were not found to be DE in the present study, since these studies examined mixed cell populations containing a high proportion of neurons, whereas ours focused on astrocytes and their precursors specifically (HD iPSC Consortium, 2017; Labadorf et al., 2015). On the other hand, we identified over 4,000 DE genes that were not identified in either study, which may be due to the fact that we used highly homogenous cell cultures rather than heterogeneous populations. GO analysis of our unique DE genes revealed enrichment of astrocyte-specific genes ($p < 0.001$, *data not shown*), lending further support to this. Taken together, these findings provide evidence that our NHP HD model recapitulates transcriptome phenotypes reported from *in vivo* and *in vitro* human HD models, provides greater resolution and statistical power for high-throughput studies of NPCs and astrocytes, and identified a set of novel DE genes potentially involved in HD progression that were not identified in previous high-throughput studies using heterogeneous cell populations.

2.5.3 Promoter-proximal chromatin accessibility dynamics during HD differentiation

To characterize genome-wide changes in chromatin accessibility and assess their association with the altered transcriptome in HD, we performed ATAC-seq (Corces et al., 2017) on HD and WT cells in parallel with RNA-seq experiments. ATAC-seq was performed in 2 replicates, displaying high correlation within all samples, and thus, were combined to obtain at least 50 million mapped reads after various quality control steps (Figure s2-3E, F; Table s2-4). We isolated non-nucleosomal fragments (< 125 bp), which correspond to genomic regions protected from the Tn5 transposase by proteins bound to the DNA (Tn5 hypersensitive sites [THSSs]). After calling peaks for each sample, differential THSSs were determined for each stage (Table 2-2; see Methods) and further separated into promoter-proximal (+/- 500 bp from transcription start site (TSS)) and distal (>500 bp from any TSS) categories for subsequent analysis. Overall, there were 2,467 differential promoter-proximal THSSs (315 HD-enriched and 2,152 WT-enriched) and 44,649 differential distal THSSs (30,588 HD-enriched and 14,061 WT-enriched), suggesting that although changes in chromatin accessibility occur genome-wide, HD cells demonstrate an overall depletion of promoter accessibility during differentiation of PSCs into astrocytes. Of note, no differential promoter-proximal THSS enrichment occurred at the *KCNJ10* locus, but differences in an intragenic distal THSS is evident between HD and WT cells during differentiation and coincide with gene expression changes at each stage (Figure 2-1B).

To examine the genome-wide relationship between gene expression and promoter accessibility during HD astrocyte differentiation, we first arranged differential promoter-proximal THSS enrichment at each stage according to the order of DE genes shown in Figure 2-1C (Figure 2-1D). Heatmaps of the distribution of ATAC-seq reads around TSSs in each sample reflect the differential THSS profiles observed for each stage (Figure 2-1E). Although changes in proximal

THSSs only correlate weakly to differential expression (Figure s2-3G, H), there are striking global differences in promoter-proximal accessibility between HD and WT cells across differentiation. For example, the majority of promoters in PSCs show slight enrichment of accessibility in HD cells, while in NPC and day 3 samples, promoter accessibility is depleted in HD cells compared to WT cells (Figure 2-1D, E).

Next, a motif analysis of differential proximal THSSs was performed. More motifs were identified for HD-depleted than HD-enriched proximal THSSs (Figure 2-1F, G; Table s2-5), which is consistent with the observed ratio of HD-enriched and WT-enriched proximal THSSs. TF motif enrichment occurred with corresponding changes in TF expression at many differential proximal THSSs across differentiation (Figure 2-1F, G). For many enriched motifs in HD-depleted proximal THSSs, changes in accessibility were evident prior to changes in TF expression (Figure 2-1G). Broadly speaking, this suggests that epigenetic alterations across HD astrocyte differentiation may precede changes in gene expression, though further studies are needed to confirm this.

Interestingly, two TF motifs showed inverse differential enrichment profiles between HD and WT cells in a stage specific manner, RFX4 and E2F1 (Figure 2-1F, G). In PSCs, the RFX4 motif is HD-enriched; however, NPC and day 3 samples show WT-enrichment of this motif, with down regulated expression at day 3. Furthermore, the RFX2 motif shows similar patterns of WT-enrichment in NPCs and at day 3 (Figure 2-1G). Interestingly, there is evidence that RFX4 is specifically expressed in the brain and is important to neurodevelopment (Sugiaman-Trapman et al., 2018; Zhang et al., 2006). Additionally, motif accessibility and expression of E2F1 is enriched in WT NPCs and in HD astrocytes. It is notable that E2F2, E2F7 and E2F8 motifs are also WT-enriched in NPCs (Figure 2-1G). The E2F TFs are well documented regulators of cell cycle progression and apoptosis (Crosby et al., 2004). Taken together, our analysis of promoter-proximal

THSSs revealed differential accessibility profiles across astrocyte differentiation along with stage-specific TF motif enrichment, which largely preceded corresponding changes in TF expression profiles. However, the majority of gene expression changes could not be explained by corresponding changes in promoter accessibility, suggesting other genomic regulatory elements, possibly enhancers, may contribute to altered transcription in HD cells.

2.5.4 Distal THSS profiles are widely altered during in vitro HD astrocyte differentiation

Genome-wide distribution of differential THSSs at each stage showed that most differences occurred distal to promoters (> 500 bp from any TSS): 96% in PSCs, 95% in NPCs, 93% in day 3, and 99% in astrocytes (Figure 2-2A, top panel). However, differential THSSs were more evenly distributed between intergenic and intragenic regions; 37% in PSCs, 45% in NPCs, 48% in day 3, and 42% in astrocytes were intragenic (Figure 2-2A, bottom panel). To gain insights into alterations in distal accessibility across HD astrocyte differentiation, hierarchical clustering was performed on distal THSSs that showed differential enrichment in at least one stage (Figure 2-2B). Scaled distal THSS reads for each sample are shown and reflect the differential THSS profiles observed at each stage of differentiation (Figure 2-2C). Distinct clusters of distal THSSs occur between HD and WT cells, especially in NPCs, at day 3 and in astrocytes (Figure 2-2B, C). While proximal THSSs showed differential enrichment at DE gene promoters in the PSC stage (Figure 2-1D), distal THSSs were strikingly similar in PSCs (Figure 2-2B, C). Alterations in distal accessibility largely appears in NPCs, when cells are still multipotent but have committed to a neural lineage. Given the body of research providing evidence for early dysregulation of a myriad of neurodevelopmental pathways in HD (Biagioli et al., 2015; HD iPSC Consortium, 2012; HD iPSC Consortium, 2017), this finding suggests that the dysregulation of distal chromatin accessibility observed in terminally differentiated HD astrocytes is established in the NPC stage.

Next, we performed motif enrichment analyses in differential distal THSSs across HD astrocyte differentiation (Figure 2-2D, E; Table s2-5). Several distal motifs show similar enrichment patterns to identified proximal motifs (Figure 2-1F, G). For example, distal WT-enrichment of RFX2, RFX3, and RFX4 motifs occurs in NPCs and astrocytes, and corresponded with DE of these TFs (Figure 2-2E). E2F1 and E2F2 motifs also show moderate, distal enrichment in WT NPCs, while the E2F7 motif is enriched in HD astrocytes (Figure 2-2D, E). Also of note is the enrichment of the FOSL2 motif at distal THSSs in HD NPCs and astrocytes, with corresponding expression changes (Figure 2-2D). While little is known about FOSL2 specifically, recent evidence suggests that targeting *FOSL2* overexpression inhibited proliferation and apoptosis in cancer cells (He et al., 2017; Ling et al., 2018). Overall, our motif analysis results indicate widespread alterations in distal TF occupancy across HD astrocyte differentiation.

2.5.5 Enhancer accessibility is altered during in vitro HD astrocyte differentiation

It has been established that intergenic and intragenic regulatory elements, such as enhancers, are bound by various TFs and directly regulate gene transcription (Shlyueva et al., 2014; Vermut et al., 2016). Additionally, enhancer activity is highly specific between cell types and across development (Shlyueva et al., 2014; Vermut et al., 2016). Given this, our finding that altered distal THSS profiles during HD astrocyte differentiation are established in the NPC stage (Figure 2-2B, C), after committing to a neural lineage, raises the question of whether these differential distal THSSs are occurring at neurodevelopmental and astrocyte-specific enhancers. In order to investigate this, we utilized published H3K27ac chromatin immunoprecipitation with sequencing (ChIP-seq) data from a study that identified putative active brain enhancers (PABEs) conserved in macaque and human brain tissues (Vermut et al., 2016). Since we used the MacaM reference genome for all our analyses, and that paper did not, we realigned their raw ChIP-seq data

to the MacaM reference genome and followed their protocol to call enhancers (Vermut et al., 2016; Zimin et al., 2014). We identified 33,285 PABEs in MacaM; of those 5,233 overlapped with 6,453 of our differential distal peaks (Figure 2-2F). All stages of differentiation showed similar ratios of differential intragenic/total enhancers as in all PABEs (Figure 2-2G); 53% in PSCs, 53% in NPCs, 55% in day 3, 62% in astrocytes, and 56% PABEs. Hierarchical clustering of differential THSS enrichment at PABEs showed distinct clusters of altered enhancer accessibility, beginning in NPCs and persisting through day 3 and astrocyte samples (Figure 2-2H), similar to what was observed for all differential distal THSSs (Figure 2-2B). Again, PSCs show the least differences between HD and WT accessible PABEs (Figure 2-2H), further supporting the idea that the dysregulated chromatin signatures observed in mature HD cells are established in the NPC stage.

2.5.6 De novo motif analysis at differentially accessible enhancers

Next, MEME-ChIP (Machanick et al., 2011) was used to perform *de novo* motif discovery analyses at differentially accessible PABEs at any stage and revealed significant enrichment of several TF motifs (Figure 2-3; Figure s2-4). Although we observed distal HD depletion of RFX2, RFX3 and RFX4 motifs across differentiation (Figure 2-2E), the RFX2 and RFX3 motifs were HD-enriched at some PABEs and WT-enriched at others in astrocytes (Figure 2-3A, B). Previous research has described tissue-specific expression profiles for the RFX TFs (Sugiaman-Trapman et al., 2018). RFX2 is most well-known for its role in regulating spermiogenesis, in which reduced expression induced apoptosis; it is also highly expressed in the brain (Sugiaman-Trapman et al., 2018; Wu et al., 2016), while RFX3 is highly expressed in fetal tissues and the brain (Sugiaman-Trapman et al., 2018). Consistent with these findings, we observed DE of *RFX3* (Figure 2-3D) at earlier stages of differentiation (NPCs and day 3), and DE of *RFX2* (Figure 2-3C) in day 3 and astrocyte samples. *RFX4* expression followed similar trends to that of *RFX2*, with reduced

expression in HD at day 3 and in astrocytes (Figure s2-4A). *RFX5*, which is reported to have broad expression profiles across a variety of tissues (Sugiaman-Trapman et al., 2018), was only DE in PSCs (Figure s2-4B). Overall, RFX motif accessibility is altered across HD astrocyte differentiation.

Additionally, the FOSL2 motif showed increasing enrichment at HD accessible PABEs (N=47; E-value=4.8e-54) from the NPC to astrocyte stages (Figure 2-3E, G), which is consistent with the observed distal enrichment of the FOSL2 motif in HD NPCs and astrocytes (Figure 2-2D). Differential expression of *FOSL2* corresponded with increased motif enrichment at HD-accessible PABEs (Figure 2-3H). FOSL2 is a member of the AP-1 TF complex, along with JUN, whose motif is also enriched in HD accessible PABEs across differentiation (N=204; E-value=4.8e-54) (Figure 2-3F, G). However, DE of *JUN* was only observed at day 3 and did not correspond with differential motif accessibility at PABEs (Figure 2-3F, I). In summary, we identified several candidate TF families, including RFX and FOSL2/JUN, that may aberrantly bind enhancers and contribute to HD pathogenesis during astrocyte differentiation; although follow-up studies are necessary to verify the specific TFs involved and to characterize TF binding dynamics across HD differentiation.

2.5.7 Gene Ontology (GO) analysis of DE genes across HD astrocyte differentiation

GO analyses, using the Kyoto encyclopedia of genes and genomes (KEGG) pathway gene sets, was performed to identify overrepresented pathways across astrocyte differentiation ($q < 0.05$; Liberzon et al., 2011). Consistent with our previous findings, PSCs had the most unique GO results (Figure 2-4A), while GO results from DE genes in NPC, day 3 and astrocyte samples were more similar to one another (Figure 2-4B, C, D; Figure s2-5A). Overrepresented KEGG pathways in these 3 stages of differentiation included *focal adhesion* (hsa04510), *ECM receptor interaction*

(hsa04512), *DNA replication* (hsa03030), *p53 signaling pathway* (hsa04115), *cell cycle* (hsa04110), *regulation of actin cytoskeleton* (hsa04810), *axon guidance* (hsa04360), *pyrimidine metabolism* (hsa00240), and *PPAR signaling pathway* (hsa03320), among others (Figure 2-4B, C, D; Figure s2-5A). All of these pathways have been reported to contribute to HD pathogenesis (Basu et al., 2013; Dickey et al., 2016; HD iPSC Consortium, 2012; HD iPSC Consortium, 2017; Hervás-Corpión et al., 2018; Labadorf et al., 2015; Molero et al., 2009, 2016; van Hagen et al., 2017), although to our knowledge, this is the first study to identify them in astrocytes specifically. Furthermore, 38.3% of the genes in the *Huntington's disease* (hsa05016) pathway were DE at one or more stage of HD astrocyte differentiation (Figure 2-4E, F; Figure s2-5B); however, the pathway is significantly overrepresented only in the PSC stage (Figure 2-4A).

Since promoter-proximal THSS enrichment did not correlate with gene expression profiles, we performed GO analysis on the nearest gene to all differential THSSs at each stage of differentiation and obtained similar results to that of the GO analysis of DE genes (Figure s2-5C-F; Table s2-6), including *ECM receptor interaction* (hsa04512), *cell cycle* (hsa04110), *apoptosis* (hsa04210), *focal adhesion* (hsa04510) and *axon guidance* (hsa04360). Additionally, various pathways involved in signaling and cancer were overrepresented in genes nearest to differential THSSs (Figure s2-5C-F). Interestingly, GO analysis based on differential THSSs in PSCs more closely resembled that of the other 3 stages (Figure s2-5C), in contrast to GO results for DE genes at the PSC stage (Figure 2-4A).

In order to specifically identify relevant trends in transcriptional dysregulation during HD astrocyte differentiation, we performed agnostic gene set enrichment analysis (GSEA) using the molecular signature database (MSigDB) at the NPC and astrocyte stages (Liberzon et al., 2011; Subramanian et al., 2005). Using this unsupervised approach, we found significant enrichment of

9 pathways between HD and WT cells (Figure 2-4G). Four cell cycle related pathways (*E2F target genes* (Hallmark; q < 0.02), *G2/M Checkpoint* (Hallmark; q < 0.02), *sister chromatid cohesion* (GO:BP; GO:0007062; q < 0.02), and *sister chromatid segregation* (GO:BP; GO:0000819; q < 0.02)) showed depletion in HD NPCs and enrichment in HD astrocytes compared to WT cells (Figure 2-4G). Notably, the inverse enrichment of E2F target gene expression in HD cells corresponds with the stage-specific trends in E2F motif enrichment we observed at both promoter-proximal and distal differential THSSs. Additionally, gene sets involved in *synapse assembly* (GO:BP; GO:0007416; q < 0.02) and *CNS development* (GO:BP; GO:0007417; q < 0.02) were enriched in HD NPCs and depleted in HD astrocytes compared to WT (Figure 2-4G). Pathways enriched in HD cells at both stages compared to WT included *apoptosis* (Hallmark; q < 0.02), *epithelial to mesenchymal transition* (EMT) (Hallmark; q < 0.02), and *inflammation* (Hallmark; q < 0.02) (Figure 2-4G). Given that these pathways have all been previously reported on, we decided to focus on pathways involved in the cell cycle, as they show both overrepresentation (*cell cycle* (hsa04110), *p53 signaling pathway* (hsa04115); Figure 2-4B, D) and the most significant enrichment (Figure 2-4G) in our DE genes.

2.5.8 Progressive up regulation of p53 signaling genes occurs during HD astrogenesis

mHTT binds to p53, resulting in dysregulation of its transcriptional activity at select genes and impacting cell cycle progression, apoptosis, and DNA damage repair (Bae et al., 2005; Lu et al., 2015; Steffan et al., 2000); however, the role of p53 signaling in HD is not well understood. Furthermore, p53 signaling and cell cycle pathways have not been examined in HD astrocytes. Results from the GO analyses of DE genes indicate that significant alterations in p53 signaling occur during HD astrocyte differentiation (Figure 2-4B, D). Over half the p53 signaling genes were found to be DE in at least one stage of astrocyte differentiation (52.7%; Figure s2-6A). Although

no changes in *p53* expression were observed, there is evidence that dysregulation of p53 in HD can be posttranslational, with upregulation at the protein level, but not in mRNA (Bae et al., 2005). Widespread transcriptional dysregulation of the p53 signaling pathway in HD samples (Figure 2-5A) included genes involved in cell cycle arrest (*Cyclin B1*; Figure 2-5A, B; Figure s2-6B), apoptosis (*TP53I3*; Figure 2-5B; Figure s2-6C), and DNA repair and damage prevention (*RRM2B*; Figure 2-5B; Figure s2-6D). Additionally, important upstream effectors of p53 signaling, $p14^{ARF}$ (also known as *CDKN2A*; Figure 2-5A, B; Figure s2-6E) and *MDM2* (Figure 2-5A, B; Figure s2-6F) were upregulated in HD NPCs, day 3, and astrocytes. A heatmap of the 38 DE genes in this pathway demonstrates the progressive up regulation of p53 signaling genes observed in HD NPC, day 3 and astrocyte samples (Figure 2-5B).

In support of this, GSEA using Hallmark gene sets showed significant enrichment of *p53 pathway* genes in HD astrocytes ($q < 0.02$; Figure 2-5C), but not HD NPCs ($q < 0.05$; Figure s2-6G), compared to WT cells. Additionally, cross sectional GSEA results indicated significant enrichment of *apoptosis pathway* gene expression in HD astrocytes ($q < 0.02$; Figure 2-5D), but not NPCs ($q < 0.18$; Figure s2-6H). Furthermore, agnostic longitudinal GSEA, comparing gene expression profiles between NPCs and astrocytes in HD and WT separately, reported a significant enrichment of the *apoptosis pathway* in HD astrocytes compared to HD NPCs ($q < 0.02$; Figure s2-6I), but not WT astrocytes ($q < 0.07$; Figure s2-6J). Taken together, our results suggest that the p53 signaling pathway is progressively dysregulated during HD astrocyte differentiation and impacts the expression of genes involved in the cell-cycle and apoptosis (Figure 2-5A-D).

2.5.9 Cellular pathways related to the cell cycle are altered during HD astrocyte differentiation

p53 upregulation has been associated with cell cycle deficits in HD models; however, the global downstream transcriptional consequences of p53 dysregulation in HD remain unknown (Lu

et al., 2015; Reynolds et al., 2018). GO analyses identified alterations of the *cell cycle pathway* in HD cells across differentiation (Figure 2-4B, D; Figure s2-5A). Further unsupervised GSEA revealed significant, temporally-dependent enrichment of multiple pathways involved in the cell cycle during astrocyte differentiation (Figure 2-4G). Cross sectional enrichment analyses demonstrated significant depletion in the expression of genes in *sister chromatid cohesion* (GO:BP; GO:0007062; $q < 0.02$; Figure 2-5E), *G2M Checkpoint* ($q < 0.02$; Figure s2-7A), and *sister chromatid segregation* (GO:BP; GO:0000819; $q < 0.02$; Figure s2-7C) pathways in HD NPCs compared to WT. In contrast, HD astrocytes displayed significant enrichment of these pathways compared to WT cells ($q < 0.02$; Figure 2-5F; Figure s2-7B, D). This inverse enrichment across differentiation is illustrated by DE of genes such as *Cyclin B1* (Figure s2-6B) and *CDK1* (Figure s2-7F), which regulate cell cycle checkpoints.

Altered expression was observed throughout the cell cycle pathway (Figure 2-5G), with nearly half the gene set (43.5%; Figure s2-7E) showing DE in at least one stage of astrocyte differentiation. While overall upregulation of cell cycle gene expression was observed between NPC and astrocyte stages in HD samples, as seen with *Cyclin D1* (Figure s2-7G), a small number of DE genes, such as *Cyclin D2* (Figure s2-7H), showed reduced expression compared to WT cells across differentiation. Figure 2-5G provides insight into the potential downstream cell cycle consequences of altered p53 signaling in HD. A heatmap showing DE of cell cycle pathway genes across all 4 stages of differentiation illustrates the inverse expression profiles of HD NPCs and HD astrocytes compared to respective WT cells (Figure 2-5H).

Taken together, our data suggest that dysregulation of p53 signaling and cell cycle pathways in HD occurs early in neural development and is progressive, with HD astrocytes showing increased expression of a majority of pathway genes compared to WT astrocytes (Figure

2-5B, H). As p53 signaling is responsible for the regulation of multiple pathways, these analyses cannot directly conclude that aberrant p53 signaling is responsible for the altered cell cycle transcription profiles observed. However, as many DE genes in the p53 pathway are also in the cell cycle pathway and both pathways show similar expression trends (Figure 2-5B, H), we continued with investigations of HD-mediated cell cycle aberrations during astrocyte differentiation

2.5.10 E2F dysregulation during HD astrocyte differentiation

Unsupervised GSEA analysis comparing HD and WT cells at the NPC or astrocyte stage consistently reported that *E2F target genes* were the most significantly enriched gene set between our samples ($q < 0.02$; Figure 2-6A, B). As with the other cell cycle pathways reported here, inverse enrichment showed significant depletion of E2F target gene expression in HD NPCs compared to WT NPCs (Figure 2-6A), while HD astrocytes showed significant enrichment compared to WT (Figure 2-6B). Furthermore, longitudinal GSEA of WT and HD samples demonstrated that in WT cells, E2F target gene expression was enriched at the NPC stage compared to the astrocytes stage ($q < 0.02$; Figure s2-8B). However, HD cells showed no significant enrichment of E2F target genes across differentiation ($q < 0.41$; Figure s2-8A), demonstrating aberrant regulation of these genes begins at the NPC stage and persists through HD astrocyte differentiation. Interestingly, findings from motif analyses of differential THSSs indicate E2F1, E2F2, E2F7, and E2F8 motifs show corresponding trends with GSEA findings; with WT-enrichment of E2F motifs observed in NPCs and HD-enrichment of the E2F1 motif observed in astrocytes (Figure 2-1F, G; Figure 2-2D, E). The stage specific, DE of *E2F1* (Figure 2-6C), which corresponded to promoter motif enrichment and expression profiles of target genes, prompted us to examine the expression of all E2F family members across astrocyte differentiation (Figure 2-

6C, D; Figure s2-8C-H). While only *E2F1* (Figure 2-6C) and *E2F7* (Figure 2-6D) demonstrated DE patterns corresponding to the GSEA results, most other E2F TFs were DE in at least one stage of astrocyte differentiation (Figure s2-8C-H).

To better characterize the interplay between altered chromatin accessibility and E2F target gene expression, we first examined promoter-proximal ATAC-seq enrichment at target genes that were DE in at least one stage (Figure s2-9A, B). Consistent with our genome-wide results, we found that differences in promoter accessibility (Figure s2-9A) did not correlate strongly with E2F target gene expression across HD differentiation (Figure s2-9B). Overall, it appears alterations in E2F target gene promoter accessibility lag behind changes in expression, suggesting other regulatory mechanisms may drive DE of E2F target genes in HD astrocytes.

This prompted us to examine the nearest differential THSSs (both proximal and distal) to E2F target gene promoters (Figure 2-6E). We observed a dramatic increase in accessibility in HD astrocytes, which more closely reflected expression profiles for corresponding E2F target genes (Figure 2-6F). Motif scanning of these nearest differential peaks associated with E2F target genes in NPCs and astrocytes revealed no specific motif enrichment in these peaks (Table s2-7). In fact, enrichment of any reported TF motif only occurred at a few THSSs in each stage, indicating multiple TFs may contribute to the observed E2F target gene dysregulation. At any stage, these nearest differential THSSs occurred within 250 kb of E2F promoters (Figure s2-9C). Surprisingly, the majority of NPC and day 3 differential THSSs occurred less than 50 kb from gene promoters, despite showing much less association with DE of target genes compared to astrocytes (Figure 2-6E, F; Figure s2-9C). Interestingly, almost 50% of E2F genes demonstrated HD enrichment at the nearest differential THSS at day 3, which coincided with upregulation of E2F genes in HD astrocytes, hinting at the possibility that these nearest differential THSSs in day 3 could be early

signatures of the upregulated expression observed in HD astrocytes. For example, E2F target gene *MCM3* was DE in NPC, day 3 and astrocyte samples (Figure 2-6G; Figure s2-9D). Although no differential promoter-proximal accessibility was observed at *MCM3*, corresponding differential THSS enrichment was observed both upstream of the promoter (around 15 kb and 30 kb), as well as up to 10 kb downstream of the transcription end site (Figure 2-6G). Notably, *MCM3* is a well-established marker of proliferation and one of six mini-chromosome maintenance (MCM) genes within the cell cycle pathway that are targeted by E2F TFs. All 6 E2F-regulated MCM genes (*MCM2, MCM3, MCM4, MCM5, MCM6, MCM7*) were DE in at least one stage of astrocyte differentiation (Figure 2-5G; Figure s2-9D-I).

In addition to cell cycle and apoptosis specific genes, E2F TFs also regulate several epigenetic factors that demonstrated DE during astrocyte differentiation. For example, the H3K27 methyltransferase, *EZH2* was downregulated in HD NPCs but overexpressed in HD astrocytes, following the expression pattern of cell cycle and apoptosis related genes across differentiation (Figure s2-9J). *DNMT1* (Figure s2-9K) and *UHRF1* (Figure s2-9L) also showed depleted expression in HD NPCs, but by day 3 of astrocyte differentiation onward, these regulators of DNA methylation were significantly overexpressed compared to WT cells. Additionally, *HMGN3* displayed DE in NPCs and astrocytes (Figure s2-9M); however, in contrast to the DE profiles of most other E2F target and cell cycle genes, *HMGN3* was significantly overexpressed in HD NPCs and depleted in HD astrocytes. HMGN3 binds to and remodels accessibility of chromatin to directly modulate transcription (West et al., 2004). Most interestingly, HMGN3 has been suggested to be important to normal astrocyte function (Ito et al., 2002; West et al., 2004). Thus, the observed *HMGN3* upregulation in HD NPCs and depletion in HD astrocytes (Figure s2-9M) is consistent with our previous findings for other astrocyte specific genes (*GFAP, APOE, LCN2*)

during HD differentiation (Figure s2-2C, D), and provides further evidence that premature initiation and incomplete terminal differentiation occurs during HD astrogenesis. In summary, we observed E2F dysregulation during HD astrocyte differentiation that not only impacted cell cycle progression and apoptosis pathways, but also caused aberrant expression of epigenetic and chromatin remodeling proteins, possibly resulting in incomplete astrocyte differentiation in HD cells.

2.6 Discussion

Here we analyzed transcription and chromatin accessibility dynamics during astrocyte differentiation in WT and transgenic HD NHP PSCs using an unbiased, integrative approach. We identified genome-wide alterations in gene expression across differentiation; however, persisting DE patterns were only evident from the NPC to astrocyte stage. PSCs displayed a more unique DE profile. DE genes identified by RNA-seq in our HD NHP cells showed considerable overlap with RNA-seq data sets from *in vitro* and *in vivo* human HD models (HD iPSC Consortium, 2017; Labadorf et al., 2015) and GO analysis of unique DE genes revealed overrepresentation of astrocyte-specific genes, providing further evidence that our HD NHP model recapitulates HD-associated phenotypes and may offer a reliable and translatable system for the investigation of the contribution and dysregulation of astrocytes in neurodegenerative diseases, as well as for the identification of potential effective therapeutic strategies.

Furthermore, we found extensive alterations in THSS enrichment and thus, TF occupancy during HD astrocyte differentiation. Overall, HD cells showed depletion of promoter-proximal accessibility; however, most differential THSSs were found at enhancers and other distal regions and were more strongly correlated to changes in gene expression than promoter accessibility. Differential distal THSSs displayed a distinct and progressive signature of dysregulation as HD

NPCs differentiate into astrocytes. Interestingly, the NPC and day 3 stages each had more than double the number of differential THSSs than either the PSC or astrocyte stage. We also identified several TFs that showed stage-specific motif enrichment in differential THSSs along with corresponding changes in expression, often in subsequent stages, such as RFX2, RFX4, and FOSL2. To our knowledge, these TFs have not been previously implicated in HD, thus warranting further investigation. Our data suggests that aberrant priming of epigenomic profiles occurs in HD NPCs, after committing to a neural lineage, and leads to compounding dysregulation of chromatin accessibility, TF binding and transcription during HD astrocyte development. As enhancer activity is known to be highly context specific and altered by disease pathology, it is important to point out that H3K27ac, which was used to define PABEs in the present study, has been shown to be altered in HD (Giralt et al., 2012; Lee et al., 2013a; McFarland et al., 2012; Sadri-Vakili et al., 2007; Shlyueva et al., 2014; Vermut et al., 2016). While our results offer the first evidence of altered chromatin accessibility across HD astrocyte differentiation, further investigations of chromatin signatures and TF binding at regulatory elements across differentiation and in various neural cell types are necessary to confirm our findings and to fully understand the interplay of epigenomic and transcriptome dysregulation in HD.

In summary, PSCs showed the most distinct differential expression and THSS profiles, while progressive aberrant trends were observed from HD NPCs to astrocytes. Based on the clustering patterns observed in both our RNA-seq and ATAC-seq data, we hypothesize that there are 2 distinct stages of HD-mediated dysregulation that occur during astrocyte development: one in PSCs, and the other begins in the NPC stage, after commitment to a neural lineage. This hypothesis is consistent with findings from a study profiling H3K27me3 and H3K4me3 dynamics during early HD differentiation, which demonstrated that HD ESCs and NPCs displayed distinct

chromatin signatures, suggesting differential HD-mediated dysregulation occurs across development (Biagioli et al., 2015). This study did not investigate any further stages of neural differentiation, but RNA-seq findings have widely reported alterations of pathways associated with neurodevelopment in HD (HD iPSC Consortium, 2012, 2017; Labadorf et al., 2015; Molero et al., 2009, 2016; Seredenina et al., 2012), indicating that early alterations may persist across development. It is possible that this dichotomy between PSCs, and NPCs and their derivatives results from the well documented impact of mHTT on neurodevelopment specifically (White et al., 1997; Wiatr et al., 2018; Yu et al., 2017); as PSCs transition to NPCs and commit to a neural lineage, neurodevelopmental programs are initiated and in the presence of mHTT, are progressively dysregulated.

Changes in gene expression determined by RNA-seq revealed alterations of pathways previously identified in HD, but not specifically in astrocytes, and implicate dysregulation of multiple cell cycle pathways, including *p53 signaling*, during HD astrogenesis. p53 acts as a TF to regulate many cellular processes and has been implicated in cell cycle dysregulation in HD (Lu et al., 2015; Reynolds et al., 2018). We observed a significant, progressive upregulation of p53 signaling genes in HD between the NPC and astrocyte stage that coincided with enrichment in cell cycle and apoptosis pathways. Notably, upstream regulators of p53 signaling, *CDKN2A* and *MDM2,* were upregulated in HD day 3 and astrocytes. In addition, the p53 pathway gene *RRM2B,* which plays a role in DNA synthesis and repair (Pontarin et al., 2012), was upregulated in HD cells at all stages of astrocyte differentiation. Interestingly, a genome-wide association study (GWAS) identified the minor allele of *RRM2B* as a genetic modifier associated with accelerated onset in HD patients (Genetic Modifiers of Huntington's Disease (GeM-HD) Consortium, 2015). Given this, we suggest *RRM2B* as a potential candidate for follow-up studies. Based on our

findings, we hypothesize that observed alterations in p53 signaling contribute, potentially via multiple mechanisms, to the progressive dysregulation of the cell cycle and HD pathogenesis during astrocyte differentiation.

Stage specific alterations in the cell cycle have been identified in mouse and human models of HD (Basu et al., 2013; Boudreau et al., 2009; Labadorf et al., 2015; Lopes et al., 2016; Lu et al., 2015; Molero et al., 2009; Pelegri et al., 2008; Reynolds et al., 2018). For example, mHTT has been shown to disrupt spindle orientation and thus, mitotic division (Lopes et al., 2016). Further molecular evidence from 293 cells expressing mHTT has demonstrated that the appearance of cell cycle arrest and mitotic defects coincides with an observed increase in p53 expression (Lu et al., 2015). Consistent with this, we observed that changes in cell cycle gene expression followed the same trends as those observed in the p53 pathway, with depletion in HD NPCs and enrichment in HD astrocytes. We also identified 4 specialized cell cycle pathways that showed substantial, significant differential enrichment between HD and WT in NPCs and astrocytes: *E2F target genes, G2/M checkpoint, sister chromatid cohesion, and sister chromatid segregation*.

Of particular interest was the E2F target gene set. E2F TFs are most widely known for their role in cell cycle regulation; with E2F1, E2F2 and E2F3 serving as activators, while E2F7 and E2F8 are repressors (Swiss et al., 2010). E2F1 is a TF that regulates the G1/S checkpoint of the cell cycle and has been shown to regulate cell death through a p53-dependent manner (Iaquinta et al., 2007; Johnson et al., 2006; Ting et al., 2014). Recent evidence suggests that E2F1 is also capable of initiating apoptosis by directly inducing the expression of *CDKN2A*, which forms a complex with MDM2 and p53 to initiate cell cycle arrest and apoptosis (Bates et al., 1998; Moroni et al., 2001). Additionally, aberrant expression of E2F TFs can cause cell cycle re-entry and apoptosis (Dirks et al., 1998; Wu et al., 2015). Consistent with these findings, we observed DE of

most E2F TFs and upregulation of target gene *CDKN2A*, along with increased p53 signaling, cell cycle, and apoptosis pathway activation in our HD astrocytes, suggesting a similar mechanism is occurring in our HD cells during differentiation. Although the roles of individual E2F TFs in p53 signaling and cell cycle dysregulation in HD are not well characterized, E2F1 dysregulation has also been implicated in neuronal death in neurodegenerative diseases such as Alzheimer's disease (Jordan-Sciutto et al., 2002) and Parkinson's disease (Hoglinger et al., 2007; Jordan-Sciutto et al., 2003), and was reported to be upregulated in human HD brains (Pelegri et al., 2008). Taken together, our results suggest that aberrant cell cycle re-entry during HD astrocyte differentiation induces apoptosis via an E2F1-p53 dependent mechanism. Future molecular studies are necessary to characterize these events in HD cells.

The present study showed global alterations in E2F motif enrichment at differential THSSs across astrocyte differentiation that coincided with E2F target gene expression profiles. We found that the nearest differential THSS to E2F target promoters more strongly associated with gene expression than promoter accessibility. Interestingly, DE profiles of E2F target genes preceded changes in nearby, differential THSS enrichment, suggesting other regulatory mechanisms might contribute to E2F dysregulation in HD astrocytes. We also provided evidence that the altered expression profiles of E2F target genes during HD astrocyte differentiation may be regulated by differential binding of multiple different TFs at distal regulatory regions. However, future studies are necessary to shed light onto the regulatory interactions underlying the DE of E2F target genes.

Interestingly, among the E2F target genes that were found to be DE during differentiation were several epigenetic factors, including regulators of histone and DNA methylation (*EZH2, DNMT1, UHRF1*) and chromatin remodelers (*HMGN3*). All three methyltransferases showed depletion in HD NPCs and upregulation in HD astrocytes. EZH2 is part of the polycomb repressive

complex 2 (PRC2), which is critical for ESC differentiation into NPCs (Jepsen et al., 2007; Orlando, 2003; Seong et al., 2009). Although HTT is known to directly interact with EZH2, the influence of mHTT on EZH2-mediated H3K27me3 is not well defined (Biagioli et al., 2015; Seong et al., 2009). Additionally, global alterations in DNA methylation in HD have been reported and were interestingly found to be differential across brain regions (Horvath et al., 2016; Ng et al., 2013), highlighting the need for extensive characterization of the HD epigenome both across neural cell types and throughout neurodevelopment. Both *DNMT1* and *UHRF1* activity are associated with the cell cycle; DNMT1-mediated DNA methylation is bound by UHRF1, which also binds histone H3 lysine 9 trimethylation (H3K9me3) to orchestrate higher, multi-layer epigenetic regulation of transcription. Of note, H3K9me3 has been reported to be enriched in HD human and mice brains (Ryu et al., 2006; Lee et al., 2013). Further, it has been demonstrated that inhibiting DNMTs provides a neuroprotective effect in HD mice (Pan et al., 2016). Given their association with less accessible chromatin and our findings that HD promoters showed depleted accessibility, while distal accessibility was largely HD enriched across differentiation, it would be interesting to more closely examine the consequences of altered *DNMT1* and *UHRF1* expression on DNA methylation and H3K9me3 dynamics during HD astrocyte differentiation.

Finally, in contrast to DE profiles for other E2F target genes, *HMGN3* expression was significantly increased in HD NPCs, but was significantly depleted in HD astrocytes. This chromatin remodeling enzyme has been shown to control astrocyte differentiation from NPCs (Nagao et al., 2014) and is important to astrocyte function (Ito et al., 2002; West et al., 2004). The present study provided evidence that multiple astrocyte specific genes, such as *HMGN3*, *GFAP*, *APOE*, and *LCN2,* are significantly upregulated early in HD differentiation (NPC and day 3 stages) both compared to corresponding WT samples and to expression levels observed in HD astrocytes.

In support of previously reported evidence from heterogenous neural populations, this finding suggests that our HD cell prematurely upregulated astrocyte differentiation pathways, but never fully develop mature astrocyte transcription profiles (HD iPSC Consortium, 2017), causing early and progressive impairments that not only impact astrocytes themselves, but may also leave their associated neuron population more vulnerable to environmental stressors and neurotoxicity (Shin et al., 2005). Notably, our HD astrocytes took on a flattened appearance in contrast to the stellate morphology of our WT astrocytes.

Dysregulation of E2F TFs and cell cycle pathways provides further support for this, as E2F TFs are also known to regulate the switch between proliferating NPCs and differentiation expression profiles that require exit from the cell cycle for commitment to a specific neural lineage, such as glial cells (Magri et al., 2014; Nygard et al., 2003; Swiss et al., 2010). In fact, E2F4 and E2F5 regulate differentiation of NPCs into specific neural lineages (Swiss et al., 2010), along with *E2F1* downregulation (Magri et al., 2014; Nygard et al., 2003). There is also evidence that each E2F TF regulates distinct gene sets in a stage-specific manner across neurodevelopment (Dirks et al., 1998; Swiss et al., 2010; Wu et al., 2015). Consistent with this, our WT NPCs showed enrichment of cell cycle pathways, specifically E2F target genes. Once induced to differentiate into astrocytes, WT cells show dramatic down regulation of cell cycle and E2F target genes by day 3, which persists in WT astrocytes. HD NPCs displayed downregulation of cell cycle and E2F target genes compared to WT cells. Upon differentiation into astrocytes, E2F TF expression is upregulated in HD cells with increased cell cycle gene expression and aberrant cell cycle re-entry that coincides with enrichment of p53 signaling and apoptosis pathways. Interestingly, HD NPC cultures exhibited slowed proliferation, with WT cultures requiring passage twice as often as HD cultures. This demonstrates our HD NHP cells were unable to properly regulate E2F TFs and

switch to the differentiation transcriptome required for the generation of mature astrocytes. This incomplete activation of astrocyte markers in HD cells may be a downstream consequence of early E2F dysregulation. Future studies should focus on identifying the initial mechanisms of E2F dysregulation and the direct downstream transcriptional consequences of aberrant E2F activity during HD astrocyte differentiation. Taken together, these results indicate that E2F TF dysregulation during astrocyte differentiation has consequences that extend beyond cell cycle regulation.

In summary, we observed E2F dysregulation that not only impacted cell cycle progression and apoptosis pathways, but also altered the expression of chromatin remodeling and epigenetic proteins, possibly resulting in suboptimal astrocyte differentiation in HD cells.

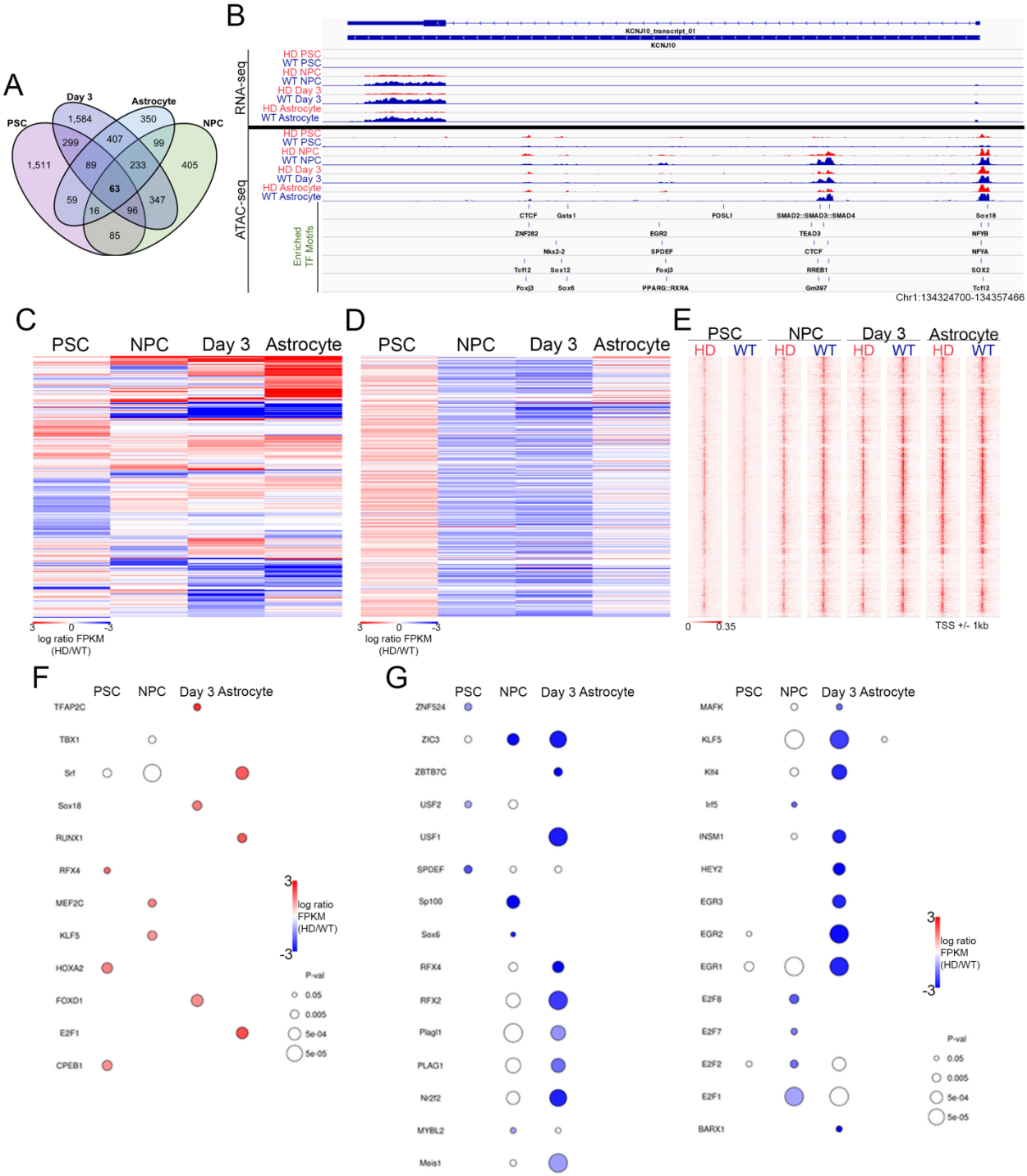
A
Day 3
Astrocyte
PSC
NPC
1,584
350
299
407
99
1,511
89
233
405
63
59
347
16
96
85
B
RNA-seq
ATAC-seq
HD PSC
WT PSC
HD NPC
WT NPC
HD Day 3
WT Day 3
HD Astrocyte
WT Astrocyte
KCNJ10_transcript_01
KCNJ10
Enriched TF Motifs
CTCF
Gata1
FOSL1
SMAD2::SMAD3::SMAD4
Sox18
ZNF282
EGR2
TEAD3
NFYB
Nkx2-2
SPDEF
CTCF
NFYA
Tcf12
Sox12
RREB1
SOX2
Foxj3
Sox6
PPARG::RXRA
Gm397
Tcf12
Chr1:134324700-134357466
C
PSC
NPC
Day 3
Astrocyte
3
0
-3
log ratio FPKM (HD/WT)
D
PSC
NPC
Day 3
Astrocyte
3
0
-3
log ratio FPKM (HD/WT)
E
PSC
NPC
Day 3
Astrocyte
HD
WT
0
0.35
TSS +/- 1kb
F
PSC
NPC
Day 3 Astrocyte
TFAP2C
TBX1
Srf
Sox18
RUNX1
RFX4
MEF2C
KLF5
HOXA2
FOXD1
E2F1
CPEB1
3
log ratio FPKM (HD/WT)
-3
P-val
0.05
0.005
5e-04
5e-05
G
PSC
NPC
Day 3 Astrocyte
ZNF524
ZIC3
ZBTB7C
USF2
USF1
SPDEF
Sp100
Sox6
RFX4
RFX2
Plagl1
PLAG1
Nr2f2
MYBL2
Meis1
PSC
NPC
Day 3 Astrocyte
MAFK
KLF5
Klf4
Irf5
INSM1
HEY2
EGR3
EGR2
EGR1
E2F8
E2F7
E2F2
E2F1
BARX1
3
log ratio FPKM (HD/WT)
-3
P-val
0.05
0.005
5e-04
5e-05

Figure 2-1. Characterization of promoter-proximal THSSs at differentially expressed genes during HD astrocyte differentiation. (A) Venn diagram showing overlap of genes differentially expressed between HD and WT cells at each stage of astrocyte differentiation. (B) Track view of RNA-seq and THSSs, as well as identified motifs within ATAC-seq peaks across the *KCNJ10* gene. HD samples are shown in red and WT samples are shown in blue. (C) Heatmap depicting 5,643 genes found DE at any stage of differentiation. Red indicates increased expression in HD cells and blue indicates reduced expression in HD cells. Each row corresponds to the same gene. (D) Heatmap depicting differential THSS enrichment at DE gene promoters. The red color represents HD enrichment and the blue color indicates HD depletion. Genes arranged according to gene order in panel C. (E) Distributions of ATAC-seq peaks around the promoter (+/- 2kb TSS) in HD and WT cells at each timepoint across differentiation. (F-G) TF motifs identified at differential promoter-proximal ATAC-seq peaks in HD (F) and WT (G) cells. Only TF motifs with significant enrichment at least at one stage were included ($p < 0.05$).

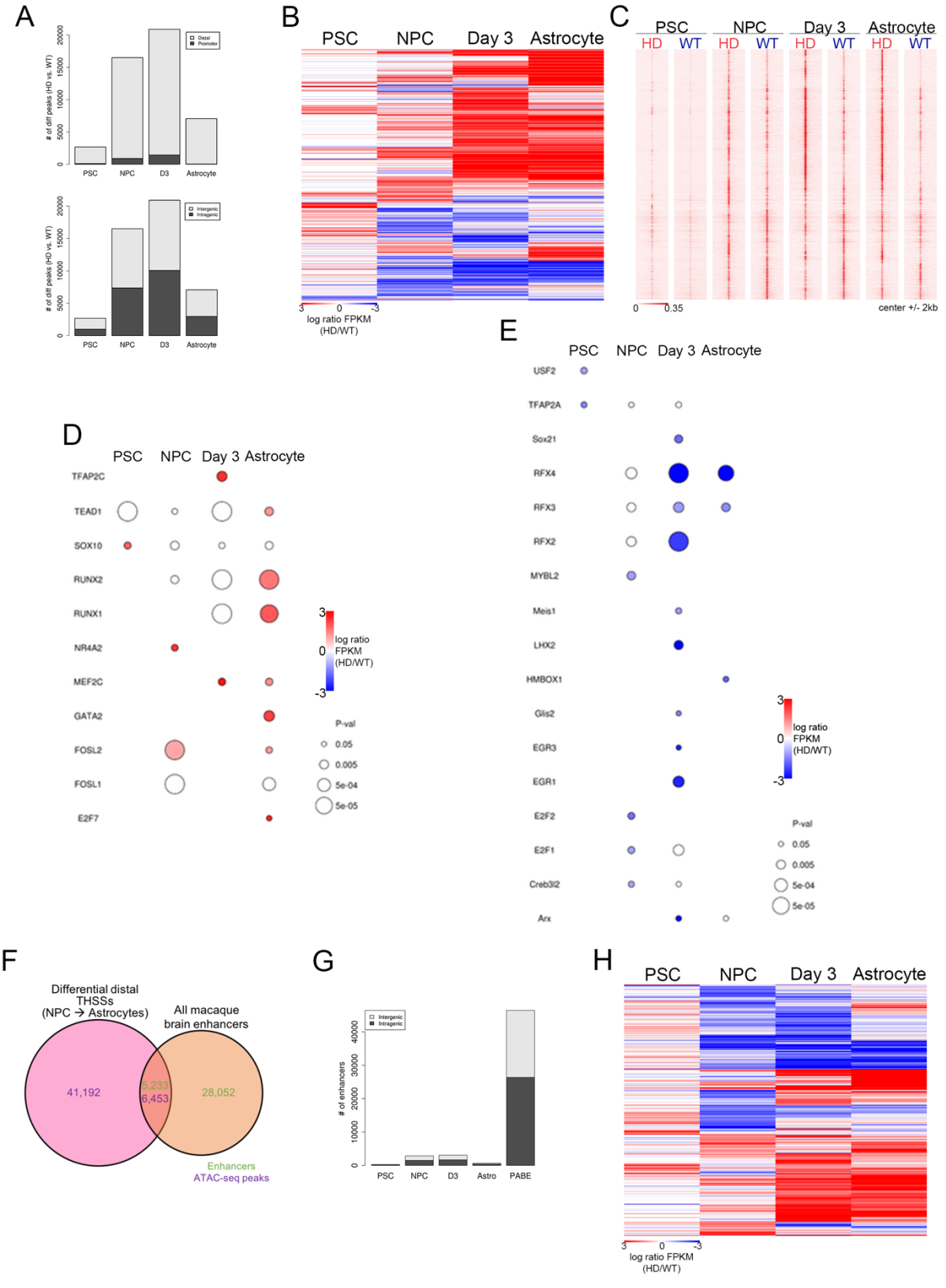
A
# of diff peaks (HD vs. WT)
Distal
Promoter
PSC
NPC
D3
Astrocyte
Intergenic
Intragenic
B
PSC
NPC
Day 3
Astrocyte
log ratio FPKM (HD/WT)
C
PSC
NPC
Day 3
Astrocyte
HD
WT
0
0.35
center +/- 2kb
D
TFAP2C
TEAD1
SOX10
RUNX2
RUNX1
NR4A2
MEF2C
GATA2
FOSL2
FOSL1
E2F7
log ratio FPKM (HD/WT)
P-val
0.05
0.005
5e-04
5e-05
E
USF2
TFAP2A
Sox21
RFX4
RFX3
RFX2
MYBL2
Meis1
LHX2
HMBOX1
Gli2
EGR3
EGR1
E2F2
E2F1
Creb3l2
Arx
F
Differential distal THSSs (NPC → Astrocytes)
All macaque brain enhancers
41,192
5,233
6,453
28,052
Enhancers
ATAC-seq peaks
G
# of enhancers
PSC
NPC
D3
Astro
PABE
H
PSC
NPC
Day 3
Astrocyte
log ratio FPKM (HD/WT)

Figure 2-2. Characterization of differential distal THSSs during HD astrocyte differentiation. (A) Genome-wide distribution of differential THSSs between HD and WT cells across differentiation identified from ATAC-seq non-nucleosomal fragments. Both distal vs. proximal (top) and intergenic vs. intragenic distributions (bottom) are reported. THSSs located +/- 500 bp from a TSS are considered proximal. (B) Heatmap depicting differential enrichment of distal ATAC-seq THSSs at each stage of differentiation. The red color represents HD enrichment and the blue color indicates HD depletion. (C) Genome-wide distributions of distal ATAC-seq THSSs from HD and WT cells at each timepoint. (D-E) TF motifs identified from distal ATAC-seq peaks that were enriched in HD (D) and WT (E) cells. Only TF motifs with significant enrichment at least at one stage were included ($p < 0.05$). (F) Venn diagram showing overlap of differential distal ATAC-seq THSSs and Putative Active Brain Enhancers (PABEs) previously published (Vermut et al., 2016). Purple denotes ATAC-seq peaks and green indicates macaque brain enhancers. (G) Genome-wide distribution of differential enhancer THSSs across HD astrocyte differentiation. (H) Heatmap depicting differential enrichment of distal ATAC-seq THSSs at PABEs during differentiation. The red color represents HD enrichment and the blue color indicates HD depletion.

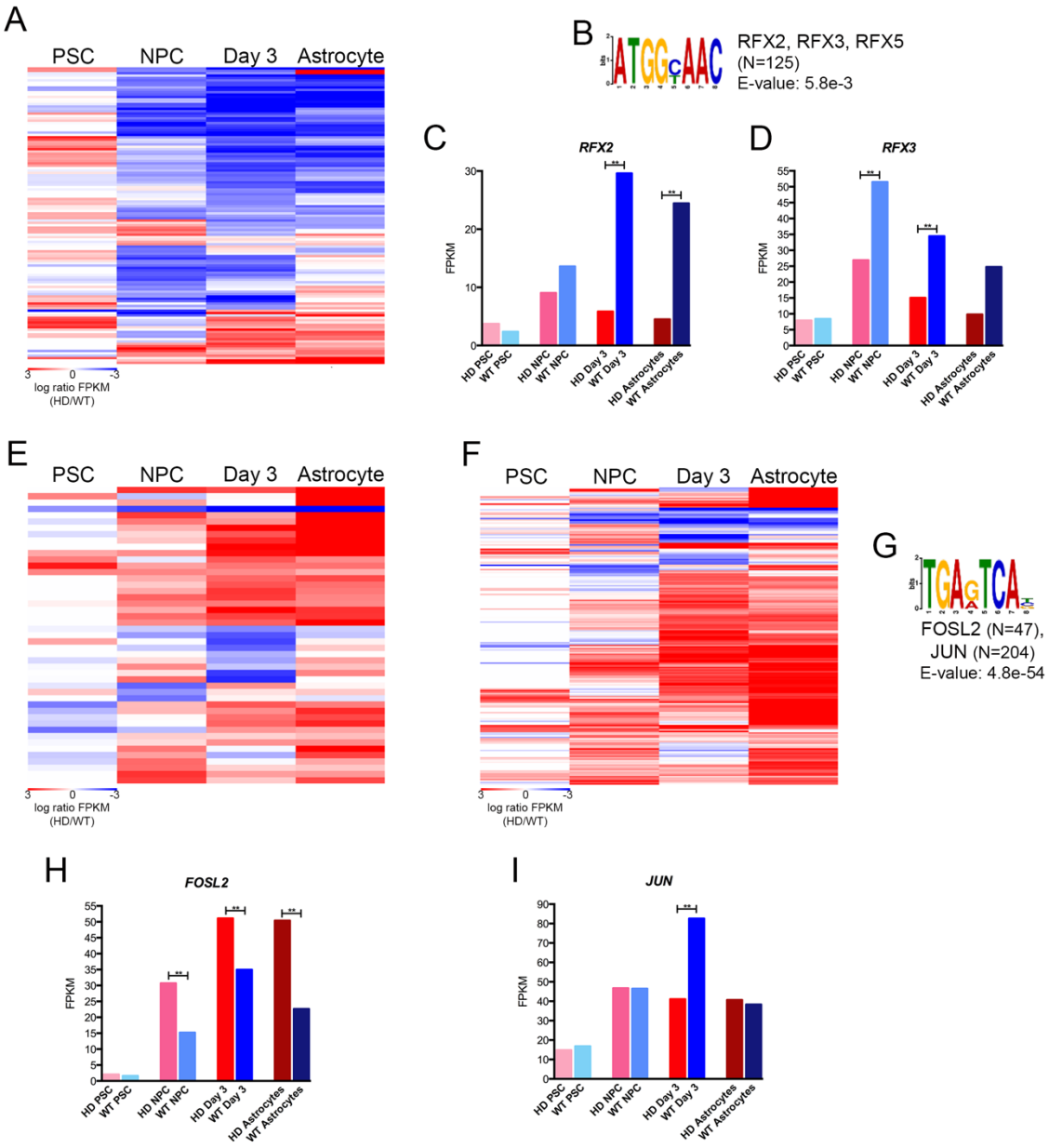
A
PSC
NPC
Day 3
Astrocyte
3
0
-3
log ratio FPKM
(HD/WT)
B
RFX2, RFX3, RFX5
(N=125)
E-value: 5.8e-3
C
RFX2
FPKM
HD PSC
WT PSC
HD NPC
WT NPC
HD Day 3
WT Day 3
HD Astrocytes
WT Astrocytes
D
RFX3
E
F
G
FOSL2 (N=47),
JUN (N=204)
E-value: 4.8e-54
H
FOSL2
I
JUN

Figure 2-3. Differences in TF binding site accessibility occur in putative enhancers at every stage of differentiation in HD cells. (A) Heatmap depicting differential ATAC-seq signal in HD and WT cells at macaque brain enhancers containing the RFX2, RFX3, and RFX5 binding sequences (N=125). The red color represents enrichment and the blue color indicates depletion of THSSs containing this RFX motif in HD cells. (B) RFX2, RFX3, and RFX5 motif found by *de novo* motif analysis at enhancers showing differential ATAC-seq. (C-D) Bar graphs generated from RNA-seq data depicting differential expression of *RFX2* (C) and *RFX3* (D) occurs during the NPC, day 3, and astrocyte stages of HD astrocyte differentiation. (E-F) Heatmap depicting differential THSSs at macaque brain enhancers containing FOSL2 (N=47; panel E) and JUN (N=204; panel F) binding sequences. Red represents HD enrichment and blue represents HD depletion. (G) The motif for FOSL2 and JUN found at enhancers showing differential ATAC-seq enrichment. (H-I) Bar graphs generated from RNA-seq for *FOSL2* (H) and *JUN* (I) expression across differentiation. All RNA-seq experiments were performed in three biological replicates and average FPKM for each sample was plotted (**$p < 0.001$, differential expression analysis).

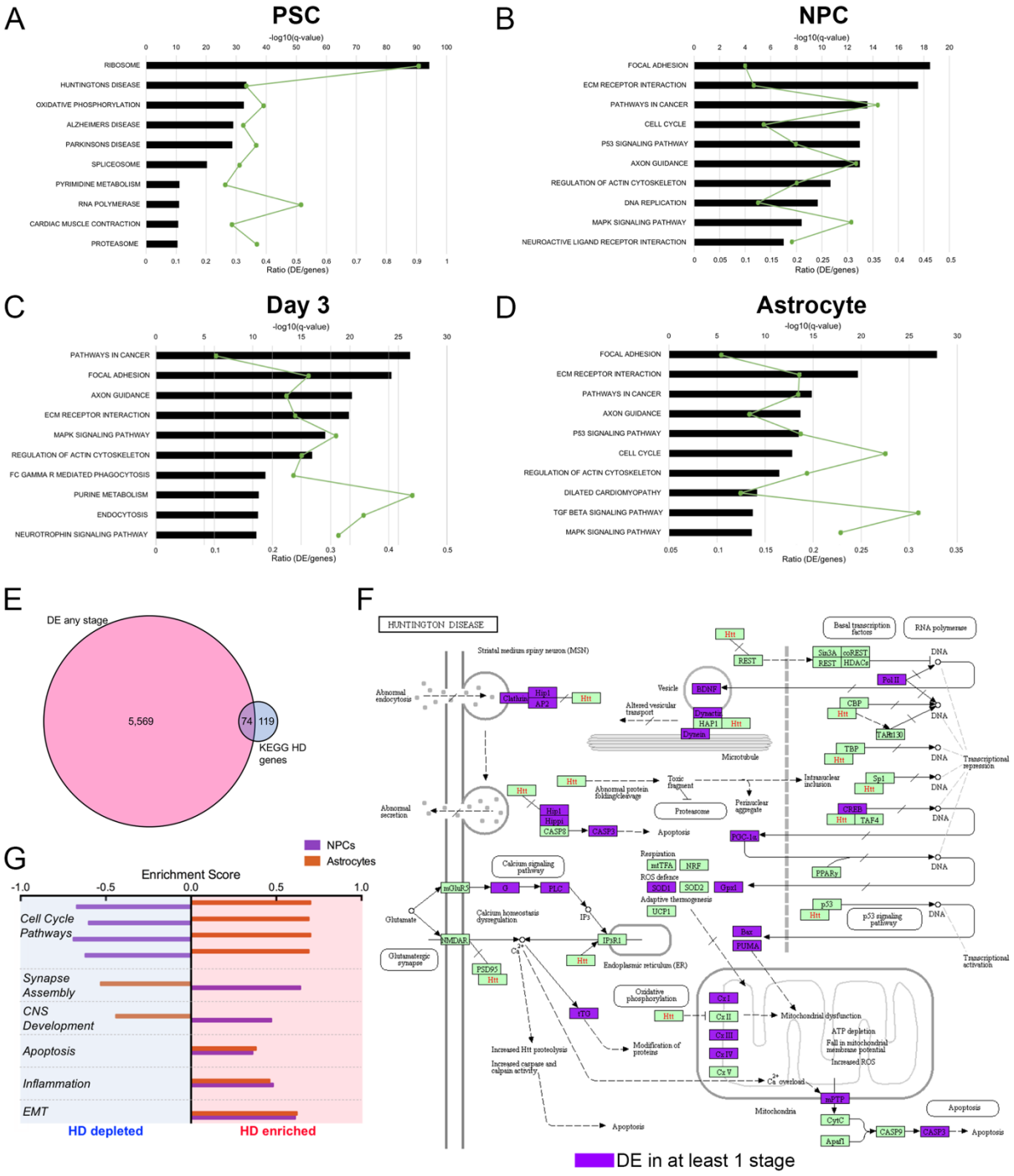
A
PSC
-log10(q-value)
RIBOSOME
HUNTINGTONS DISEASE
OXIDATIVE PHOSPHORYLATION
ALZHEIMERS DISEASE
PARKINSONS DISEASE
SPLICEOSOME
PYRIMIDINE METABOLISM
RNA POLYMERASE
CARDIAC MUSCLE CONTRACTION
PROTEASOME
Ratio (DE/genes)
B
NPC
-log10(q-value)
FOCAL ADHESION
ECM RECEPTOR INTERACTION
PATHWAYS IN CANCER
CELL CYCLE
P53 SIGNALING PATHWAY
AXON GUIDANCE
REGULATION OF ACTIN CYTOSKELETON
DNA REPLICATION
MAPK SIGNALING PATHWAY
NEUROACTIVE LIGAND RECEPTOR INTERACTION
Ratio (DE/genes)
C
Day 3
-log10(q-value)
PATHWAYS IN CANCER
FOCAL ADHESION
AXON GUIDANCE
ECM RECEPTOR INTERACTION
MAPK SIGNALING PATHWAY
REGULATION OF ACTIN CYTOSKELETON
FC GAMMA R MEDIATED PHAGOCYTOSIS
PURINE METABOLISM
ENDOCYTOSIS
NEUROTROPHIN SIGNALING PATHWAY
Ratio (DE/genes)
D
Astrocyte
-log10(q-value)
FOCAL ADHESION
ECM RECEPTOR INTERACTION
PATHWAYS IN CANCER
AXON GUIDANCE
P53 SIGNALING PATHWAY
CELL CYCLE
REGULATION OF ACTIN CYTOSKELETON
DILATED CARDIOMYOPATHY
TGF BETA SIGNALING PATHWAY
MAPK SIGNALING PATHWAY
Ratio (DE/genes)
E
DE any stage
5,569
74
119
KEGG HD genes
F
HUNTINGTON DISEASE
Striatal medium spiny neuron (MSN)
Basal transcription factors
RNA polymerase
Abnormal endocytosis
Vesicle
Altered vesicular transport
Microtubule
Abnormal protein folding/cleavage
Toxic fragment
Intranuclear inclusion
Perinuclear aggregate
Proteasome
Abnormal secretion
Apoptosis
Transcriptional repression
Transcriptional activation
Calcium signaling pathway
Respiration
ROS defence
Adaptive thermogenesis
Glutamate
Calcium homeostasis dysregulation
Glutamatergic synapse
Endoplasmic reticulum (ER)
Oxidative phosphorylation
Mitochondrial dysfunction
ATP depletion
Fall in mitochondrial membrane potential
Increased ROS
Increased Htt proteolysis
Increased caspase and calpain activity
Modification of proteins
Mitochondria
p53 signaling pathway
DE in at least 1 stage
G
NPCs
Astrocytes
Enrichment Score
Cell Cycle Pathways
Synapse Assembly
CNS Development
Apoptosis
Inflammation
EMT
HD depleted
HD enriched

Figure 2-4. RNA-seq identifies multiple pathways that are altered across HD astrocyte differentiation. (A-D) Top ten KEGG pathways reported from GO analyses of DE genes at the PSC (A), NPC (B), day 3 (C) and astrocyte (D) stages. Pathways are ranked by -log10 (q-value), determined by Benjamini-Hochberg procedures, with threshold set to $q < 0.05$. Line graphs show the ratio of DE genes in each KEGG pathway. (E) DE genes at any stage show overlap with the KEGG Huntington's Disease pathway. (F) Huntington's disease pathway showing DE genes (in purple) in HD cells at any stage of astrocyte differentiation. (G) Bar plot depicting the enrichment scores of the top 9 most enriched gene sets, which comprise 6 functional categories. Negative enrichment scores (left; blue) reflect HD depleted gene sets, and positive enrichment scores (right; red) represent HD enriched gene sets. NPC GSEA results are shown in purple and astrocyte GSEA results are shown in orange.

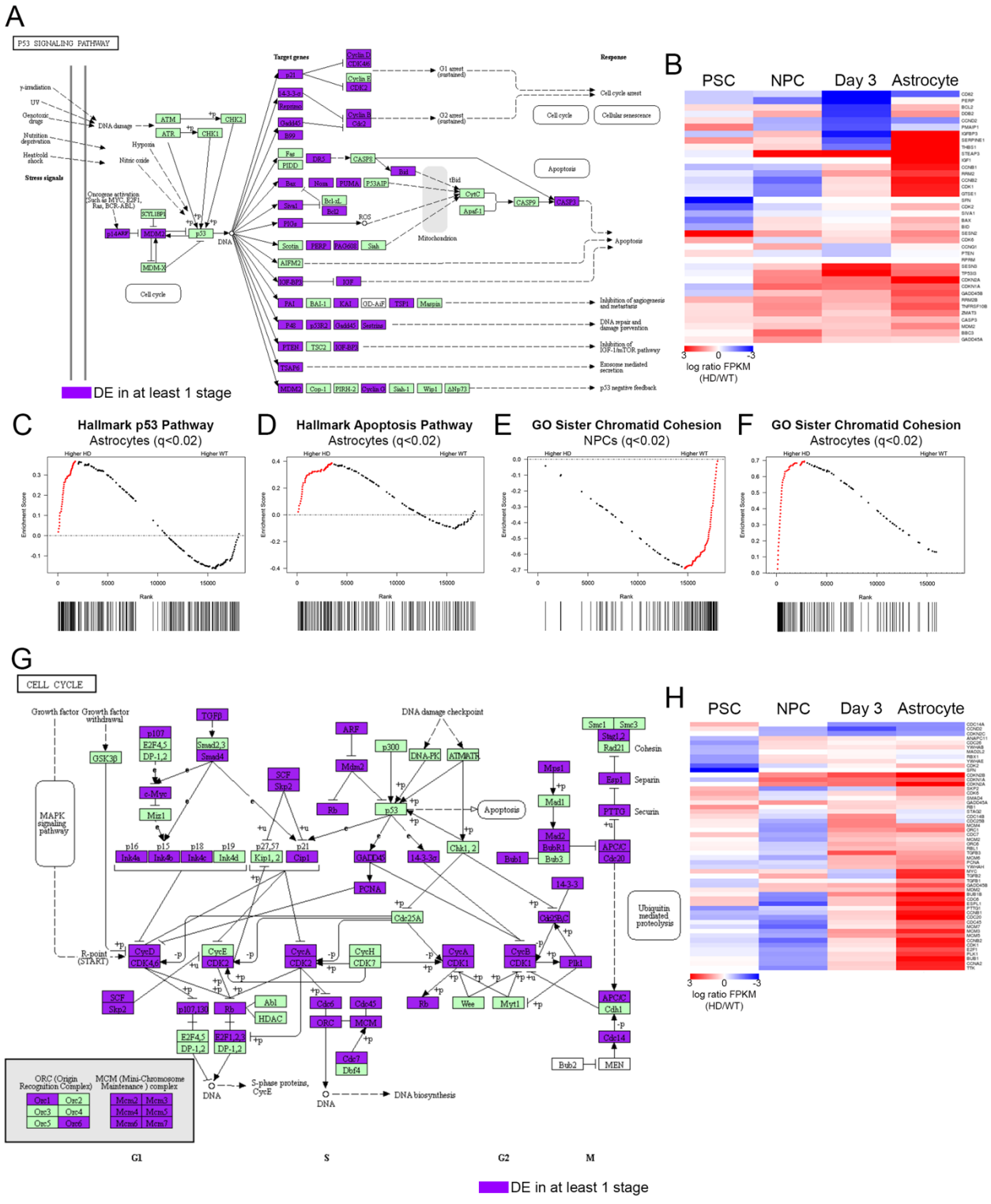
A
P53 SIGNALING PATHWAY
DE in at least 1 stage
B
PSC
NPC
Day 3
Astrocyte
log ratio FPKM (HD/WT)
C
Hallmark p53 Pathway
Astrocytes (q<0.02)
D
Hallmark Apoptosis Pathway
Astrocytes (q<0.02)
E
GO Sister Chromatid Cohesion
NPCs (q<0.02)
F
GO Sister Chromatid Cohesion
Astrocytes (q<0.02)
Higher HD
Higher WT
Enrichment Score
Rank
G
CELL CYCLE
MAPK signaling pathway
Ubiquitin mediated proteolysis
ORC (Origin Recognition Complex)
MCM (Mini-Chromosome Maintenance) complex
S-phase proteins, CycE
DNA biosynthesis
G1
S
G2
M
DE in at least 1 stage
H
PSC
NPC
Day 3
Astrocyte
log ratio FPKM (HD/WT)

Figure 2-5. RNA-seq revealed dysregulation of p53 signaling and cell cycle pathways across HD differentiation. (A) p53 signaling pathway diagram showing DE genes (in purple) in HD cells at any stage of astrocyte differentiation. (B) Heatmap depicting 38 DE genes in the p53 signaling pathway at each stage of differentiation. Red indicates increased expression in HD cells and blue indicates reduced expression in HD cells. Each row corresponds to the same gene and gene names are displayed to the right of the plot. (C-F) Cross sectional GSEA enrichment plots. For GSEA plots, the black lines indicate the position of pathway genes in the expression data rank-sorted between HD and WT samples. Red dots indicate leading edge genes. q-values are FDR corrected p-values with alpha=0.02, or the equivalent. (G) Diagram of the KEGG cell cycle pathway showing genes DE (purple) in HD cells. (H) Heatmap depicting 54 DE cell cycle genes in the p53 signaling pathway at each stage of differentiation. Red indicates increased expression in HD cells and blue indicates reduced expression in HD cells. Each row corresponds to the same gene and gene names are displayed to the right of the plot.

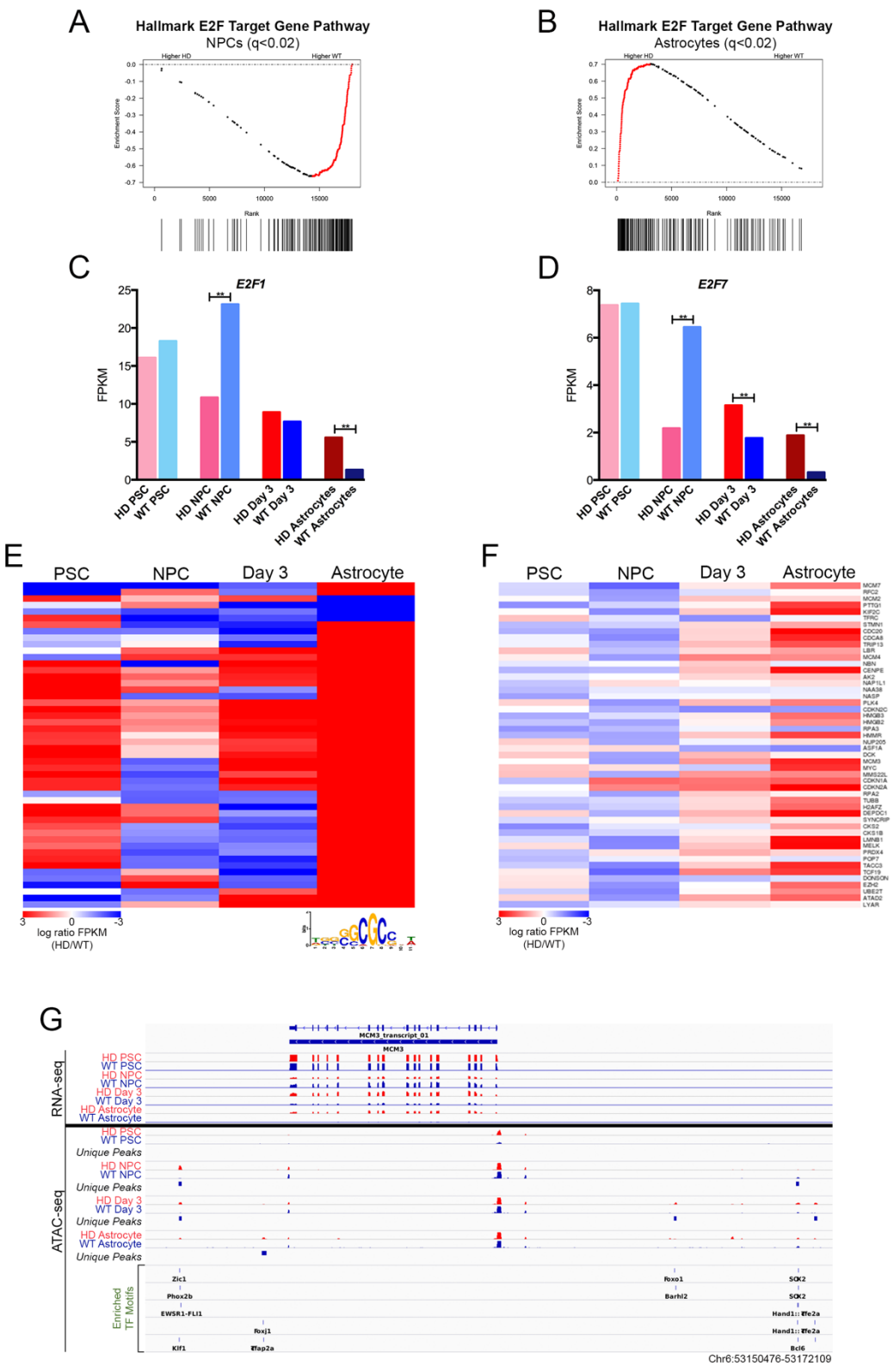
A
Hallmark E2F Target Gene Pathway
NPCs (q<0.02)
Higher HD
Higher WT
Enrichment Score
Rank
B
Hallmark E2F Target Gene Pathway
Astrocytes (q<0.02)
Higher HD
Higher WT
Enrichment Score
Rank
C
E2F1
FPKM
HD PSC
WT PSC
HD NPC
WT NPC
HD Day 3
WT Day 3
HD Astrocytes
WT Astrocytes
D
E2F7
FPKM
HD PSC
WT PSC
HD NPC
WT NPC
HD Day 3
WT Day 3
HD Astrocytes
WT Astrocytes
E
PSC
NPC
Day 3
Astrocyte
log ratio FPKM
(HD/WT)
F
PSC
NPC
Day 3
Astrocyte
log ratio FPKM
(HD/WT)
G
MCM3_transcript_01
MCM3
RNA-seq
HD PSC
WT PSC
HD NPC
WT NPC
HD Day 3
WT Day 3
HD Astrocyte
WT Astrocyte
ATAC-seq
HD PSC
WT PSC
Unique Peaks
HD NPC
WT NPC
Unique Peaks
HD Day 3
WT Day 3
Unique Peaks
HD Astrocyte
WT Astrocyte
Unique Peaks
Enriched TF Motifs
Zic1
Phox2b
EWSR1-FLI1
Klf1
Foxj1
Tfap2a
Foxo1
Barhl2
SOX2
SOX2
Hand1::Tfe2a
Hand1::Tfe2a
Bcl6
Chr6:53150476-53172109

Figure 2-6. Aberrant E2F regulation coincides with increased p53 signaling and cell cycle gene expression in HD astrocytes. (A-B) Cross sectional GSEA enrichment plots shows significant depletion of E2F target gene expression in HD NPCs (A) and significant enrichment in HD astrocytes (B) compared to WT cells. Black lines indicate E2F target gene positions in rank-sorted expression data between HD and WT samples. Red dots indicate leading edge genes. q-values are FDR corrected p-values with alpha=0.02, or the equivalent. (C-D) RNA-seq expression data for *E2F1* (C) and *E2F7* (D) showing differential expression corresponding with motif accessibility. Average FPKM for each sample was plotted (**$p < 0.001$, differential expression analysis). (E) Heatmap depicting nearest differential ATAC-seq peaks to E2F target genes that are DE in at least one stage of astrocyte differentiation. Both proximal and distal peaks are included. Nearest differential ATAC-seq peaks are arranged according to hierarchical clustering, and correspond to the gene order in panel F. The E2F1 motif is shown below the heatmap. (F) Heatmap depicting differential expression of E2F target genes across differentiation. Each row corresponds to the same gene and gene names are displayed to the right of the plot. For both heat maps, red represents HD enrichment and blue indicates HD depletion. (G) Track view of RNA-seq and ATAC-seq data, as well as motifs present in differential peaks, at *MCM3*, an example E2F target gene. HD signal is shown in red and WT in blue. Significant differential peaks are indicated in the tracks below ATAC-seq tracks at each stage. TF motifs enriched in differential peaks are displayed at the bottom.

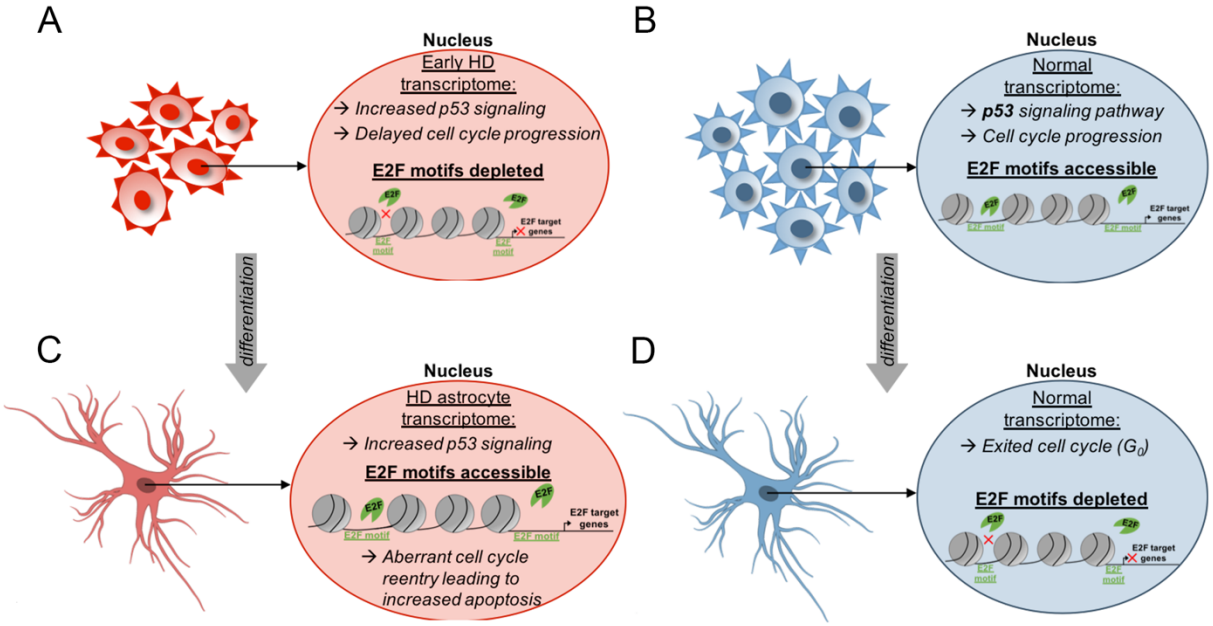
A
Nucleus
Early HD transcriptome:
→ Increased p53 signaling
→ Delayed cell cycle progression
E2F motifs depleted
E2F target genes
differentiation
B
Nucleus
Normal transcriptome:
→ p53 signaling pathway
→ Cell cycle progression
E2F motifs accessible
E2F target genes
differentiation
C
Nucleus
HD astrocyte transcriptome:
→ Increased p53 signaling
E2F motifs accessible
E2F target genes
→ Aberrant cell cycle reentry leading to increased apoptosis
D
Nucleus
Normal transcriptome:
→ Exited cell cycle (G0)
E2F motifs depleted
E2F target genes

Figure 2-7. Schematic model showing cell cycle, p53 signaling, and E2F target gene regulation across HD astrocyte differentiation. (A) HD NPCs show increased expression of p53 signaling genes, decreased expression of cell cycle and E2F target genes, which coincides with depleted promoter-proximal and distal accessibility of the E2F TF motif, while WT NPCs (B) show normal cell cycle progression and accessible E2F TF motifs genome-wide. (C) HD astrocytes show upregulation of p53 signaling, apoptosis, cell cycle and E2F target gene expression, along with increased E2F TF motif accessibility, suggesting cell cycle reentry leading to apoptosis. (D) In comparison, WT astrocytes show depleted accessibility of E2F TF motifs, and have low expression of p53 signaling, E2F target and cell cycle genes, indicating they are quiescent.

Table 2-1. Number of DE genes at each stage of astrocyte differentiation

	Total DE	Up in HD	Down in HD
PSC	2,218	881 (39.7%)	1,337 (60.3%)
NPC	1,344	618 (46%)	726 (54%)
Day 3	3,118	1,405 (45.1%)	1,713 (54.9%)
Astrocyte	1,316	729 (55.4%)	587 (44.6%)

Table 2-2. Number of differential ATAC-seq peaks at each stage of differentiation

	Total	HD Enriched	HD Depleted
PSC	2,676	1,923 (71.9%)	753 (28.1%)
NPC	16,497	9,437 (57.2%)	7,060 (42.8%)
Day 3	20,883	13,201 (63.2%)	7,682 (36.8%)
Astrocyte	7,060	6,342 (89.8%)	718 (10.2%)

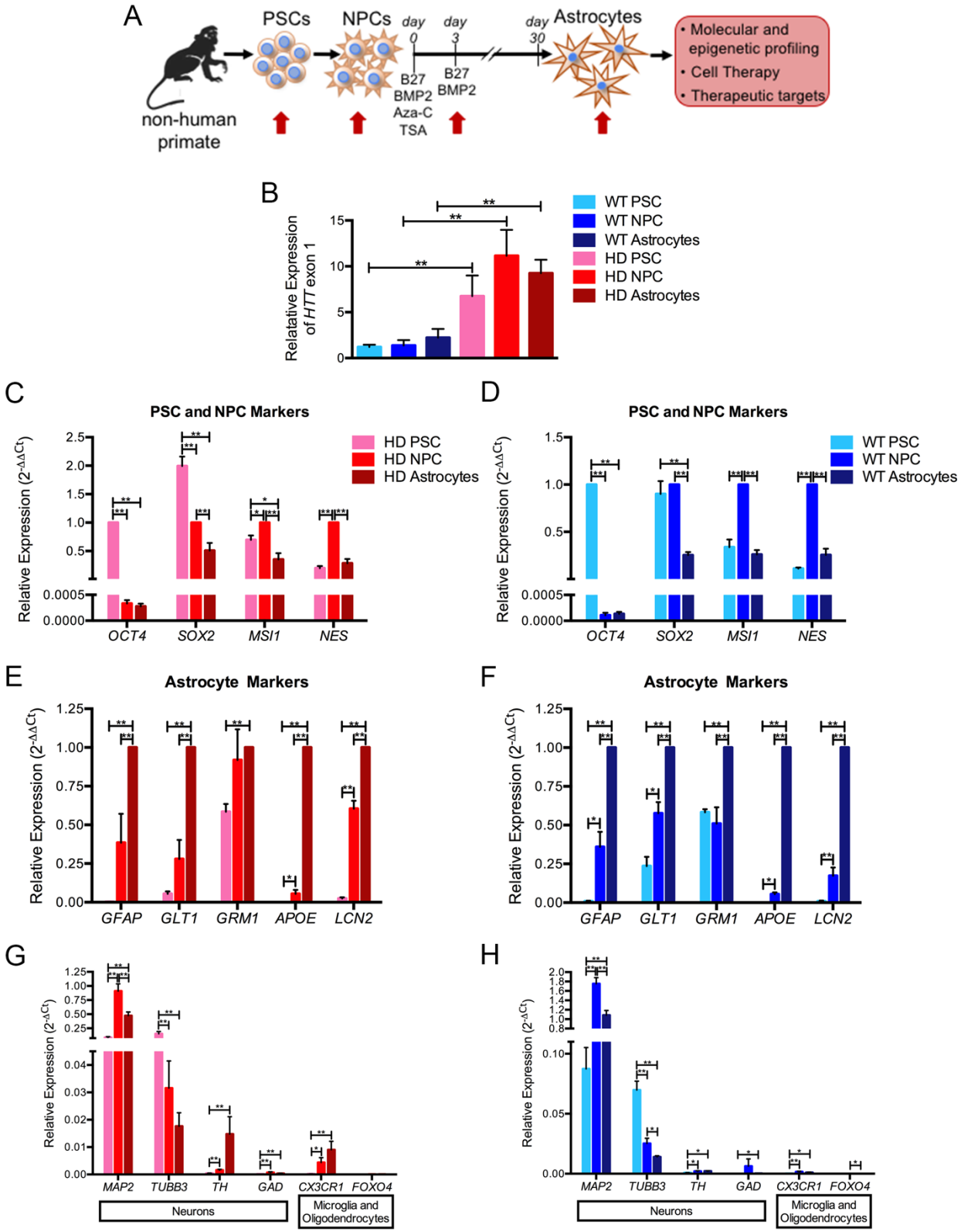
A
PSCs
NPCs
day 0
day 3
day 30
Astrocytes
B27 BMP2 Aza-C TSA
B27 BMP2
non-human primate
• Molecular and epigenetic profiling
• Cell Therapy
• Therapeutic targets
B
Relative Expression of HTT exon 1
WT PSC
WT NPC
WT Astrocytes
HD PSC
HD NPC
HD Astrocytes
C
PSC and NPC Markers
Relative Expression (2-ΔΔCt)
HD PSC
HD NPC
HD Astrocytes
OCT4
SOX2
MSI1
NES
D
PSC and NPC Markers
WT PSC
WT NPC
WT Astrocytes
E
Astrocyte Markers
GFAP
GLT1
GRM1
APOE
LCN2
F
Astrocyte Markers
G
Relative Expression (2-ΔCt)
MAP2
TUBB3
TH
GAD
CX3CR1
FOXO4
Neurons
Microglia and Oligodendrocytes
H

Figure s2-1. Model Validation. (A) Model of study design. Pluripotent stem cells (PSCs) were derived from HD and WT nonhuman primates (NHPs). Neural progenitor cells (NPCs) were further differentiated *in vitro* into astrocytes using a 30-day differentiation protocol. Time points for samples used in this study are indicated by red arrows. (B) qRT-PCR analysis of *HTT* exon 1 expression relative to *HTT* exon 26 expression during *in vitro* astrocyte differentiation of WT and HD NHP cell lines. Expression of both exons is normalized to *GAPDH* expression. (C-H) qRT-PCR analysis demonstrates differentiation efficiency. HD (C, E, G) and WT (D, F, H) NHP cells show appropriate expression of lineage specific markers, with decreases in PSC/NPC markers (C-D), increases in astrocyte markers (E-F), and repression of markers for other neural lineages (G-H) during astrocyte differentiation. All qRT-PCR experiments were performed in triplicate, using three biological replicates. Data and error bars are represented as mean ± SEM (**$p < 0.01$ and *$p < 0.05$, ANOVA).

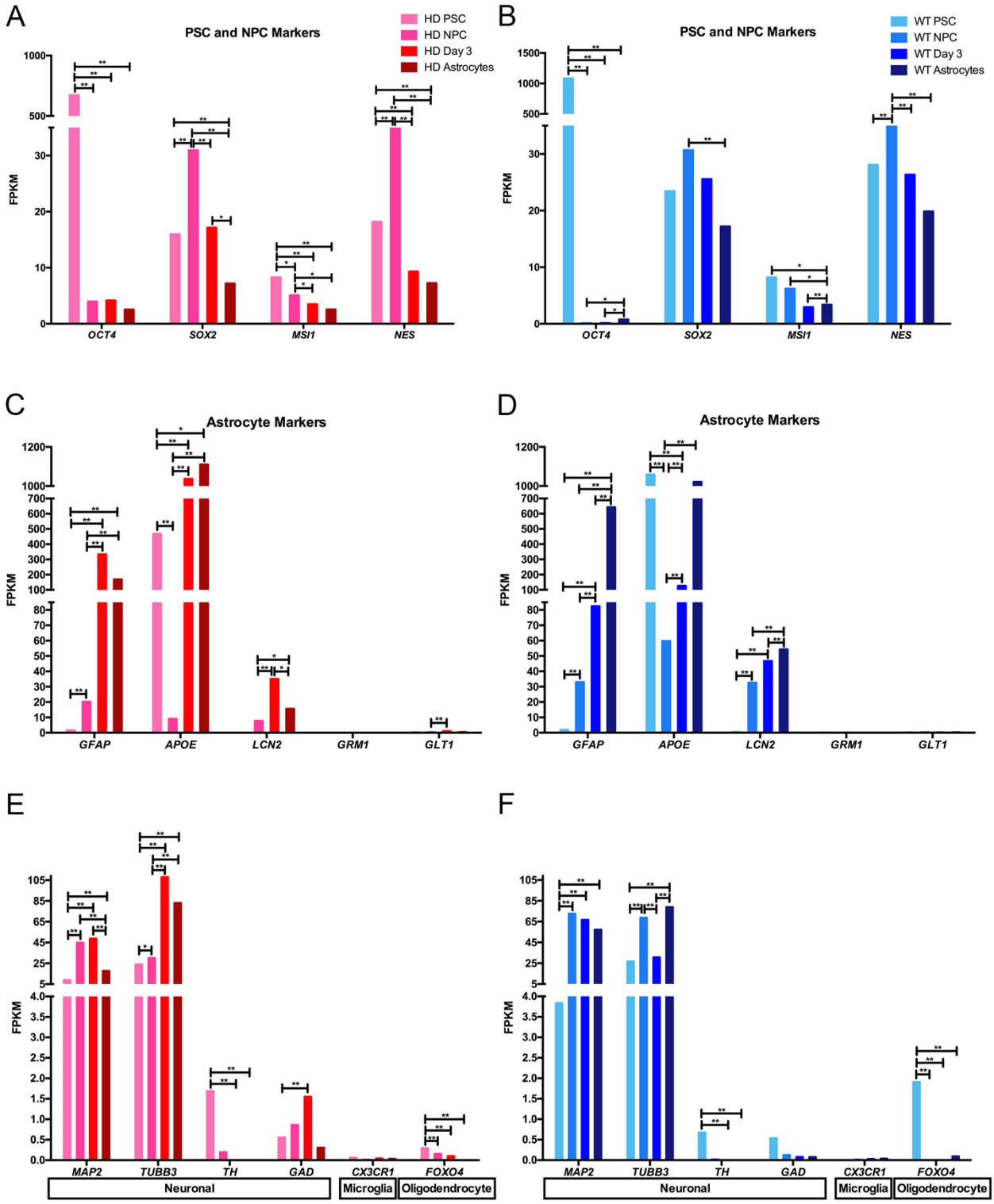
A
PSC and NPC Markers
HD PSC
HD NPC
HD Day 3
HD Astrocytes
FPKM
OCT4
SOX2
MSI1
NES
B
PSC and NPC Markers
WT PSC
WT NPC
WT Day 3
WT Astrocytes
FPKM
OCT4
SOX2
MSI1
NES
C
Astrocyte Markers
FPKM
GFAP
APOE
LCN2
GRM1
GLT1
D
Astrocyte Markers
FPKM
GFAP
APOE
LCN2
GRM1
GLT1
E
FPKM
MAP2
TUBB3
TH
GAD
CX3CR1
FOXO4
Neuronal
Microglia
Oligodendrocyte
F
FPKM
MAP2
TUBB3
TH
GAD
CX3CR1
FOXO4
Neuronal
Microglia
Oligodendrocyte

Figure s2-2. Model Validation. (A-F) Bar graphs of RNA-seq signal of cell-type markers during *in vitro* astrocyte differentiation in HD (A, C, E) and WT (B, D, F) cells. (A-B) PSC and NPC markers are downregulated during differentiation. (C-D) Several astrocyte markers become induced during astrocyte differentiation. (E-F) Markers for neuronal and glial cell types are largely repressed over the course of astrocyte differentiation. All RNA-seq experiments were performed in three biological replicates and average FPKM for each sample was plotted (**$p < 0.001$ and *$p < 0.01$, differential expression analysis).

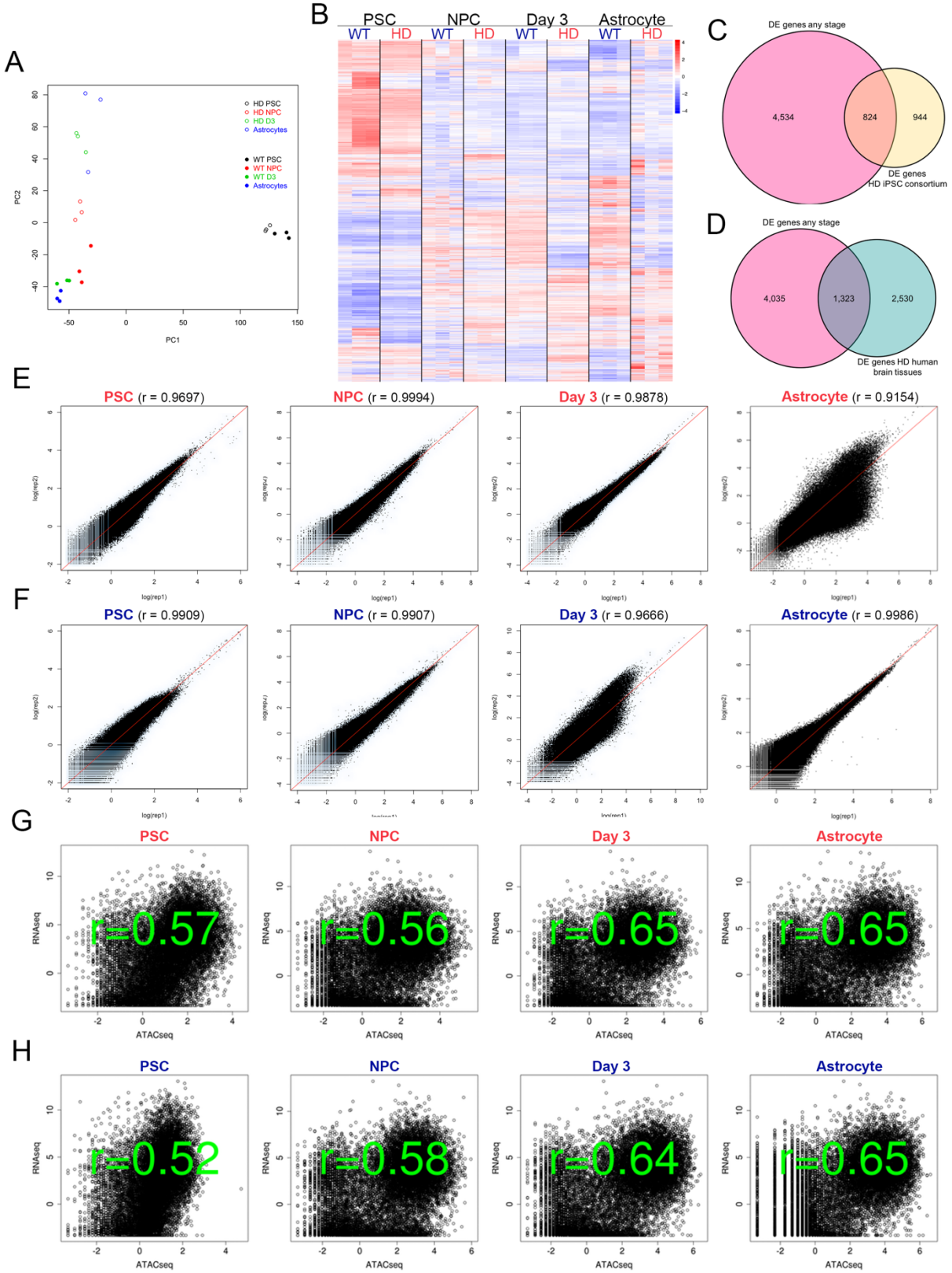
A
HD PSC
HD NPC
HD D3
Astrocytes
WT PSC
WT NPC
WT D3
Astrocytes
PC1
PC2
B
PSC
NPC
Day 3
Astrocyte
WT
HD
C
DE genes any stage
4,534
824
944
DE genes
HD iPSC consortium
D
DE genes any stage
4,035
1,323
2,530
DE genes HD human
brain tissues
E
PSC (r = 0.9697)
NPC (r = 0.9994)
Day 3 (r = 0.9878)
Astrocyte (r = 0.9154)
log(rep1)
log(rep2)
F
PSC (r = 0.9909)
NPC (r = 0.9907)
Day 3 (r = 0.9666)
Astrocyte (r = 0.9986)
G
PSC
NPC
Day 3
Astrocyte
r=0.57
r=0.56
r=0.65
r=0.65
RNAseq
ATACseq
H
PSC
NPC
Day 3
Astrocyte
r=0.52
r=0.58
r=0.64
r=0.65

Figure s2-3. Related to Figure 2-1. (A) Principal component analysis (PCA) of log2 transformed normalized read counts (variance stabilizing transformation, DESeq2) from RNA-seq experiments in HD (outline) and WT (solid) cell lines for all 4 time points, PSC (black), NPC (red), Day 3 (green), and astrocyte (blue). PC1 and PC2 capture 51% and 13% of the data variance respectively. (B) Heatmap of log_2 transformed normalized read counts (variance stabilizing transformation, DESeq2) of transcripts differentially expressed (FDR adjusted, alpha=0.02, n=5,062) between different differentiation stages and between WT and transgenic samples. Expression values of each transcript (rows) are scaled to unit variance across samples (columns) to normalize expression between transcripts. Transcripts are organized by unsupervised hierarchical clustering (euclidean distance, complete linkage) and samples are organized by differentiation stage and genotype (WT or HD). (C) Venn diagram showing overlap of differentially expressed (DE) genes identified at any stage of HD astrocyte differentiation and DE genes identified by the HD iPSC Consortium (2017). DE genes from the iPSC consortium study not annotated in MacaM were not counted. (D) Venn diagram of overlapping DE genes across HD differentiation and DE genes identified in post-mortem HD brain tissues by Labadorf et al. (2015). DE genes from the Labadorf et al. (2015) not annotated in MacaM were not counted. (E-F) Scatterplots between two ATAC-seq replicates for HD (E) and WT (F) cells at each stage of differentiation. (G-H) Scatterplots of RNA-seq gene FPKM values vs. ATAC-seq FPKM values at the promoters (TSS +/- 500bp) of the corresponding genes for HD (G) and WT (H) cells at each stage of differentiation. r = Pearson's correlation coefficient.

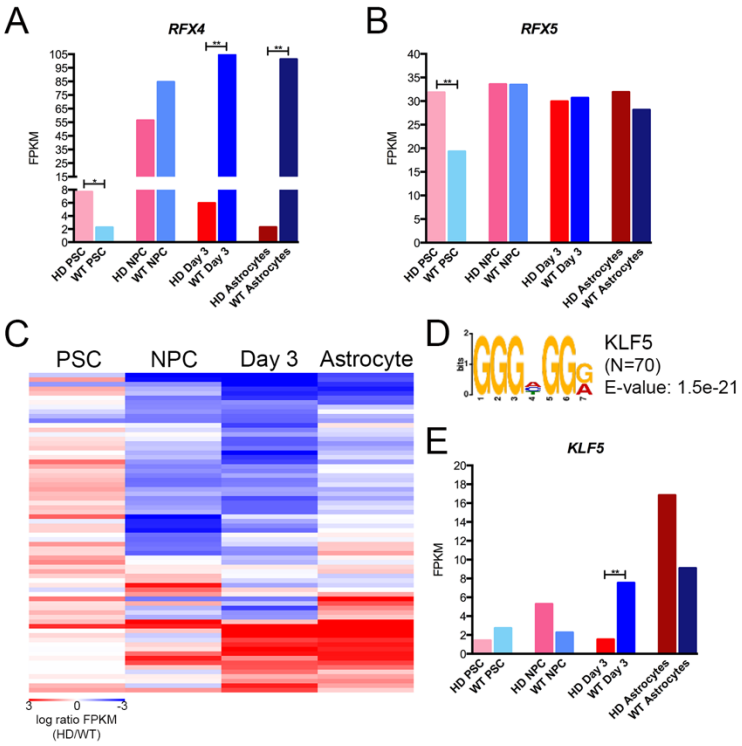
A
RFX4
FPKM
HD PSC
WT PSC
HD NPC
WT NPC
HD Day 3
WT Day 3
HD Astrocytes
WT Astrocytes
B
RFX5
C
PSC
NPC
Day 3
Astrocyte
log ratio FPKM
(HD/WT)
D
KLF5
(N=70)
E-value: 1.5e-21
E
KLF5

Figure s2-4. Related to Figure 2-3. (A-B) Bar graphs generated from RNA-seq data depicting differential expression of *RFX4* (A) and *RFX5* (B) occurs in at least one stage of *in vitro* astrocyte differentiation. RNA-seq experiments were performed in three biological replicates and average FPKM for each sample was plotted. (C) Heatmap depicting normalized differential ATAC-seq signal in HD and WT cells at macaque brain enhancers overlapping a differential THSS that contains the KLF5 motif (N=70). The red color represents HD-enrichment and the blue color indicates WT-enrichment. (D) KLF5 motif found at enhancers that overlap a differential THSS. (E) Bar graph generated from RNA-seq data of *KLF5* expression across *in vitro* astrocyte differentiation. RNA-seq experiments were performed in three biological replicates and average FPKM for each sample was plotted. **$p < 0.001$, differential expression analysis.

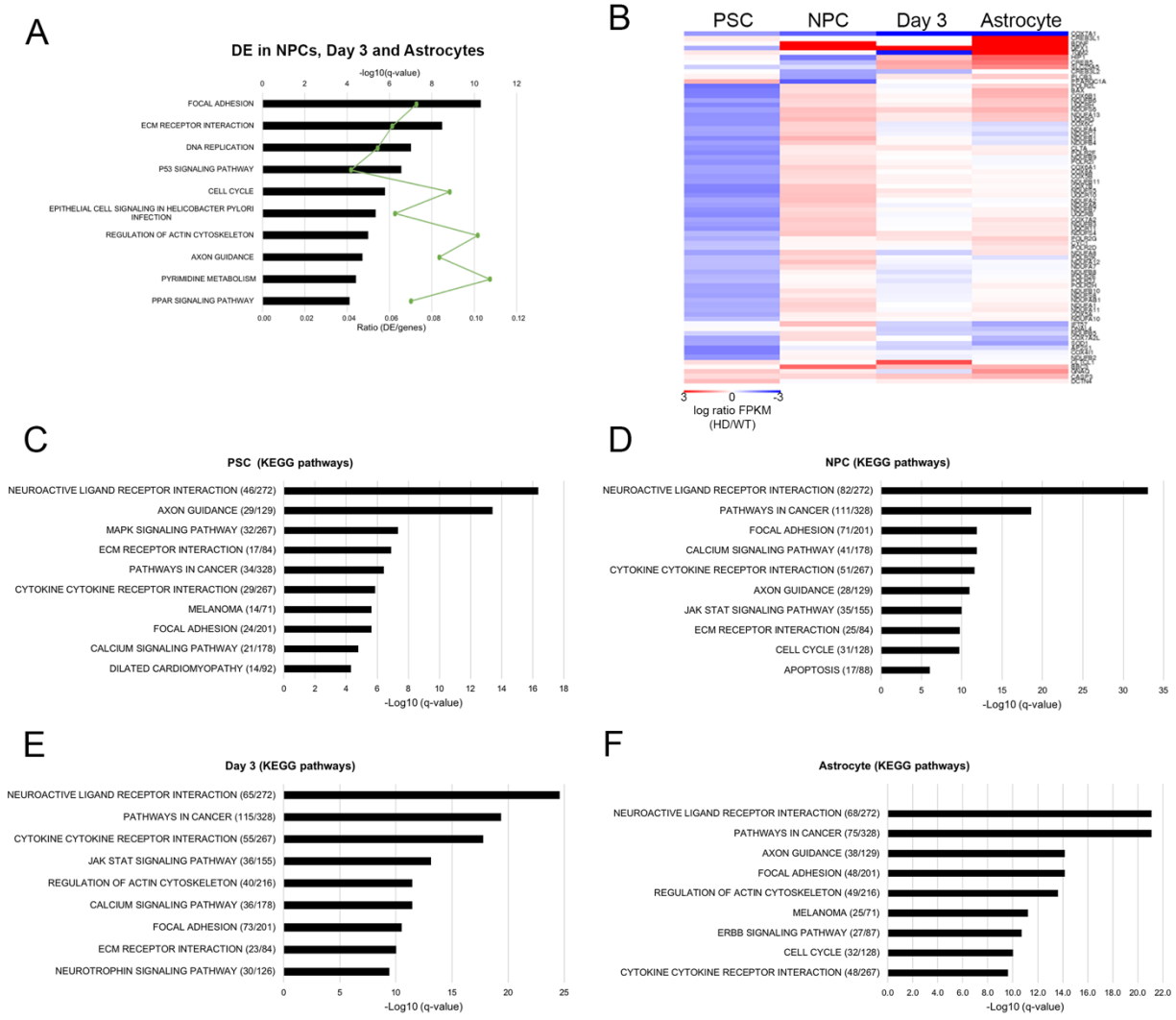
A
DE in NPCs, Day 3 and Astrocytes
-log10(q-value)
FOCAL ADHESION
ECM RECEPTOR INTERACTION
DNA REPLICATION
P53 SIGNALING PATHWAY
CELL CYCLE
EPITHELIAL CELL SIGNALING IN HELICOBACTER PYLORI INFECTION
REGULATION OF ACTIN CYTOSKELETON
AXON GUIDANCE
PYRIMIDINE METABOLISM
PPAR SIGNALING PATHWAY
Ratio (DE/genes)
B
PSC
NPC
Day 3
Astrocyte
log ratio FPKM
(HD/WT)
C
PSC (KEGG pathways)
NEUROACTIVE LIGAND RECEPTOR INTERACTION (46/272)
AXON GUIDANCE (29/129)
MAPK SIGNALING PATHWAY (32/267)
ECM RECEPTOR INTERACTION (17/84)
PATHWAYS IN CANCER (34/328)
CYTOKINE CYTOKINE RECEPTOR INTERACTION (29/267)
MELANOMA (14/71)
FOCAL ADHESION (24/201)
CALCIUM SIGNALING PATHWAY (21/178)
DILATED CARDIOMYOPATHY (14/92)
-Log10 (q-value)
D
NPC (KEGG pathways)
NEUROACTIVE LIGAND RECEPTOR INTERACTION (82/272)
PATHWAYS IN CANCER (111/328)
FOCAL ADHESION (71/201)
CALCIUM SIGNALING PATHWAY (41/178)
CYTOKINE CYTOKINE RECEPTOR INTERACTION (51/267)
AXON GUIDANCE (28/129)
JAK STAT SIGNALING PATHWAY (35/155)
ECM RECEPTOR INTERACTION (25/84)
CELL CYCLE (31/128)
APOPTOSIS (17/88)
-Log10 (q-value)
E
Day 3 (KEGG pathways)
NEUROACTIVE LIGAND RECEPTOR INTERACTION (65/272)
PATHWAYS IN CANCER (115/328)
CYTOKINE CYTOKINE RECEPTOR INTERACTION (55/267)
JAK STAT SIGNALING PATHWAY (36/155)
REGULATION OF ACTIN CYTOSKELETON (40/216)
CALCIUM SIGNALING PATHWAY (36/178)
FOCAL ADHESION (73/201)
ECM RECEPTOR INTERACTION (23/84)
NEUROTROPHIN SIGNALING PATHWAY (30/126)
-Log10 (q-value)
F
Astrocyte (KEGG pathways)
NEUROACTIVE LIGAND RECEPTOR INTERACTION (68/272)
PATHWAYS IN CANCER (75/328)
AXON GUIDANCE (38/129)
FOCAL ADHESION (48/201)
REGULATION OF ACTIN CYTOSKELETON (49/216)
MELANOMA (25/71)
ERBB SIGNALING PATHWAY (27/87)
CELL CYCLE (32/128)
CYTOKINE CYTOKINE RECEPTOR INTERACTION (48/267)
-Log10 (q-value)

Figure s2-5. Related to Figure 2-4. (A) GO analyses of DE genes at the NPC, day 3 and astrocyte stages. Pathways are ranked by -log10 (q-value), determined by the Benjamini-Hochberg procedure. All pathways shown satisfy $q < 0.05$. Line graphs show the ratio of DE genes in each KEGG pathway. (B) Heatmap depicting DE genes in the KEGG Huntington pathway (N=74) at each stage. PSCs show a different pattern of dysregulation compared to the other stages of HD astrocyte differentiation. The red color represents genes that are upregulated in HD and the blue color represents genes that are downregulated in HD. Each row corresponds to the same gene. (C-F) GO analysis of the closest gene to each differential THSS. (C), NPC (D), day 3 (E) and astrocyte (F) stages, with KEGG pathways using GO analysis. The top 10 significant pathways are ranked by -log10 (q-value), determined by Benjamini-Hochberg procedures; all pathways shown satisfy $q < 0.05$.

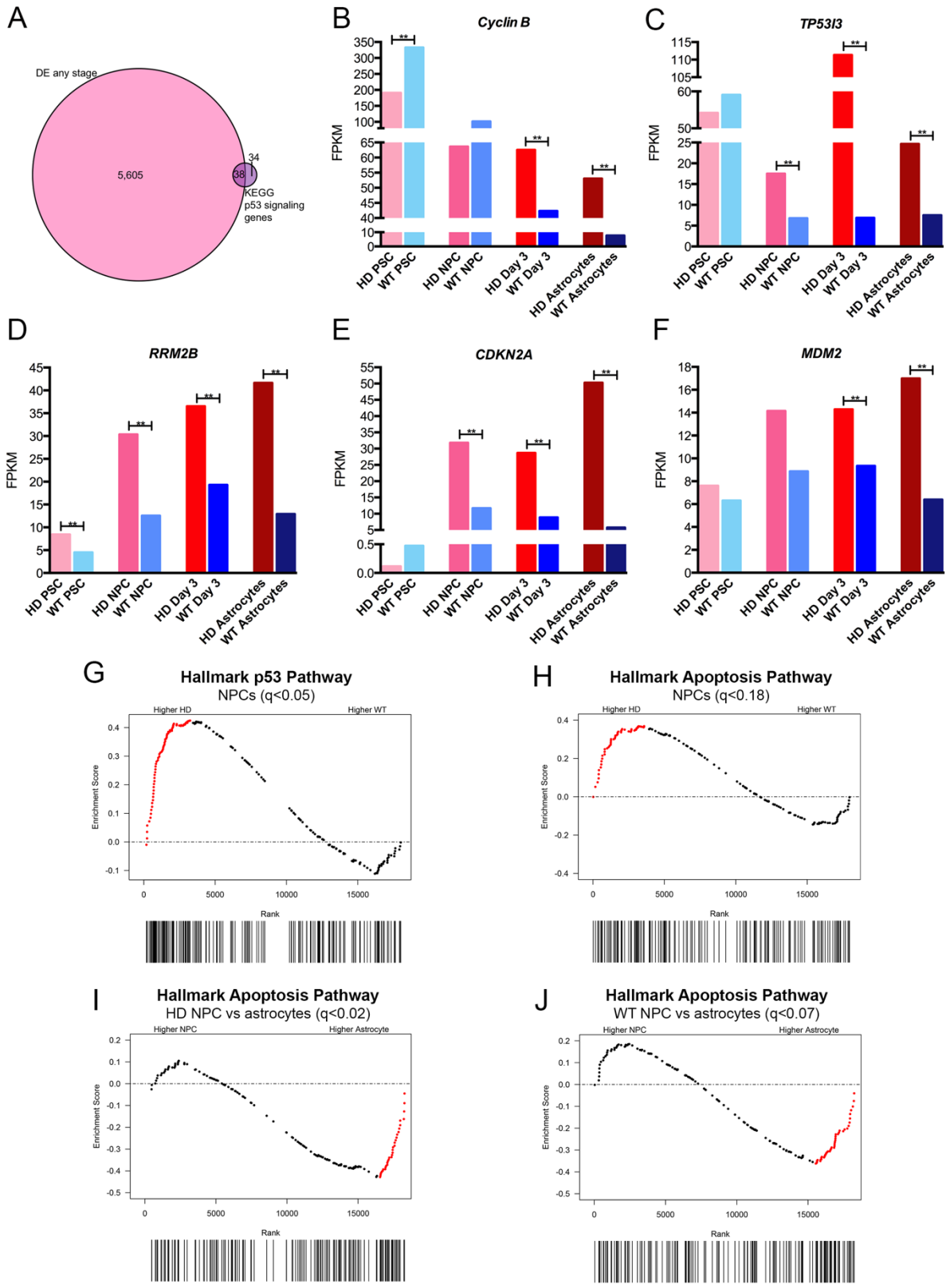
A
DE any stage
5,605
34
38
KEGG
p53 signaling
genes
B
Cyclin B
C
TP53I3
D
RRM2B
E
CDKN2A
F
MDM2
FPKM
HD PSC
WT PSC
HD NPC
WT NPC
HD Day 3
WT Day 3
HD Astrocytes
WT Astrocytes
G
Hallmark p53 Pathway
NPCs (q<0.05)
H
Hallmark Apoptosis Pathway
NPCs (q<0.18)
I
Hallmark Apoptosis Pathway
HD NPC vs astrocytes (q<0.02)
J
Hallmark Apoptosis Pathway
WT NPC vs astrocytes (q<0.07)
Higher HD
Higher WT
Higher NPC
Higher Astrocyte
Enrichment Score
Rank

Figure s2-6. Related to Figure 2-5. (A) Venn diagram showing overlap of DE genes at any stage with the KEGG p53 signaling pathway gene set. (B-F) Bar graphs of RNA-seq data for example DE genes in the p53 pathway. All RNA-seq experiments were performed in three biological replicates and average FPKM for each sample was plotted (**$p < 0.001$, differential expression analysis). (G-J) GSEA enrichment plots. Cross sectional GSEA displays no significant enrichment of p53 signaling (G) or apoptosis (H) gene expression in HD NPCs. (I-J) Longitudinal GSEA of DE genes reveals significant enrichment of apoptosis pathway genes in HD astrocytes compared to HD NPCs (I), but not in WT cell lines (J). Red dots indicate leading edge genes. q-values are FDR corrected p-values with alpha=0.02, or the equivalent.

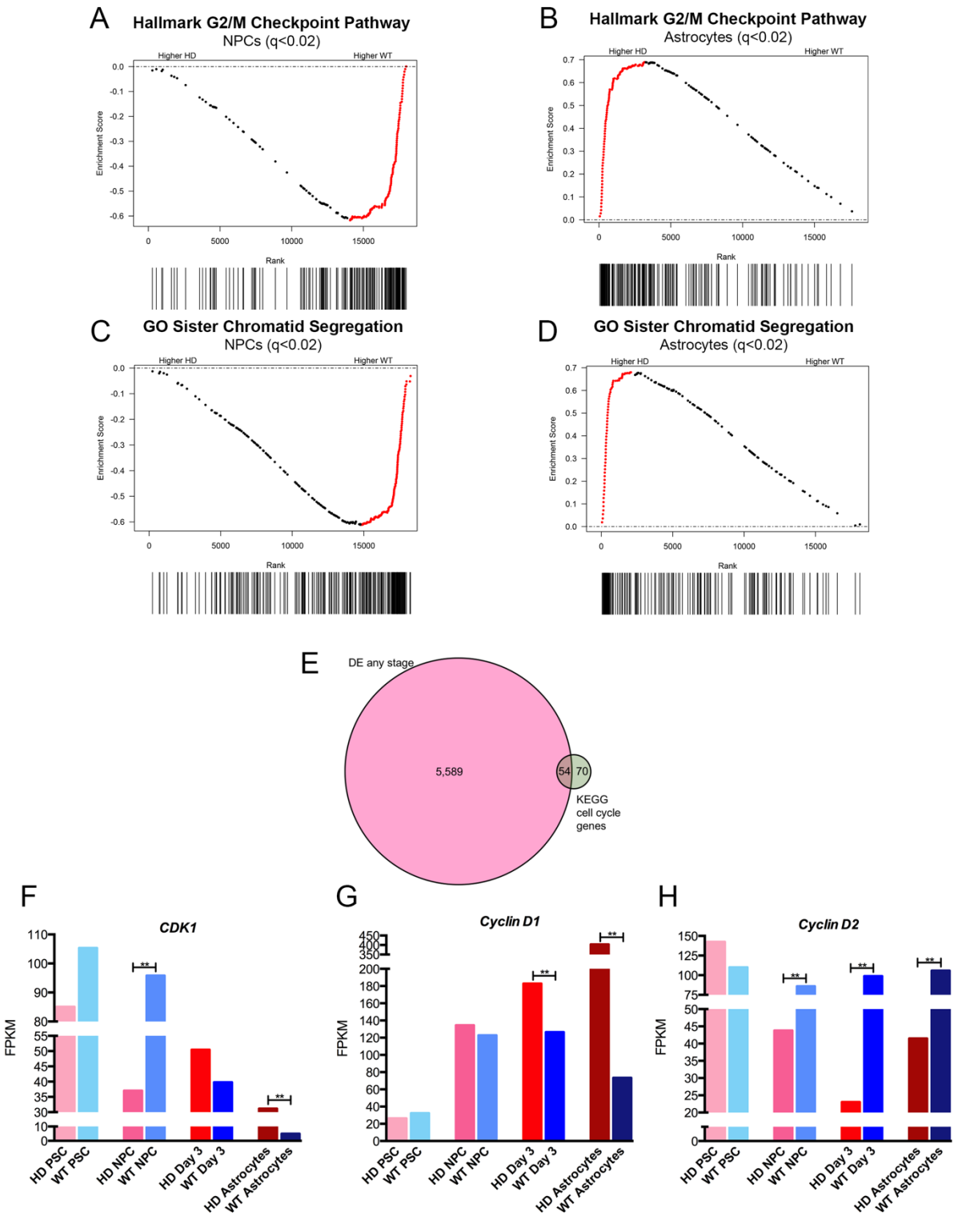
A
Hallmark G2/M Checkpoint Pathway
NPCs (q<0.02)
Higher HD
Higher WT
Enrichment Score
Rank
B
Hallmark G2/M Checkpoint Pathway
Astrocytes (q<0.02)
C
GO Sister Chromatid Segregation
NPCs (q<0.02)
D
GO Sister Chromatid Segregation
Astrocytes (q<0.02)
E
DE any stage
5,589
54
70
KEGG
cell cycle
genes
F
CDK1
G
Cyclin D1
H
Cyclin D2
FPKM
HD PSC
WT PSC
HD NPC
WT NPC
HD Day 3
WT Day 3
HD Astrocytes
WT Astrocytes

Figure s2-7. Related to Figure 2-5. (A-D) Cross sectional GSEA revealed an inverse enrichment of cell cycle pathways during HD astrocyte differentiation. (A-B) GSEA of DE genes revealed depleted expression of G2/M checkpoint genes in HD NPCs (A) and enriched expression in HD astrocytes (B). (C-D) Genes involved in sister chromatid segregation are also inversely enriched in our DE gene set, with depletion in HD NPCs (C) and enrichment in HD astrocytes (D) compared to WT cells. Black lines indicate the position of pathway genes in rank-sorted expression data from HD and WT samples. Red dots indicate leading edge genes. q-values are FDR corrected p-values with alpha=0.02, or the equivalent. (E) Venn diagram showing overlap of DE genes at any stage with the KEGG cell cycle pathway gene set. All KEGG cell cycle pathway genes are counted, even those not annotated in MacaM. (F-H) Example cell cycle genes showing differential expression via RNA-seq. All RNA-seq experiments were performed in three biological replicates and average FPKM for each sample was plotted (**$p < 0.001$, differential expression analysis).

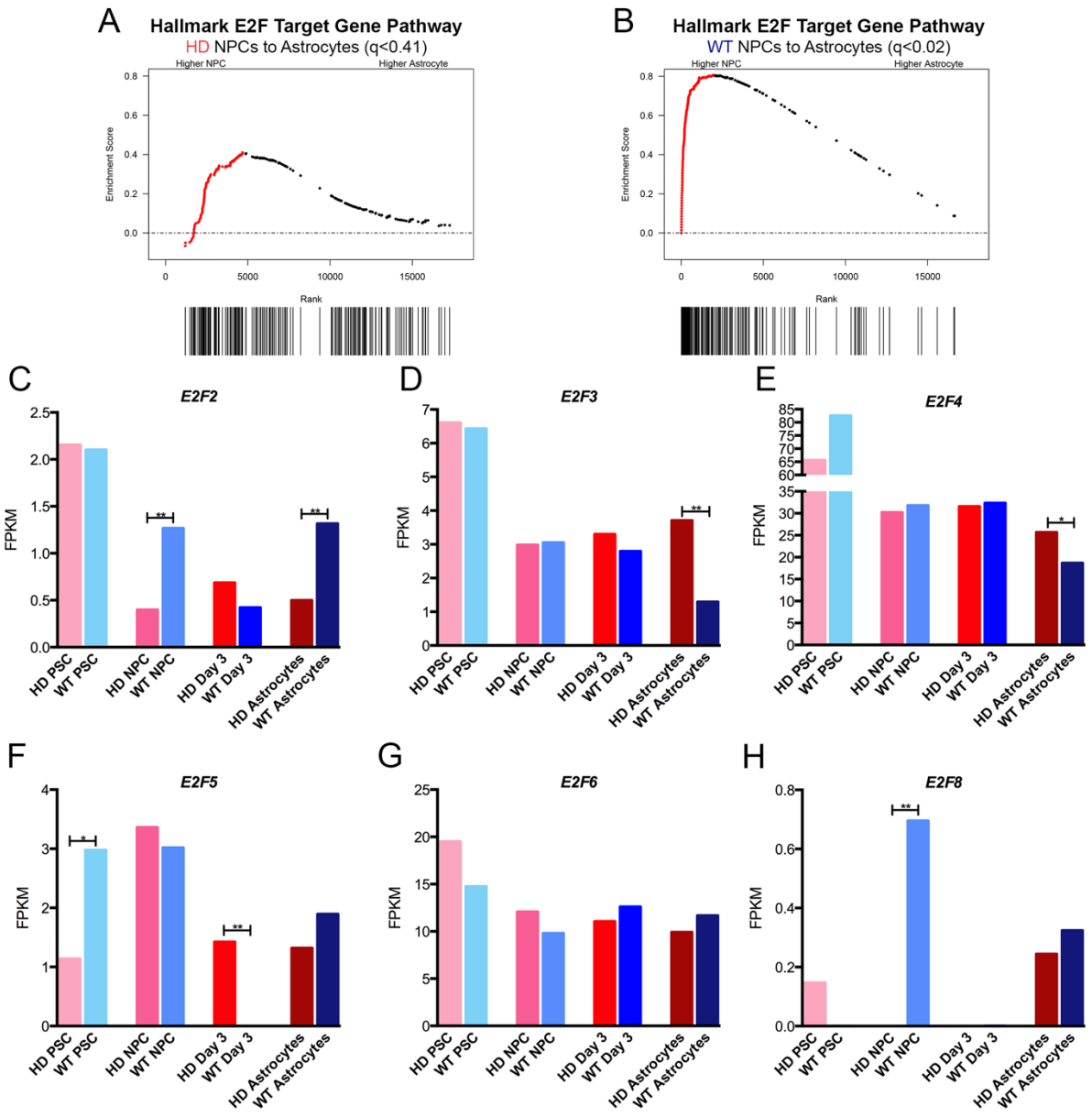
A
Hallmark E2F Target Gene Pathway
HD NPCs to Astrocytes (q<0.41)
Higher NPC
Higher Astrocyte
Enrichment Score
Rank
B
Hallmark E2F Target Gene Pathway
WT NPCs to Astrocytes (q<0.02)
Higher NPC
Higher Astrocyte
Enrichment Score
Rank
C
E2F2
FPKM
D
E2F3
FPKM
E
E2F4
FPKM
F
E2F5
FPKM
G
E2F6
FPKM
H
E2F8
FPKM
HD PSC
WT PSC
HD NPC
WT NPC
HD Day 3
WT Day 3
HD Astrocytes
WT Astrocytes

Figure s2-8. Related to Figure 2-6. (A-B) Longitudinal GSEA revealed enrichment of E2F target genes in WT (B) but not HD (A) astrocytes. Black lines indicate the position of pathway genes in rank-sorted expression data from HD and WT samples. Red dots indicate leading edge genes. q-values are FDR corrected p-values with alpha=0.02, or the equivalent. (C-H) Bar graphs generated from RNA-seq data depicting differential expression of E2F family members, *E2F2* (C), *E2F3* (D), *E2F4* (E), *E2F5* (F), *E2F6* (G), *E2F8* (H). RNA-seq experiments were performed in three biological replicates and average FPKM for each sample was plotted (**$p < 0.001$ and *$p < 0.01$, differential expression analysis).

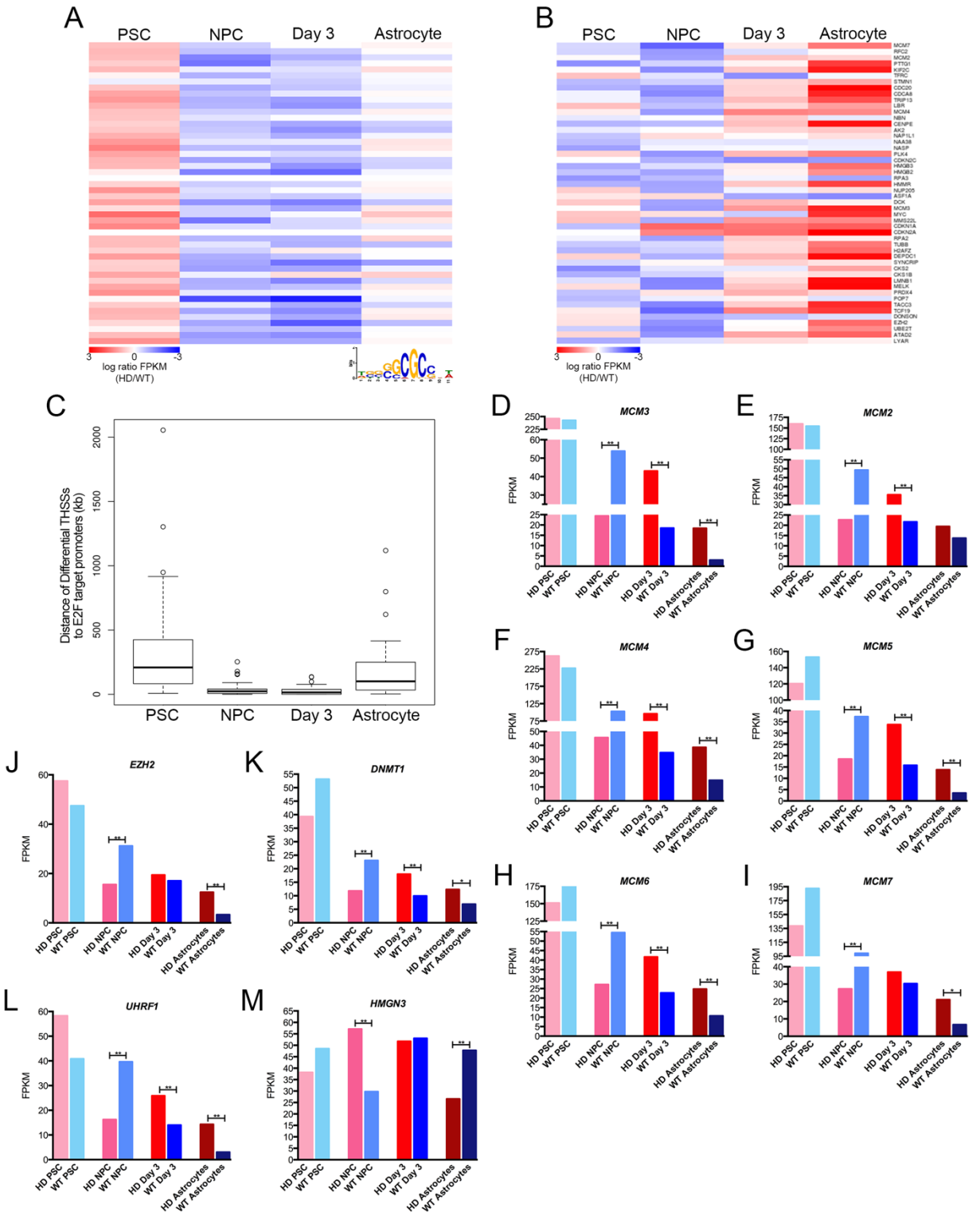
A
PSC
NPC
Day 3
Astrocyte
log ratio FPKM (HD/WT)
B
PSC
NPC
Day 3
Astrocyte
log ratio FPKM (HD/WT)
C
Distance of Differential THSSs to E2F target promoters (kb)
PSC
NPC
Day 3
Astrocyte
D
MCM3
E
MCM2
F
MCM4
G
MCM5
H
MCM6
I
MCM7
J
EZH2
K
DNMT1
L
UHRF1
M
HMGN3
FPKM
HD PSC
WT PSC
HD NPC
WT NPC
HD Day 3
WT Day 3
HD Astrocytes
WT Astrocytes

Figure s2-9. Related to Figure 2-6. (A) Heatmap depicting differential ATAC-seq signal at DE E2F target gene promoters shows depleted accessibility in HD NPCs and at day 3, while HD and WT astrocytes display similar E2F target promoter accessibility. Promoter-proximal ATAC-seq peaks are arranged according to the order of the genes in panel B. The E2F1 motif is shown below the heatmap. (B) Heatmap of differential E2F target gene expression at each stage of differentiation. The same heatmap is shown in Figure 6 but is included here for comparison with panel A. Gene names are displayed to the right of the plot. For both heat maps, red represents HD enrichment and blue indicates HD depletion. (C) Boxplot of the distribution of distances from each DE E2F gene promoter to the nearest differential THSS at each stage across astrocyte differentiation. (D-I) RNA-seq data for all six MCM proteins regulated by E2F TFs; *MCM3* (D), *MCM2* (E), *MCM4* (F), *MCM5* (G), *MCM6* (H), *MCM7* (I), all of which showed DE in at least one stage of differentiation. (J-M) Inverse DE profiles for several epigenetic regulators that are E2F target genes; *EZH2* (J), *DNMT1* (K), *UHRF1* (L) and *HMGN3* (M). RNA-seq experiments were performed in three biological replicates and average FPKM for each sample was plotted (**$p < 0.001$ and *$p < 0.01$, differential expression analysis).

Table s2-1. qRT-PCR primers

Gene Symbol	SYBR Forward Primer	SYBR Reverse Primer
***HTT* Exon 1**	GCGACCCTGGAAAAGCTGAT	CTGCTGCTGCTGGAAGGACT
***HTT* Exon 26**	ACCCTGCTCTCGTCAGCTTGG	AGCAAGTTTCCGGCCAAAAT
SOX2	CACAGCGCCCGCATGTACAA	AGTTCGCTGTCCTGCCCTCA
MSI1	CACAGCCCAAGATGGTGACT	TCCACCTTCCCAAACTGCTC
NES	TGGCAAGAGGCCGGTACA	CCGTATTTGTCCTTCACCTTC
GFAP	CCAGCTCGCGGTTCTCATAC	CTCATGGACTTTCAGGGCGT
GLT1	ATGCACGACAGTCACCTCAG	AGGATGACACCAAACACCGT
GRM1	CTCGGGCATGCATTGTGAAA	GCGTTCTTGTTAGCAGTCCC
APOE	GGGTCGCTTTTGGGATTACC	CTCATCCATCAGCGTCGTCA
LCN2	AGGGAATGCAGTTGGCAGAA	GGAGGTCACGTTGTAGCTCT
MAP2	ATCTTTCTCCTCTGGCTTCCG	GGTGTGGTGGCTGGAAGGTA
TUBB3	GCCAAGTTCTGGGAAGTCAT	GGCACGTACTTGTGAGAGGA
TH	GAACTTCTGGGGTCGCTCC	ACCTCAAGACTTACCGGCTT
GAD	CCACGTTTTTGGCGAACG	CAGTGTCGCTTTTTCGGTGT
CX3CR1	AAAACGAATGCCTTGGTGAC	AGGAAAAACACGACGACCAC
FOXO4	ACCATGGATGTGTTAGGGGC	CCCTGTGTGTAAATGGGGGA
UBC	CCACTCTGCACTTGGTCCTG	CCAGTTGGGAATGCAACAACTTTA
	TaqMan® Primer Context Sequence	
OCT4	CCCTGGGGGTTCTATTTGGGAAGGT	
UBC	TCCTTTCAATAAAGTTGTTGCATTC	

Table s2-3. 63 genes differentially expressed at every stage of HD astrocyte differentiation

Ensembl ID	Gene Symbol
ENSG00000161533	*ACOX1*
ENSG00000106992	*AK1*
ENSG00000145246	*ATP10D*
ENSG00000119280	*C1orf198*
ENSG00000151465	*CDC123*
ENSG00000179604	*CDC42EP4*
ENSG00000117724	*CENPF*
ENSG00000205423	*CNEP1R1*
ENSG00000106714	*CNTNAP3*
ENSG00000060718	*COL11A1*
ENSG00000084636	*COL16A1*
ENSG00000164692	*COL1A2*
ENSG00000139219	*COL2A1*
ENSG00000204262	*COL5A2*
ENSG00000057019	*DCBLD2*
ENSG00000065357	*DGKA*
ENSG00000069345	*DNAJA2*
ENSG00000143476	*DTL*
ENSG00000089248	*ERP29*
ENSG00000121769	*FABP3*
ENSG00000164687	*FABP5*
ENSG00000066468	*FGFR2*
ENSG00000140718	*FTO*
ENSG00000100626	*GALNTL1*
ENSG00000198814	*GK*
ENSG00000167699	*GLOD4*
ENSG00000233276	*GPX1*
ENSG00000089472	*HEPH*
ENSG00000095066	*HOOK2*
ENSG00000204389	*HSPA1A*
ENSG00000110906	*KCTD10*
ENSG00000109790	*KLHL5*
ENSG00000184445	*KNTC1*
ENSG00000113083	*LOX*
ENSG00000011009	*LYPLA2*
ENSG00000165943	*MOAP1*
ENSG00000130287	*NCAN*
ENSG00000064300	*NGFR*
ENSG00000116962	*NID1*
ENSG00000146938	*NLGN4X*
ENSG00000118257	*NRP2*
ENSG00000119630	*PGF*
ENSG00000174307	*PHLDA3*
ENSG00000165443	*PHYHIPL*
ENSG00000123560	*PLP1*
ENSG00000177084	*POLE*
ENSG00000100033	*PRODH*
ENSG00000107317	*PTGDS*
ENSG00000173482	*PTPRM*
ENSG00000115963	*RND3*
ENSG00000137393	*RNF144B*
ENSG00000048392	*RRM2B*
ENSG00000133318	*RTN3*
ENSG0000013346	*SLC2A11*
ENSG00000133195	*SLC39A11*
ENSG00000196517	*SLC6A9*
ENSG00000187122	*SLIT1*
ENSG00000172164	*SNTB1*
ENSG00000125355	*TMEM255A*
ENSG00000106537	*TSPAN13*
ENSG00000175063	*UBE2C*
ENSG00000158773	*USF1*
ENSG00000156925	*ZIC3*

Table s2-4. Summary of ATAC-seq data

	Total Reads	Uniquely Mapped Reads	% Duplicate Reads	Total unique reads	Total TF Reads (50-115 bp)
WT PSC ***Rep 1***	241,018,632	149,150,459 (61.88%)	21.25%	137,920,614	41,783,968
WT PSC ***Rep 2***	120,805,711	71,486,579 (59.17%)	22.48%		
WT NPC ***Rep 1***	66,302,541	51,881,442 (78.25%)	14.64%	86,184,309	33,862,889
WT NPC ***Rep 2***	66,010,778	49,064,142 (74.33%)	14.6%		
WT Day 3 ***Rep 1***	92,043,238	62,256,890 (67.64%)	23.71%	77,978,180	28,776,687
WT Day 3 ***Rep 2***	72,492,369	43,421,114 (59.9%)	29.8%		
WT Astrocyte ***Rep 1***	61,787,804	35,798,982 (57.94%)	56.5%	52,276,328	19,968,105
WT Astrocyte ***Rep 2***	209,610,003	129,726,447 (61.89%)	78.01%		
HD PSC ***Rep 1***	47,048,659	33,371,731 (70.93%)	11.54%	83,017,985	34,104,663
HD PSC ***Rep 2***	87,955,432	62,762,506 (71.35%)	14.76%		
HD NPC ***Rep 1***	69,581,921	50,247,187 (72.21%)	15.1%	82,993,975	29,456,864
HD NPC ***Rep 2***	71,810,845	49,249,549 (68.58%)	18.11%		
HD Day 3 ***Rep 1***	83,955,653	62,789,374 (74.79%)	10.30%	95,398,477	34,964,708
HD Day 3 ***Rep 2***	70,554,693	49,834,029 (70.63%)	12.16%		
HD Astrocyte ***Rep 1***	115,179,171	85,510,489 (74.24%)	53.48%	88,746,911	32,141,037
HD Astrocyte ***Rep 2***	115,147,594	72,575,752 (63.03%)	38.5%		

Table s2-7. Motifs enriched in nearest differential peaks associated with E2F target genes

Motif	NPC	Astrocytes
SOX17	4	1
ZFX	4	
FOSL2	3	
TCF3	3	
ZIC3	3	1
ALX1	2	
CTCF	2	
E2F8	2	
FOSL1	2	1
KLF1	2	
MSC	2	
NR2F2	2	
PAX2	2	
RARG	2	
RFX4	2	
SP1	2	
TFAP2C	2	1
ZSCAN4	2	
ARID3A	1	
ASCL2	1	
E2F3	1	
E2F4	1	
E2F6	1	1
EGR1	1	
ELK1	1	
ETV4	1	
ETV6	1	
EWSR1-FLT1	1	
FOS	1	2

Motif	NPC	Astrocytes
FOXA2	1	
FOXC1	1	
FOXI1	1	1
FOXP1	1	
GATA3	1	
HAND1::TCFE2A	1	1
HIC1	1	
HMX1	1	
JUNDM2	1	1
KLF12	1	
KLF4	1	
MAX	1	
MYBL2	1	
NFATC1	1	
NFYA	1	
NHLH1	1	
NKX3-2	1	
POU2F1	1	
PPARG::RXRA	1	
RUNX1	1	1
SMAD3	1	
SOX10	1	
SOX2	1	
SP2	1	
SP4	1	
TCFAP2A	1	2
TFAP4	1	
TLX1::NFIC	1	1
ZFP281	1	

Motif	NPC	Astrocytes
ZFP423	1	
ZIC1	1	
ZNF263	1	
ZNF713	1	
BHLHE40	1	2
CEBPA		1
DLX1		1
ETS1		1
FOXK1		1
GCM1		1
GLIS1		1
GM397		1
HBP1		1
HNF4A		1
HOXC12		1
IRF5		1
MEF2C		1
MEIS1		1
MESP1		1
NEUROD2		1
NFE2		1
NKX2-4		1
NR2E1		1
PKNOX2		1
PLAG1		1
POU3F3		1
RREB1		1
RUNX2		1
RXRA		1
SOX3		1

Motif	NPC	Astrocytes
SOX9		1
SPIC		1
TEAD3		1
YY2		1
ZBTB49		1
ZNF232		1
ZNF75A		1

Chapter 3: General Discussion and Future Directions

3.1 Summary

Characterizing the aberrant transcriptome and epigenome of non-neural cell types, such as astrocytes, in Huntington's disease (HD) is of great importance to understanding the intercellular mechanisms of the disease, and for identifying effective therapeutic strategies to delay or prevent disease progression. Not only has it been well established that HD cells exhibit widespread transcriptional and epigenetic dysregulation, but also recent evidence suggest astrocyte dysfunction contributes to HD pathogenesis (Arregui et al., 2011; Biagioli et al., 2015; Bradford et al., 2009; Giralt et al., 2012; HD iPSC Consortium, 2012; Jia et al., 2012; Labadorf et al., 2015; Lee et al., 2013a; Lopes et al., 2016; Seredenina et al., 2012; Shin et al., 2005; Tong et al., 2014). However, the genomic impact of mHTT expression on astrocytes remains to be investigated. Here, we differentiated pluripotent stem cells (PSCs) from HD non-human primates (NHP) into astrocytes and used a multi -omics approach to characterize chromatin accessibility and transcription across astrocyte differentiation in HD. Our *in vitro* NHP model of astrocyte differentiation provides a unique opportunity to study HD pathogenesis and evaluate potential therapies in an animal model that more closely resembles the neuroanatomy and neurophysiology of humans compared to rodent models of HD.

We demonstrate that HD NHP cells exhibit altered transcription profiles at every stage of astrocyte differentiation, although PSCs showed the most distinct transcriptome of the 4 stages examined. ATAC-seq studies also revealed genome-wide changes in chromatin accessibility across differentiation, with most changes occurring distal to promoters. Promoter-proximal accessibility was overall depleted in HD cells and distal differences in ATAC-seq peaks showed both HD enrichment and depletion. However, PSCs again showed the most unique chromatin

signatures compared to the other stages (neural progenitor cells (NPCs), day 3, and astrocytes). Difference in proximal accessibility did not strongly correlate with gene expression. Differential distal ATAC-seq enrichment displayed progressive trends across the NPC, day 3 and astrocyte samples. When compared to previously defined macaque putative active brain enhancers, distal THSSs overlapped with over 5,000 enhancers (Vermut et al., 2016). Within this subset of enhancers showing differential accessibility, the strong trends from NPC to astrocytes were maintained, suggesting that alerted accessibility signatures begin in NPCs, once cells have committed to a neural lineage.

Differential gene expression determined by RNA-seq experiments identified several pathways previously reported to be dysregulated in HD, including, *p53 signaling*, *apoptosis* and *cell cycle*. As none of these are documented in HD astrocytes specifically, we further examined this dysregulation. We found that over half the genes in the p53 signaling pathway were differentially expressed (DE) in HD cells. Moreover, HD astrocytes showed upregulation of p53 genes compared to WT astrocytes. Gene set enrichment analysis (GSEA) of our differentially expressed genes revealed both apoptosis and cell cycle genes are impacted in HD cells. Since both of these pathways are downstream of p53 signaling, we took a closer look at these pathways. Although the apoptosis pathway demonstrated significant enrichment in HD astrocytes, several cell cycle pathways demonstrated a more significant, inverse enrichment between both NPCs and astrocytes. The genes in these cell cycle related pathways showed decreased expression in HD NPCs and increased expression in HD astrocytes compared to WT cells.

E2F target genes were the most significantly enriched gene set at both the NPC and astrocyte stage, demonstrating the inverse correlation observed for all cell cycle pathways. Interestingly, motifs for several E2F family members showed enrichment in differential promoter-

proximal and distal THSSs across astrocyte differentiation, which corresponded with DE profiles for E2F target genes. Additionally, E2F transcription factors (TFs) themselves were DE in at least one stage of HD differentiation. Although accessibility at E2F target gene promoters was not correlated with expression of these genes, the nearest differential THSS was strongly associated with target gene expression profiles at the NPC, day 3, and astrocyte stages. Changes in E2F target gene expression were observed prior to changes in accessibility in HD cells. Lastly, E2F TFs regulate several epigenetic factors that were found to be DE during astrocyte differentiation, including *EZH2, DNMT1, HMGN3,* and *UHRFL.*

3.2 Discussion and Future Directions

Results from this study provide evidence that HD astrocytes demonstrate global dysregulation that begins early in development and may be driven by different mechanisms than in neuron populations. Global chromatin accessibility was highly differential across astrocyte differentiation. Regions of differential accessibility distal to promoters, including at a set of enhancers, showed strong trends in NPCs, day 3 samples and astrocytes, once cells have committed to a neural lineage. While our findings suggest that altered accessibility at distal, regulatory elements occurs across HD astrocyte differentiation, our analysis was limited by the lack of available annotations for astrocyte-specific enhancers in the macaque genome. Widespread alterations in epigenetic modifications have been documented in HD, but evidence for their association with transcription is conflicted (Biagioli et al., 2015; Giralt et al., 2012; Jiang et al., 2006; Labadorf et al., 2015; Nucifora et al., 2001; Steffan et al., 2000; Thomas et al., 2008; Valor et al., 2013). While some of this may be due to different models and cell populations, it is well established that regulatory elements, such as enhancers, are bound by TFs and regulate gene transcription in a highly context-specific manner (Shlyueva et al., 2014; Vermut et al., 2016).

Epigenomic studies aimed to classify differential accessibility and TF binding at enhancers across neurodevelopment and in different neural cell types may help elucidate the complex interplay of epigenomic and transcriptome dysregulation in HD.

We also report that HD NHP cells show altered transcription at every stage of astrocyte differentiation. It is interesting to note that PSCs showed the most distinct gene expression and chromatin accessibility profiles of the 4 stages, again highlighting that although dysregulation occurs during pluripotency, aberrancies observed in terminally differentiated neural cells are established in the NPC stage, after committing to a neural lineage. While several previously reported pathways were identified to be dysregulated in our NHP model of *in vitro* HD astrocyte differentiation, multiple cell cycle related pathways showed consistent enrichment in our DE genes including *p53 signaling*, *E2F target genes*, *cell cycle pathway* and *apoptosis*. There is some evidence for alterations in the cell cycle in mouse and human models of HD (Basu et al., 2013; Boudreau et al., 2009; Labadorf et al., 2015; Lopes et al., 2016; Lu et al., 2015; Molero et al., 2009; Pelegri et al., 2008; Reynolds et al., 2018). For example, 293 cells expressing mHTT showed cell cycle arrest, mitotic defects, and increased p53 expression (Lu et al., 2015). However, E2F dysregulation and its effect on p53 signaling and the cell cycle during HD pathogenesis has not been examined.

The E2F TFs are master regulators of cell cycle progression and are also reported to regulate apoptosis through activation of the p53 signaling pathway (Iaquinta et al., 2007; Johnson et al., 2006; Ting et al., 2014). Each E2F TFs regulates a specific set of genes in a context-depended manner across neurodevelopment (Dirks et al., 1998; Swiss et al., 2010; Wu et al., 2015). In fact, *E2F1* downregulation occurs during neural differentiation of NPCs (Magri et al., 2014; Nygard et al., 2003), and E2F4 and E2F5 coordinate differentiation into specific neural lineages (Swiss et

al., 2010). Furthermore, upregulation of *E2F1* in terminally differentiated cells leads to aberrant cell cycle re-entry and apoptosis (Dirks et al., 1998; Wu et al., 2015). Interestingly, we observed upregulation of the E2F target gene *CDKN2A*, which is an upstream activator of p53 signaling, and increased p53 signaling, cell cycle, and apoptosis gene expression in our HD astrocytes. Our results suggest that aberrant E2F regulation may activate cell-cycle re-entry and p53-mediated apoptosis in HD astrocytes. Future studies should aim to better characterize the downstream consequences of E2F dysregulation in HD astrocytes.

For example, to investigate cell cycle progression in our NHP model of HD astrogenesis, flow cytometry with propidium iodide (PI) could be employed to measure DNA content in samples at each stage of astrocyte differentiation, but NPCs and astrocytes specifically, to determine the distribution of cells in different phases of the cell cycle. These studies should be performed in parallel with an apoptosis assay, such as flow cytometry with Annexin V or TUNEL, which detects apoptotic DNA fragmentation, to provide insight into any consequences in cell cycle aberrancies. It is worth noting that Caspase 3 was observed to be DE in the later stages of astrocyte differentiation, and given its central role in apoptosis, western blotting for cleaved Caspase 3 should also be performed along with TUNEL or other apoptosis assays.

We also observed global enrichment of E2F TF motifs that corresponded with E2F target gene expression trends across differentiation. However, while promoter accessibility at E2F target genes did not correspond with gene expression, the nearest differential THSS to E2F target gene promoters associated with the expression of the target gene, especially in the astrocyte stage. This finding highlights the idea that these regions of differential distal accessibility may be the site of past or future interactions with E2F promoters during astrocyte differentiation. Further investigations using examining E2F TF binding using ChIP-seq and Hi-C techniques are necessary

to confirm this and elucidate the extent to which aberrant promoter-enhancers interactions contribute to the HD transcriptome and pathogenesis. Furthermore, to better elucidate the role of E2F TFs in HD, knock-down and over expression experiments, starting with E2F1 and E2F7, in parallel with RNA-seq should be performed in our *in vitro* model of astrocyte differentiation. Not only would these experiments complement E2F TF ChIP-seq analyses but would also provide insight into the direct downstream transcriptional consequences of E2F TF dysregulation across HD astrocyte differentiation. Results from studies such as these could be further validated in an *in vivo* HD mouse model, with selective knock-down or over expression of E2F TFs in astrocytes specifically.

Several epigenetic enzymes were among the E2F target genes reported to be DE during HD astrocyte differentiation. For example, modulators of histone and DNA methylation, *EZH2*, *DNMT1*, and *UHRF1*, are dysregulated across differentiation. EZH2 is part of the PRC2 complex and is responsible for trimethylation of H3K27, which is altered during neurodevelopment in HD (Jepsen et al., 2007; Orlando, 2003; Seong et al., 2010; von Schimmelmann et al., 2016). Additionally, DNMT1 methylates DNA in a cell-cycle dependent manner, and UHRF1 binds this methylation along with trimethylation of H3K9 to coordinate and integrate multiple layers of epigenetic information and maintain appropriate transcriptional profiles (Avvakumov et al., 2008; Bostick et al., 2007; Hashimoto et al., 2010; Liu et al., 2013; Zhang et al., 2011). Global alterations in DNA methylation in HD have been reported and were interestingly found to be differential across brain regions (Horvath et al., 2016; Ng et al., 2013), highlighting the need for extensive characterization of HD epigenome and transcriptional dysregulation both in different neural cell types, such as astrocytes, and throughout neurodevelopment. Additionally, H3K9me3 has been reported to be enriched in HD human and mice brains (Lee et al., 2013b; Ryu et al., 2006). Given

their association with less accessible chromatin and our findings that HD promoters showed depleted accessibility, while distal accessibility was largely HD enriched across astrocyte differentiation, it would be interesting to more closely examine the consequences of increased *DNMT1* and *UHRF1* expression on DNA methylation and H3K9me3 dynamics during astrocyte differentiation using bisulfite sequencing and ChIP-seq. Further, it has been demonstrated that inhibiting DNMTs provides a neuroprotective effect in HD mice (Pan et al., 2016). Future studies using DNMT inhibitors in our *in vitro* model of HD astrogenesis would help uncover astrocyte-specific dysregulation of DNA methylation and when paired with bisulfite sequencing and RNA-seq experiments, could identify potential downstream transcriptional consequences of E2F dysregulation of *DNMT1*. In order to fully understand the aberrant interplay between epigenetics and transcription during HD pathogenesis, the integration of multiple layers of epigenetic information needs to be examined and considered. To that end, ChIP-seq experiments investigating H3K9me3 enrichment and UHRF1 binding, both with and without DNMT inhibitor treatment in HD cells would reveal insights into the interplay of multiple epigenetic modifications leading to dysregulation in HD.

Additionally, several DE E2F target genes were chromatin remodelers; most notably, *HMGN3*, which has been shown to be important to astrocyte differentiation and function (Ito et al., 2002; Nagao et al., 2014; West et al., 2004). In contrast with most other E2F target genes, *HMGN3* was upregulated in HD NPCs and downregulated in HD astrocytes. Evidence from heterogeneous *in vitro* and *in vivo* neural populations has suggested that HD cells upregulate neuronal differentiation genes prematurely and show failure to successfully differentiate into mature neurons (HD iPSC Consortium, 2017; Labadorf et al., 2015). In addition to *HMGN3*, we found several other astrocyte genes (*GFAP, APOE*, and *LCN2*) to be significantly overexpressed

early in astrocyte differentiation but become downregulated in HD astrocytes compared to WT cells, providing evidence that this phenomenon is not unique to neuron populations and also occurs during astrogenesis. As neuronal function and survival relies on astrocyte function and WT astrocytes provide neuroprotection that leads to an improved phenotype in HD neurons, targeting of early astrocyte dysfunction may serve as a potential effective therapeutic strategy for HD that warrants further investigation (Allen et al., 2009; Belanger et al., 2011; Bradford et al., 2009; Clarke et al., 2013; Shin et al., 2005).

3.3 Conclusion

In this study, we characterized chromatin accessibility and transcription during *in vitro* astrocyte differentiation using HD NHP cells. Widespread differences in chromatin accessibility suggest aberrant astrogenic signatures are established in the progenitor stage, after committing to a neural lineage. Distal accessibility at regulatory elements such as enhancers showed the strongest trends and warrant further in-depth characterization. Global changes in transcription also occurred across astrocyte differentiation, with multiple cell cycle related pathways impacted. E2F target genes showed significant dysregulation, specifically in HD NPCs through astrocytes, and were upstream of other altered cell cycle pathways, including p53 signaling. We also provide evidence that E2F dysregulation not only affected cell cycle progression, potentially leading to aberrant cell cycle re-entry and activation of the apoptosis pathway, but also impacted the expression of several epigenetic factors, potentially contributing to premature but incomplete astrocyte differentiation in HD cells.

References

Achour, M., Le Gras, S., Keime, C., Parmentier, F., Lejeune, F.X., Boutillier, A.L., Neri, C., Davidson, I., and Merienne, K. (2015). Neuronal identity genes regulated by super-enhancers are preferentially down-regulated in the striatum of Huntington's disease mice. Hum Mol Genet *24*, 3481-3496.

Allen NJ, and BA., B. (2009). Neuroscience: Glia - more than just brain glue. Nature *457*, 675-677.

Arregui, L., Benitez, J.A., Razgado, L.F., Vergara, P., and Segovia, J. (2011). Adenoviral astrocyte-specific expression of BDNF in the striata of mice transgenic for Huntington's disease delays the onset of the motor phenotype. Cell Mol Neurobiol *31*, 1229-1243.

Arteaga-Bracho, E.E., Gulinello, M., Winchester, M.L., Pichamoorthy, N., Petronglo, J.R., Zambrano, A.D., Inocencio, J., De Jesus, C.D., Louie, J.O., Gokhan, S.*, et al.* (2016). Postnatal and adult consequences of loss of huntingtin during development: Implications for Huntington's disease. Neurobiol Dis *96*, 144-155.

Auerbach W, H.M., Hilditch-Maguire P, Wadghiri YZ, Wheeler VC, Cohen SI, Joyner AL, MacDonald ME, Turnbull DH (2001). The HD mutation causes progressive lethal neurological disease in mice expressing reduced levels of huntingtin. Hum Mol Genet *10*, 2515-2523.

Avvakumov, G.V., Walker, J.R., Xue, S., Li, Y., Duan, S., Bronner, C., Arrowsmith, C.H., and Dhe-Paganon, S. (2008). Structural basis for recognition of hemi-methylated DNA by the SRA domain of human UHRF1. Nature *455*, 822-825.

Aylward, E.H., Harrington, D.L., Mills, J.A., Nopoulos, P.C., Ross, C.A., Long, J.D., Liu, D., Westervelt, H.K., Paulsen, J.S., Investigators, P.-H.*, et al.* (2013). Regional atrophy associated with cognitive and motor function in prodromal Huntington disease. J Huntingtons Dis *2*, 477-489.

Aylward, E.H., Liu, D., Nopoulos, P.C., Ross, C.A., Pierson, R.K., Mills, J.A., Long, J.D., Paulsen, J.S., Investigators, P.-H., and Coordinators of the Huntington Study, G. (2012). Striatal volume contributes to the prediction of onset of Huntington disease in incident cases. Biol Psychiatry *71*, 822-828.

Aylward, E.H., Nopoulos, P.C., Ross, C.A., Langbehn, D.R., Pierson, R.K., Mills, J.A., Johnson, H.J., Magnotta, V.A., Juhl, A.R., Paulsen, J.S.*, et al.* (2011). Longitudinal change in regional brain volumes in prodromal Huntington disease. J Neurol Neurosurg Psychiatry *82*, 405-410.

Bae, B.I., Xu, H., Igarashi, S., Fujimuro, M., Agrawal, N., Taya, Y., Hayward, S.D., Moran, T.H., Montell, C., Ross, C.A.*, et al.* (2005). p53 mediates cellular dysfunction and behavioral abnormalities in Huntington's disease. Neuron *47*, 29-41.

Baquet, Z.C., Gorski, J.A., and Jones, K.R. (2004). Early striatal dendrite deficits followed by neuron loss with advanced age in the absence of anterograde cortical brain-derived neurotrophic factor. J Neurosci *24*, 4250-4258.

Barres, B.A. (2008). The mystery and magic of glia: a perspective on their roles in health and disease. Neuron *60*, 430-440.

Basu, M., Bhattacharyya, N.P., and Mohanty, P.K. (2013). Comparison of modules of wild type and mutant Huntingtin and TP53 protein interaction networks: implications in biological processes and functions. PLoS One *8*, e64838.

Bates, S., Phillips, A.C., Clark, P.A., Stott, F., Peters, G., Ludwig, R.L., and Vousden, K.H. (1998). p14ARF links the tumour suppressors RB and p53. Nature *395*, 124-125.

Becanovic, K., Pouladi, M.A., Lim, R.S., Kuhn, A., Pavlidis, P., Luthi-Carter, R., Hayden, M.R., and Leavitt, B.R. (2010). Transcriptional changes in Huntington disease identified using genome-wide expression profiling and cross-platform analysis. Hum Mol Genet *19*, 1438-1452.

Belanger, M., Allaman, I., and Magistretti, P.J. (2011). Brain energy metabolism: focus on astrocyte-neuron metabolic cooperation. Cell Metab *14*, 724-738.

Belanger, M., and Magistretti, P.J. (2009). The role of astroglia in neuroprotection. Dialogues Clin Neurosci *11*, 281-295.

Biagioli, M., Ferrari, F., Mendenhall, E.M., Zhang, Y., Erdin, S., Vijayvargia, R., Vallabh, S.M., Solomos, N., Manavalan, P., Ragavendran, A.*, et al.* (2015). Htt CAG repeat expansion confers pleiotropic gains of mutant huntingtin function in chromatin regulation. Hum Mol Genet *24*, 2442-2457.

Bjorkqvist, M., Wild, E.J., Thiele, J., Silvestroni, A., Andre, R., Lahiri, N., Raibon, E., Lee, R.V., Benn, C.L., Soulet, D.*, et al.* (2008). A novel pathogenic pathway of immune activation detectable before clinical onset in Huntington's disease. J Exp Med *205*, 1869-1877.

Bostick, M., Kim, J.K., Esteve, P.O., Clark, A., Pradhan, S., and Jacobsen, S.E. (2007). UHRF1 plays a role in maintaining DNA methylation in mammalian cells. Science *317*, 1760-1764.

Boudreau, R.L., McBride, J.L., Martins, I., Shen, S., Xing, Y., Carter, B.J., and Davidson, B.L. (2009). Nonallele-specific silencing of mutant and wild-type huntingtin demonstrates therapeutic efficacy in Huntington's disease mice. Mol Ther *17*, 1053-1063.

Bradford, J., Shin, J.Y., Roberts, M., Wang, C.E., Li, X.J., and Li, S. (2009). Expression of mutant huntingtin in mouse brain astrocytes causes age-dependent neurological symptoms. Proc Natl Acad Sci U S A *106*, 22480-22485.

Buenrostro, J.D., Giresi, P.G., Zaba, L.C., Chang, H.Y., Greenleaf, W.J. (2013). Transposition of native chromatin for fast and sensitive epigenomic profiling of open chromatin, DNA-binding proteins and nucleosome position. Nat Methods *10,* 1213-1218.

Carter, R.L., Chen, Y., Kunkanjanawan, T., Xu, Y., Moran, S.P., Putkhao, K., Yang, J., Huang, A.H., Parnpai, R., and Chan, A.W. (2014). Reversal of cellular phenotypes in neural cells derived from Huntington's disease monkey-induced pluripotent stem cells. Stem Cell Reports *3*, 585-593.

Cattaneo, E., Rigamonti, D., Goffredo, D., Zuccato, C., Squitieri, F., and Sipione, S. (2001). Loss of normal huntingtin function: new developments in Huntington's disease research. Trends Neurosci *24*, 182-188.

Cattaneo, E., Zuccato, C., and Tartari, M. (2005). Normal huntingtin function: an alternative approach to Huntington's disease. Nat Rev Neurosci *6*, 919-930.

Chan, A.W., Cheng, P.H., Neumann, A., and Yang, J.J. (2010). Reprogramming Huntington monkey skin cells into pluripotent stem cells. Cell Reprogram *12*, 509-517.

Chan, H.M., and La Thangue, N.B. (2001). p300/CBP proteins: HATs for transcriptional bridges and scaffolds. J Cell Sci *114*, 2363-2373.

Chou, S.Y., Weng, J.Y., Lai, H.L., Liao, F., Sun, S.H., Tu, P.H., Dickson, D.W., and Chern, Y. (2008). Expanded-polyglutamine huntingtin protein suppresses the secretion and production of a chemokine (CCL5/RANTES) by astrocytes. J Neurosci *28*, 3277-3290.

Clarke, L.E., and Barres, B.A. (2013). Emerging roles of astrocytes in neural circuit development. Nat Rev Neurosci *14*, 311-321.

Colombo, J.A., Reisin, H.D. (2004). Interlaminar astroglia of the cerebral cortex: A marker of the primate brain. Brain Res *1006*, 126-131.

Colombo, J.A., Yanez, A., Puissant, V., Lipina, S. (1995). Long, interlaminar astroglial cell processes in the cortex of adult monkeys. J Neurosci Res *40*, 551-556.

Conforti, P., Camnasio, S., Mutti, C., Valenza, M., Thompson, M., Fossale, E., Zeitlin, S., MacDonald, M.E., Zuccato, C., and Cattaneo, E. (2013). Lack of huntingtin promotes neural stem cells differentiation into glial cells while neurons expressing huntingtin with expanded polyglutamine tracts undergo cell death. Neurobiol Dis *50*, 160-170.

Corces, M.R., Trevino, A.E., Hamilton, E.G., Greenside, P.G., Sinnott-Armstrong, N.A., Vesuna, S., Satpathy, A.T., Rubin, A.J., Montine, K.S., Wu, B.*, et al.* (2017). An improved ATAC-seq protocol reduces background and enables interrogation of frozen tissues. Nat Methods *14*, 959-962.

Crook, Z.R., and Housman, D.E. (2013). Surveying the landscape of Huntington's disease mechanisms, measurements, and medicines. J Huntingtons Dis *2*, 405-436.

Crosby, M.E., and Almasan, A. (2004). Opposing roles of E2Fs in cell proliferation and death. Cancer Biol Ther *3*, 1208-1211.

Davies, S.W., Turmaine, M., Cozens, B.A., DiFiglia, M., Sharp, A.H., Ross, C.A., Scherzinger, E., Wanker, E.E., Mangiarini, L., and Bates, G.P. (1997). Formation of neuronal intranuclear inclusions underlies the neurological dysfunction in mice transgenic for the HD mutation. Cell *90*, 537-548.

Deng, Y.P., Albin, R.L., Penney, J.B., Young, A.B., Anderson, K.D., and Reiner, A. (2004). Differential loss of striatal projection systems in Huntington's disease: a quantitative immunohistochemical study. J Chem Neuroanat *27*, 143-164.

Dickey, A.S., Pineda, V.V., Tsunemi, T., Liu, P.P., Miranda, H.C., Gilmore-Hall, S.K., Lomas, N., Sampat, K.R., Buttgereit, A., Torres, M.J.*, et al.* (2016). PPAR-delta is repressed in Huntington's disease, is required for normal neuronal function and can be targeted therapeutically. Nat Med *22*, 37-45.

DiFiglia, M., Sapp, E., Chase, K.O., Davies, S.W., Bates, G.P., Vonsattel, J.P., and Aronin, N. (1997). Aggregation of huntingtin in neuronal intranuclear inclusions and dystrophic neurites in brain. Science *277*, 1990-1993.

Dirks, P.B., Rutka, J.T., Hubbard, S.L., Mondal, S., and Hamel, P.A. (1998). The E2F-family proteins induce distinct cell cycle regulatory factors in p16-arrested, U343 astrocytoma cells. Oncogene *17*, 867-876.

Dobin, A., Davis, C.A., Schlesinger, F., Drenkow, J., Zaleski, C., Jha, S., Batut, P., Chaisson, M., and Gingeras, T.R. (2013). STAR: ultrafast universal RNA-seq aligner. Bioinformatics *29*, 15-21.

Dong, X., Tsuji, J., Labadorf, A., Roussos, P., Chen, J.F., Myers, R.H., Akbarian, S., and Weng, Z. (2015). The Role of H3K4me3 in Transcriptional Regulation Is Altered in Huntington's Disease. PLoS One *10*, e0144398.

Dragatsis, I., Levine, M.S., and Zeitlin, S. (2000). Inactivation of Hdh in the brain and testis results in progressive neurodegeneration and sterility in mice. Nat Genet *26*, 300-306.

Drouet, V., Ruiz, M., Zala, D., Feyeux, M., Auregan, G., Cambon, K., Troquier, L., Carpentier, J., Aubert, S., Merienne, N.*, et al.* (2014). Allele-specific silencing of mutant huntingtin in rodent brain and human stem cells. PLoS One *9*, e99341.

Duff, K., Paulsen, J.S., Beglinger, L.J., Langbehn, D.R., Stout, J.C., and Predict, H.D.I.o.t.H.S.G. (2007). Psychiatric symptoms in Huntington's disease before diagnosis: the predict-HD study. Biol Psychiatry *62*, 1341-1346.

Durr, A., Hahn-Barma, V., Brice, A., Pecheux, C., Dode, C., and Feingold, J. (1999). Homozygosity in Huntington's disease. J Med Genet *36*, 172-173.

Ehrnhoefer, D.E., Skotte, N.H., Ladha, S., Nguyen, Y.T., Qiu, X., Deng, Y., Huynh, K.T., Engemann, S., Nielsen, S.M., Becanovic, K.*, et al.* (2014). p53 increases caspase-6 expression and activation in muscle tissue expressing mutant huntingtin. Hum Mol Genet *23*, 717-729.

Faideau, M., Kim, J., Cormier, K., Gilmore, R., Welch, M., Auregan, G., Dufour, N., Guillermier, M., Brouillet, E., Hantraye, P.*, et al.* (2010). In vivo expression of polyglutamine-expanded huntingtin by mouse striatal astrocytes impairs glutamate transport: a correlation with Huntington's disease subjects. Hum Mol Genet *19*, 3053-3067.

Fossale, E., Seong, I.S., Coser, K.R., Shioda, T., Kohane, I.S., Wheeler, V.C., Gusella, J.F., MacDonald, M.E., and Lee, J.M. (2011). Differential effects of the Huntington's disease CAG mutation in striatum and cerebellum are quantitative not qualitative. Hum Mol Genet *20*, 4258-4267.

Francelle, L., Lotz, C., Outeiro, T., Brouillet, E., and Merienne, K. (2017). Contribution of Neuroepigenetics to Huntington's Disease. Front Hum Neurosci *11*, 17.

Gagnon, K.T., Pendergraff, H.M., Deleavey, G.F., Swayze, E.E., Potier, P., Randolph, J., Roesch, E.B., Chattopadhyaya, J., Damha, M.J., Bennett, C.F.*, et al.* (2010). Allele-selective inhibition of mutant huntingtin expression with antisense oligonucleotides targeting the expanded CAG repeat. Biochemistry *49*, 10166-10178.

Gauthier, L.R., Charrin, B.C., Borrell-Pages, M., Dompierre, J.P., Rangone, H., Cordelieres, F.P., De Mey, J., MacDonald, M.E., Lessmann, V., Humbert, S.*, et al.* (2004). Huntingtin controls neurotrophic support and survival of neurons by enhancing BDNF vesicular transport along microtubules. Cell *118*, 127-138.

Genetic Modifiers of Huntington’s Disease (GeM-HD) Consortium. (2015). Identification of Genetic Factors that Modify Clinical Onset of Huntington’s Disease. Cell *162*, 516–526.

Gharami, K., Xie, Y., An, J.J., Tonegawa, S., and Xu, B. (2008). Brain-derived neurotrophic factor over-expression in the forebrain ameliorates Huntington's disease phenotypes in mice. J Neurochem *105*, 369-379.

Gibbs, M.E., Hutchinson, D., and Hertz, L. (2008). Astrocytic involvement in learning and memory consolidation. Neurosci Biobehav Rev *32*, 927-944.

Gil, J.M., and Rego, A.C. (2008). Mechanisms of neurodegeneration in Huntington's disease. Eur J Neurosci *27*, 2803-2820.

Giralt, A., Puigdellivol, M., Carreton, O., Paoletti, P., Valero, J., Parra-Damas, A., Saura, C.A., Alberch, J., and Gines, S. (2012). Long-term memory deficits in Huntington's disease are associated with reduced CBP histone acetylase activity. Hum Mol Genet *21*, 1203-1216.

Godin, J.D., Colombo, K., Molina-Calavita, M., Keryer, G., Zala, D., Charrin, B.C., Dietrich, P., Volvert, M.L., Guillemot, F., Dragatsis, I.*, et al.* (2010). Huntingtin is required for mitotic spindle orientation and mammalian neurogenesis. Neuron *67*, 392-406.

Goehler, H., Lalowski, M., Stelzl, U., Waelter, S., Stroedicke, M., Worm, U., Droege, A., Lindenberg, K.S., Knoblich, M., Haenig, C.*, et al.* (2004). A protein interaction network

links GIT1, an enhancer of huntingtin aggregation, to Huntington's disease. Mol Cell *15*, 853-865.

Goldberg, Y.P., Telenius, H., and Hayden, M.R. (1994). The molecular genetics of Huntington's disease. Curr Opin Neurol *7*, 325-332.

Gomez-Tortosa, E., MacDonald, M.E., Friend, J.C., Taylor, S.A., Weiler, L.J., Cupples, L.A., Srinidhi, J., Gusella, J.F., Bird, E.D., Vonsattel, J.P.*, et al.* (2001). Quantitative neuropathological changes in presymptomatic Huntington's disease. Ann Neurol *49*, 29-34.

Gourine, A.V., Kasymov, V., Marina, N., Tang, F., Figueiredo, M.F., Lane, S., Teschemacher, A.G., Spyer, K.M., Deisseroth, K., and Kasparov, S. (2010). Astrocytes control breathing through pH-dependent release of ATP. Science *329*, 571-575.

Grant, C.E., Bailey, T.L., and Noble, W.S. (2011). FIMO: scanning for occurrences of a given motif. Bioinformatics *27*, 1017-1018.

Hadzi, T.C., Hendricks, A.E., Latourelle, J.C., Lunetta, K.L., Cupples, L.A., Gillis, T., Mysore, J.S., Gusella, J.F., MacDonald, M.E., Myers, R.H.*, et al.* (2012). Assessment of cortical and striatal involvement in 523 Huntington disease brains. Neurology *79*, 1708-1715.

Halassa, M.M., Florian, C., Fellin, T., Munoz, J.R., Lee, S.Y., Abel, T., Haydon, P.G., and Frank, M.G. (2009). Astrocytic modulation of sleep homeostasis and cognitive consequences of sleep loss. Neuron *61*, 213-219.

Halliday, G.M., McRitchie, D.A., Macdonald, V., Double, K.L., Trent, R.J., and McCusker, E. (1998). Regional specificity of brain atrophy in Huntington's disease. Exp Neurol *154*, 663-672.

Hardingham, G.E., and Bading, H. (2010). Synaptic versus extrasynaptic NMDA receptor signalling: implications for neurodegenerative disorders. Nat Rev Neurosci *11*, 682-696.

Harjes, P., and Wanker, E.E. (2003). The hunt for huntingtin function: interaction partners tell many different stories. Trends Biochem Sci *28*, 425-433.

Hashimoto, H., Vertino, P.M., and Cheng, X. (2010). Molecular coupling of DNA methylation and histone methylation. Epigenomics *2*, 657-669.

HD iPSC Consortium (2012). Induced Pluripotent Stem Cells from Patients with Huntington's Disease Show CAG-Repeat-Expansion-Associated Phenotypes. Cell Stem Cell *11*, 264-278.

HD iPSC Consortium (2017). Developmental alterations in Huntington's disease neural cells and pharmacological rescue in cells and mice. Nat Neurosci *20*, 648-660.

He, J., Mai, J., Li, Y., Chen, L., Xu, H., Zhu, X., and Pan, Q. (2017). miR-597 inhibits breast cancer cell proliferation, migration and invasion through FOSL2. Oncol Rep *37*, 2672-2678.

Hedreen, J.C., and Folstein, S.E. (1995). Early loss of neostriatal striosome neurons in Huntington's disease. J Neuropathol Exp Neurol *54*, 105-120.

Hervas-Corpion, I., Guiretti, D., Alcaraz-Iborra, M., Olivares, R., Campos-Caro, A., Barco, A., and Valor, L.M. (2018). Early alteration of epigenetic-related transcription in Huntington's disease mouse models. Sci Rep *8*, 9925.

Hinton, S.C., Paulsen, J.S., Hoffmann, R.G., Reynolds, N.C., Zimbelman, J.L., and Rao, S.M. (2007). Motor timing variability increases in preclinical Huntington's disease patients as estimated onset of motor symptoms approaches. J Int Neuropsychol Soc *13*, 539-543.

Hodges, A., Strand, A.D., Aragaki, A.K., Kuhn, A., Sengstag, T., Hughes, G., Elliston, L.A., Hartog, C., Goldstein, D.R., Thu, D.*, et al.* (2006). Regional and cellular gene expression changes in human Huntington's disease brain. Hum Mol Genet *15*, 965-977.

Hoglinger, G.U., Breunig, J.J., Depboylu, C., Rouaux, C., Michel, P.P., Alvarez-Fischer, D., Boutillier, A.L., Degregori, J., Oertel, W.H., Rakic, P.*, et al.* (2007). The pRb/E2F cell-cycle pathway mediates cell death in Parkinson's disease. Proc Natl Acad Sci U S A *104*, 3585-3590.

Horvath, S., Langfelder, P., Kwak, S., Aaronson, J., Rosinski, J., Vogt, T.F., Eszes, M., Faull, R.L., Curtis, M.A., Waldvogel, H.J.*, et al.* (2016). Huntington's disease accelerates epigenetic aging of human brain and disrupts DNA methylation levels. Aging (Albany NY) *8*, 1485-1512.

Housman, D. (1995). Gain of glutamines, gain of function?. Nat Genet *10*, 3-4.

Hsiao, H.Y., Chen, Y.C., Chen, H.M., Tu, P.H., and Chern, Y. (2013). A critical role of astrocyte-mediated nuclear factor-kappaB-dependent inflammation in Huntington's disease. Hum Mol Genet *22*, 1826-1842.

Hu, J., Dodd, D.W., Hudson, R.H., and Corey, D.R. (2009). Cellular localization and allele-selective inhibition of mutant huntingtin protein by peptide nucleic acid oligomers containing the fluorescent nucleobase [bis-o-(aminoethoxy)phenyl]pyrrolocytosine. Bioorg Med Chem Lett *19*, 6181-6184.

Iaquinta, P.J., and Lees, J.A. (2007). Life and death decisions by the E2F transcription factors. Curr Opin Cell Biol *19*, 649-657.

Illuzzi, J.L., Vickers, C.A., and Kmiec, E.B. (2011). Modifications of p53 and the DNA damage response in cells expressing mutant form of the protein huntingtin. J Mol Neurosci *45*, 256-268.

Ito, Y., and Bustin, M. (2002). Immunohistochemical Localization of the Nucleosome-Binding Protein HMGN3 in Mouse Brain. J Histochem Cytochem *50(9)*, 1273-1275.

Jansen, A.H., van Hal, M., Op den Kelder, I.C., Meier, R.T., de Ruiter, A.A., Schut, M.H., Smith, D.L., Grit, C., Brouwer, N., Kamphuis, W.*, et al.* (2017). Frequency of nuclear mutant huntingtin inclusion formation in neurons and glia is cell-type-specific. Glia *65*, 50-61.

Jepsen, K., Solum, D., Zhou, T., McEvilly, R.J., Kim, H.J., Glass, C.K., Hermanson, O., and Rosenfeld, M.G. (2007). SMRT-mediated repression of an H3K27 demethylase in progression from neural stem cell to neuron. Nature *450*, 415-419.

Jia, H., Morris, C.D., Williams, R.M., Loring, J.F., and Thomas, E.A. (2014). HDAC inhibition imparts beneficial transgenerational effects in Huntington's disease mice via altered DNA and histone methylation. Proc Natl Acad Sci U S A *112*, E56-64.

Jia, H., Pallos, J., Jacques, V., Lau, A., Tang, B., Cooper, A., Syed, A., Purcell, J., Chen, Y., Sharma, S.*, et al.* (2012). Histone deacetylase (HDAC) inhibitors targeting HDAC3 and HDAC1 ameliorate polyglutamine-elicited phenotypes in model systems of Huntington's disease. Neurobiol Dis *46*, 351-361.

Jiang, H., Poirier, M.A., Liang, Y., Pei, Z., Weiskittel, C.E., Smith, W.W., DeFranco, D.B., and Ross, C.A. (2006). Depletion of CBP is directly linked with cellular toxicity caused by mutant huntingtin. Neurobiol Dis *23*, 543-551.

Jin, J., Cheng, Y., Zhang, Y., Wood, W., Peng, Q., Hutchison, E., Mattson, M.P., Becker, K.G., and Duan, W. (2012). Interrogation of brain miRNA and mRNA expression profiles

reveals a molecular regulatory network that is perturbed by mutant huntingtin. J Neurochem *123*, 477-490.

Johnson, D.G., and Degregori, J. (2006). Putting the Oncogenic and Tumor Suppressive Activities of E2F into Context. Curr Mol Med *6*, 731-738.

Jordan-Sciutto, K.L., Dorsey, R., Chalovich, E.M., Hammond, R.R., and Achim, C.L. (2003). Expression patterns of retinoblastoma protein in Parkinson disease. J Neuropathol Exp Neurol *62*, 68-74.

Jordan-Sciutto, K.L., Malaiyandi, L.M., and Bowser, R. (2002). Altered distribution of cell cycle transcriptional regulators during Alzheimer disease. J Neuropathol Exp Neurol *61*, 358-367.

Khakh, B.S., Beaumont, V., Cachope, R., Munoz-Sanjuan, I., Goldman, S.A., and Grantyn, R. (2017). Unravelling and Exploiting Astrocyte Dysfunction in Huntington's Disease. Trends Neurosci *40*, 422-437.

Kim, D., Pertea, G., Trapnell, C., Pimentel, H., Kelley, R., and Salzberg, S.L. (2013). TopHat2: accurate alignment of transcriptomes in the presence of insertions, deletions and gene fusions. Genome Biol *14*.

Kocerha, J., Xu, Y., Prucha, M.S., Zhao, D., and Chan, A.W. (2014). microRNA-128a dysregulation in transgenic Huntington's disease monkeys. Mol Brain *7*, 46.

Labadorf, A., Hoss, A.G., Lagomarsino, V., Latourelle, J.C., Hadzi, T.C., Bregu, J., MacDonald, M.E., Gusella, J.F., Chen, J.F., Akbarian, S.*, et al.* (2015). RNA Sequence Analysis of Human Huntington Disease Brain Reveals an Extensive Increase in Inflammatory and Developmental Gene Expression. PLoS One *10*, e0143563.

Labbadia, J., and Morimoto, R.I. (2013). Huntington's disease: underlying molecular mechanisms and emerging concepts. Trends Biochem Sci *38*, 378-385.

Landles, C., and Bates, G.P. (2004). Huntingtin and the molecular pathogenesis of Huntington's disease. Fourth in molecular medicine review series. EMBO Rep *5*, 958-963.

Langbehn, D.R., Hayden, M.R., Paulsen, J.S., and and the, P.-H.D.I.o.t.H.S.G. (2010). CAG-repeat length and the age of onset in Huntington disease (HD): a review and validation study of statistical approaches. Am J Med Genet B Neuropsychiatr Genet *153B*, 397-408.

Langfelder, P., Cantle, J.P., Chatzopoulou, D., Wang, N., Gao, F., Al-Ramahi, I., Lu, X.H., Ramos, E.M., El-Zein, K., Zhao, Y.*, et al.* (2016). Integrated genomics and proteomics define huntingtin CAG length-dependent networks in mice. Nat Neurosci *19*, 623-633.

Langmead, B., and Salzberg, S.L. (2012). Fast gapped-read alignment with Bowtie 2. Nat Methods *9*, 357-359.

Laowtammathron, C., Cheng, E., Cheng, P.H., Snyder, B.R., Yang, S.H., Johnson, Z., Lorthongpanich, C., Kuo, H.C., Parnpai, R., and Chan, A.W. (2010). Monkey hybrid stem cells develop cellular features of Huntington's disease. BMC Cell Biol *11*, 12.

Lee, J., Hwang, Y.J., Kim, K.Y., Kowall, N.W., and Ryu, H. (2013a). Epigenetic mechanisms of neurodegeneration in Huntington's disease. Neurotherapeutics *10*, 664-676.

Lee, J., Hwang, Y.J., Shin, J.Y., Lee, W.C., Wie, J., Kim, K.Y., Lee, M.Y., Hwang, D., Ratan, R.R., Pae, A.N.*, et al.* (2013b). Epigenetic regulation of cholinergic receptor M1 (CHRM1) by histone H3K9me3 impairs Ca(2+) signaling in Huntington's disease. Acta Neuropathol *125*, 727-739.

Lee, J.K., Mathews, K., Schlaggar, B., Perlmutter, J., Paulsen, J.S., Epping, E., Burmeister, L., and Nopoulos, P. (2012). Measures of growth in children at risk for Huntington disease. Neurology *79*, 668-674.

Li, S., and Li, X.J. (2006). Multiple pathways contribute to the pathogenesis of Huntington disease. Mol Neurodegener *1*, 19.

Li, S.H., Schilling, G., Young, W.S., 3rd, Li, X.J., Margolis, R.L., Stine, O.C., Wagster, M.V., Abbott, M.H., Franz, M.L., Ranen, N.G.*, et al.* (1993). Huntington's disease gene (IT15) is widely expressed in human and rat tissues. Neuron *11*, 985-993.

Liberzon, A., Subramanian, A., Pinchback, R., Thorvaldsdottir, H., Tamayo, P., and Mesirov, J.P. (2011). Molecular signatures database (MSigDB) 3.0. Bioinformatics *27*, 1739-1740.

Lin, C.H., Tallaksen-Greene, S., Chien, W.M., Cearley, J.A., Jackson, W.S., Crouse, A.B., Ren, S., Li, X.J., Albin, R.L., and Detloff, P.J. (2001). Neurological abnormalities in a knock-in mouse model of Huntington's disease. Hum Mol Genet *10*, 137-144.

Ling, L., Zhang, S.H., Zhi, L.D., Li, H., Wen, Q.K., Li, G., and Zhang, W.J. (2018). MicroRNA-30e promotes hepatocyte proliferation and inhibits apoptosis in cecal ligation and puncture-induced sepsis through the JAK/STAT signaling pathway by binding to FOSL2. Biomed Pharmacother *104*, 411-419.

Liu, X., Gao, Q., Li, P., Zhao, Q., Zhang, J., Li, J., Koseki, H., and Wong, J. (2013). UHRF1 targets DNMT1 for DNA methylation through cooperative binding of hemi-methylated DNA and methylated H3K9. Nat Commun *4*, 1563.

Lobsiger, C.S., and Cleveland, D.W. (2007). Glial cells as intrinsic components of non-cell-autonomous neurodegenerative disease. Nat Neurosci *10*, 1355-1360.

Lopes, C., Aubert, S., Bourgois-Rocha, F., Barnat, M., Rego, A.C., Deglon, N., Perrier, A.L., and Humbert, S. (2016). Dominant-Negative Effects of Adult-Onset Huntingtin Mutations Alter the Division of Human Embryonic Stem Cells-Derived Neural Cells. PLoS One *11*, e0148680.

Love, M.I., Huber, W., and Anders, S. (2014). Moderated estimation of fold change and dispersion for RNA-seq data with DESeq2. Genome Biol *15*, 550.

Lu, M., Boschetti, C., and Tunnacliffe, A. (2015). Long Term Aggresome Accumulation Leads to DNA Damage, p53-dependent Cell Cycle Arrest, and Steric Interference in Mitosis. J Biol Chem *290*, 27986-28000.

Luthi-Carter, R., Strand, A., Peters, N.L., Solano, S.M., Hollingsworth, Z.R., Menon, A.S., Frey, A.S., Spektor, B.S., Penney, E.B., Schilling, G.*, et al.* (2000). Decreased expression of striatal signaling genes in a mouse model of Huntington's disease. Hum Mol Genet *9*, 1259-1271.

Lynch, G., Kramar, E.A., Rex, C.S., Jia, Y., Chappas, D., Gall, C.M., and Simmons, D.A. (2007). Brain-derived neurotrophic factor restores synaptic plasticity in a knock-in mouse model of Huntington's disease. J Neurosci *27*, 4424-4434.

MacDonald, M.E., Barnes, G., Srinidhi, J., Duyao, M.P., Ambrose, C.M., Myers, R.H., Gray, J., Conneally, P.M., Young, A., Penney, J.*, et al.* (1993). Gametic but not somatic instability of CAG repeat length in Huntington's disease. J Med Genet *30*, 982-986.

Machanick, P., and Bailey, T.L. (2011). MEME-ChIP: motif analysis of large DNA datasets. Bioinformatics *27*, 1696-1697.

Magri, L., Swiss, V.A., Jablonska, B., Lei, L., Pedre, X., Walsh, M., Zhang, W., Gallo, V., Canoll, P., and Casaccia, P. (2014). E2F1 coregulates cell cycle genes and chromatin components during the transition of oligodendrocyte progenitors from proliferation to differentiation. J Neurosci *34*, 1481-1493.

Majumder, A., Dhara, S.K., Swetenburg, R., Mithani, M., Cao, K., Medrzycki, M., Fan, Y., and Stice, S.L. (2013). Inhibition of DNA methyltransferases and histone deacetylases induces astrocytic differentiation of neural progenitors. Stem Cell Res *11*, 574-586.

Mangiarini, L., Sathasivam, K., Seller, M., Cozens, B., Harper, A., Hetherington, C., Lawton, M., Trottier, Y., Lehrach, H., Davies, S.W.*, et al.* (1996). Exon 1 of the HD gene with an expanded CAG repeat is sufficient to cause a progressive neurological phenotype in transgenic mice. Cell *87*, 493-506.

Maragakis, N.J., and Rothstein, J.D. (2006). Mechanisms of Disease: astrocytes in neurodegenerative disease. Nat Clin Pract Neurol *2*, 679-689.

Marcel, V., Nguyen Van Long, F., and Diaz, J.J. (2018). 40 Years of Research Put p53 in Translation. Cancers (Basel) *10*.

Marco, S., Giralt, A., Petrovic, M.M., Pouladi, M.A., Martinez-Turrillas, R., Martinez-Hernandez, J., Kaltenbach, L.S., Torres-Peraza, J., Graham, R.K., Watanabe, M.*, et al.* (2013). Suppressing aberrant GluN3A expression rescues synaptic and behavioral impairments in Huntington's disease models. Nat Med *19*, 1030-1038.

Marmorstein, R., and Zhou, M.M. (2014). Writers and readers of histone acetylation: structure, mechanism, and inhibition. Cold Spring Harb Perspect Biol *6*, a018762.

McFarland, K.N., Das, S., Sun, T.T., Leyfer, D., Xia, E., Sangrey, G.R., Kuhn, A., Luthi-Carter, R., Clark, T.W., Sadri-Vakili, G.*, et al.* (2012). Genome-wide histone acetylation is altered in a transgenic mouse model of Huntington's disease. PLoS One *7*, e41423.

McMurray, C.T. (2010). Mechanisms of trinucleotide repeat instability during human development. Nat Rev Genet *11*, 786-799.

Milnerwood, A.J., Cummings, D.M., Dallerac, G.M., Brown, J.Y., Vatsavayai, S.C., Hirst, M.C., Rezaie, P., and Murphy, K.P. (2006). Early development of aberrant synaptic plasticity in a mouse model of Huntington's disease. Hum Mol Genet *15*, 1690-1703.

Milnerwood, A.J., Gladding, C.M., Pouladi, M.A., Kaufman, A.M., Hines, R.M., Boyd, J.D., Ko, R.W., Vasuta, O.C., Graham, R.K., Hayden, M.R.*, et al.* (2010). Early increase in extrasynaptic NMDA receptor signaling and expression contributes to phenotype onset in Huntington's disease mice. Neuron *65*, 178-190.

Molero, A.E., Arteaga-Bracho, E.E., Chen, C.H., Gulinello, M., Winchester, M.L., Pichamoorthy, N., Gokhan, S., Khodakhah, K., and Mehler, M.F. (2016). Selective expression of mutant huntingtin during development recapitulates characteristic features of Huntington's disease. Proc Natl Acad Sci U S A *113*, 5736-5741.

Molero, A.E., Gokhan, S., Gonzalez, S., Feig, J.L., Alexandre, L.C., and Mehler, M.F. (2009). Impairment of developmental stem cell-mediated striatal neurogenesis and pluripotency genes in a knock-in model of Huntington's disease. Proc Natl Acad Sci U S A *106*, 21900-21905.

Moroni, M.C., Hickman, E.S., Lazzerini Denchi, E., Caprara, G., Colli, E., Cecconi, F., Muller, H., and Helin, K. (2001). Apaf-1 is a transcriptional target for E2F and p53. Nat Cell Biol *3*, 552-558.

Nagao, M., Lanjakornsiripan, D., Itoh, Y., Kishi, Y., Ogata, T., Gotoh, Y. (2014). High mobility group nucleosome-binding family proteins promote astrocyte differentiation of neural precursor cells. Stem Cells *32*, 2983–2997.

Nasir, J., Floresco, S.B., O'Kusky, J.R., Diewert, V.M., Richman, J.M., Zeisler, J., Borowski, A., Marth, J.D., Phillips, A.G., and Hayden, M.R. (1995). Targeted disruption of the

Huntington's disease gene results in embryonic lethality and behavioral and morphological changes in heterozygotes. Cell *81*, 811-823.

Ng, C.W., Yildirim, F., Yap, Y.S., Dalin, S., Matthews, B.J., Velez, P.J., Labadorf, A., Housman, D.E., and Fraenkel, E. (2013). Extensive changes in DNA methylation are associated with expression of mutant huntingtin. Proc Natl Acad Sci U S A *110*, 2354-2359.

Nguyen, G.D., Gokhan, S., Molero, A.E., and Mehler, M.F. (2013). Selective roles of normal and mutant huntingtin in neural induction and early neurogenesis. PLoS One *8*, e64368.

Nopoulos, P., Magnotta, V.A., Mikos, A., Paulson, H., Andreasen, N.C., and Paulsen, J.S. (2007). Morphology of the cerebral cortex in preclinical Huntington's disease. Am J Psychiatry *164*, 1428-1434.

Nucifora, F.C., Jr., Sasaki, M., Peters, M.F., Huang, H., Cooper, J.K., Yamada, M., Takahashi, H., Tsuji, S., Troncoso, J., Dawson, V.L.*, et al.* (2001). Interference by huntingtin and atrophin-1 with cbp-mediated transcription leading to cellular toxicity. Science *291*, 2423-2428.

Nygard, M., Wahlstrom, G.M., Gustafsson, M.V., Tokumoto, Y.M., and Bondesson, M. (2003). Hormone-dependent repression of the E2F-1 gene by thyroid hormone receptors. Mol Endocrinol *17*, 79-92.

O'Kusky, J.R., Nasir, J., Cicchetti, F., Parent, A., and Hayden, M.R. (1999). Neuronal degeneration in the basal ganglia and loss of pallido-subthalamic synapses in mice with targeted disruption of the Huntington's disease gene. Brain Res *818*, 468-479.

Oberheim, N.A., Takano, T., Han, X., He, W., Lin, J.H., Wang, F., Xu, Q., Wyatt, J.D., Pilcher, W., Ojemann, J.G.*, et al.* (2009). Uniquely hominid features of adult human astrocytes. J Neurosci *29*, 3276-3287.

Okamoto, S., Pouladi, M.A., Talantova, M., Yao, D., Xia, P., Ehrnhoefer, D.E., Zaidi, R., Clemente, A., Kaul, M., Graham, R.K.*, et al.* (2009). Balance between synaptic versus extrasynaptic NMDA receptor activity influences inclusions and neurotoxicity of mutant huntingtin. Nat Med *15*, 1407-1413.

Oliveira, J.M. (2010). Mitochondrial bioenergetics and dynamics in Huntington's disease: tripartite synapses and selective striatal degeneration. J Bioenerg Biomembr *42*, 227-234.

Ordway, J.M., Tallaksen-Greene, S., Gutekunst, C.A., Bernstein, E.M., Cearley, J.A., Wiener, H.W., Dure, L.S.t., Lindsey, R., Hersch, S.M., Jope, R.S.*, et al.* (1997). Ectopically expressed CAG repeats cause intranuclear inclusions and a progressive late onset neurological phenotype in the mouse. Cell *91*, 753-763.

Orlando, V. (2003). Polycomb, epigenomes, and control of cell identity. Cell *112*, 599-606.

Orr, H.T., and Zoghbi, H.Y. (2007). Trinucleotide repeat disorders. Annu Rev Neurosci *30*, 575-621.

Pan, Y., Daito, T., Sasaki, Y., Chung, Y.H., Xing, X., Pondugula, S., Swamidass, S.J., Wang, T., Kim, A.H., and Yano, H. (2016). Inhibition of DNA Methyltransferases Blocks Mutant Huntingtin-Induced Neurotoxicity. Scientific Reports *6*.

Paulsen, J.S., Long, J.D., Johnson, H.J., Aylward, E.H., Ross, C.A., Williams, J.K., Nance, M.A., Erwin, C.J., Westervelt, H.J., Harrington, D.L.*, et al.* (2014). Clinical and Biomarker Changes in Premanifest Huntington Disease Show Trial Feasibility: A Decade of the PREDICT-HD Study. Front Aging Neurosci *6*, 78.

Payseur, B.A., Jing, P., Haasl, R.J. (2011). A genomic portrait of human microsatellite variation. Mol Biol Evol *28*, 303-312.

Pelegri, C., Duran-Vilaregut, J., del Valle, J., Crespo-Biel, N., Ferrer, I., Pallas, M., Camins, A., Vilaplana, J. (2008). Cell cycle activation in striatal neurons from Huntington's disease patients and rats treated with 3-nitropropionic acid. Int J Dev Neurosci *26*, 665-671.

Phatnani, H., and Maniatis, T. (2015). Astrocytes in neurodegenerative disease. Cold Spring Harb Perspect Biol *7*.

Pontarin, G., Ferraro, P., Bee, L., Reichard, P., Bianchi, V. (2012). Mammalian ribonucleotide reductase subunit p53R2 is required for mitochondrial DNA replication and DNA repair in quiescent cells. Proc Natl Acad Sci USA *109*, 13302–13307.

Ratovitski, T., Arbez, N., Stewart, J.C., Chighladze, E., and Ross, C.A. (2015). PRMT5-mediated symmetric arginine dimethylation is attenuated by mutant huntingtin and is impaired in Huntington's disease (HD). Cell Cycle *14*, 1716-1729.

Raymond, L.A., Andre, V.M., Cepeda, C., Gladding, C.M., Milnerwood, A.J., and Levine, M.S. (2011). Pathophysiology of Huntington's disease: time-dependent alterations in synaptic and receptor function. Neuroscience *198*, 252-273.

Reynolds, R.H., Petersen, M.H., Willert, C.W., Heinrich, M., Nymann, N., Dall, M., Treebak, J.T., Bjorkqvist, M., Silahtaroglu, A., Hasholt, L.*, et al.* (2018). Perturbations in the p53/miR-34a/SIRT1 pathway in the R6/2 Huntington's disease model. Mol Cell Neurosci *88*, 118-129.

Ritch, J.J., Valencia, A., Alexander, J., Sapp, E., Gatune, L., Sangrey, G.R., Sinha, S., Scherber, C.M., Zeitlin, S., Sadri-Vakili, G.*, et al.* (2012). Multiple phenotypes in Huntington disease mouse neural stem cells. Mol Cell Neurosci *50*, 70-81.

Rosas, H.D., Salat, D.H., Lee, S.Y., Zaleta, A.K., Pappu, V., Fischl, B., Greve, D., Hevelone, N., and Hersch, S.M. (2008). Cerebral cortex and the clinical expression of Huntington's disease: complexity and heterogeneity. Brain *131*, 1057-1068.

Ross, C.A., and Tabrizi, S.J. (2011). Huntington's disease: from molecular pathogenesis to clinical treatment. The Lancet Neurology *10*, 83-98.

Ruzo, A., Croft, G.F., Metzger, J.J., Galgoczi, S., Gerber, L.J., Pellegrini, C., Wang, H., Jr., Fenner, M., Tse, S., Marks, A.*, et al.* (2018). Chromosomal instability during neurogenesis in Huntington's disease. Development *145*.

Ryu, H., Lee, J., Hagerty, S.W., Soh, B.Y., McAlpin, S.E., Cormier, K.A., Smith, K.M., and Ferrante, R.J. (2006). ESET/SETDB1 gene expression and histone H3 (K9) trimethylation in Huntington's disease. Proc Natl Acad Sci U S A *103*, 19176-19181.

Sadri-Vakili, G., Bouzou, B., Benn, C.L., Kim, M.O., Chawla, P., Overland, R.P., Glajch, K.E., Xia, E., Qiu, Z., Hersch, S.M.*, et al.* (2007). Histones associated with downregulated genes are hypo-acetylated in Huntington's disease models. Hum Mol Genet *16*, 1293-1306.

Sapp E1, S.C., Chase K, Bhide PG, Young AB, Penney J, Vonsattel JP, Aronin N, DiFiglia M. (1997). Huntingtin localization in brains of normal and Huntington's disease patients. Ann Neurol *42*, 604-612.

Saudou, F., Finkbeiner, S., Devys, D., and Greenberg, M.E. (1998). Huntingtin acts in the nucleus to induce apoptosis but death does not correlate with the formation of intranuclear inclusions. Cell *95*, 55-66.

Saudou, F., and Humbert, S. (2016). The Biology of Huntingtin. Neuron *89*, 910-926.

Scherzinger, E., Lurz, R., Turmaine, M., Mangiarini, L., Hollenbach, B., Hasenbank, R., Bates, G.P., Davies, S.W., Lehrach, H., and Wanker, E.E. (1997). Huntingtin-encoded

polyglutamine expansions form amyloid-like protein aggregates in vitro and in vivo. Cell *90*, 549-558.

Schippling, S., Schneider, S.A., Bhatia, K.P., Munchau, A., Rothwell, J.C., Tabrizi, S.J., and Orth, M. (2009). Abnormal motor cortex excitability in preclinical and very early Huntington's disease. Biol Psychiatry *65*, 959-965.

Seong, I.S., Woda, J.M., Song, J.J., Lloret, A., Abeyrathne, P.D., Woo, C.J., Gregory, G., Lee, J.M., Wheeler, V.C., Walz, T.*, et al.* (2010). Huntingtin facilitates polycomb repressive complex 2. Hum Mol Genet *19*, 573-583.

Seredenina, T., and Luthi-Carter, R. (2012). What have we learned from gene expression profiles in Huntington's disease? Neurobiol Dis *45*, 83-98.

Shao, J., and Diamond, M.I. (2007). Polyglutamine diseases: emerging concepts in pathogenesis and therapy. Human Molecular Genetics *16*, R115-R123.

Shao, Z., Zhang, Y., Yuan, G.C., Orkin, S.H., and Waxman, D.J. (2012). MAnorm: a robust model for quantitative comparison of ChIP-Seq data sets. Genome Biol *13*, R16.

Sharp, A.H., Loev, S.J., Schilling, G., Li, S.H., Li, X.J., Bao, J., Wagster, M.V., Kotzuk, J.A., Steiner, J.P., Lo, A.*, et al.* (1995). Widespread expression of Huntington's disease gene (IT15) protein product. Neuron *14*, 1065-1074.

Shin, J.Y., Fang, Z.H., Yu, Z.X., Wang, C.E., Li, S.H., and Li, X.J. (2005). Expression of mutant huntingtin in glial cells contributes to neuronal excitotoxicity. J Cell Biol *171*, 1001-1012.

Shlyueva, D., Stampfel, G., and Stark, A. (2014). Transcriptional enhancers: from properties to genome-wide predictions. Nat Rev Genet *15*, 272-286.

Sica, R.E. (2015). Could astrocytes be the primary target of an offending agent causing the primary degenerative diseases of the human central nervous system? A hypothesis. Med Hypotheses *84*, 481-489.

Sieradzan, K.A., Mechan, A.O., Jones, L., Wanker, E.E., Nukina, N., and Mann, D.M. (1999). Huntington's disease intranuclear inclusions contain truncated, ubiquitinated huntingtin protein. Exp Neurol *156*, 92-99.

Skotte, N.H., Andersen, J.V., Santos, A., Aldana, B.I., Willert, C.W., Norremolle, A., Waagepetersen, H.S., and Nielsen, M.L. (2018). Integrative Characterization of the R6/2 Mouse Model of Huntington's Disease Reveals Dysfunctional Astrocyte Metabolism. Cell Rep *23*, 2211-2224.

Snell, R.G., MacMillan, J.C., Cheadle, J.P., Fenton, I., Lazarou, L.P., Davies, P., MacDonald, M.E., Gusella, J.F., Harper, P.S., and Shaw, D.J. (1993). Relationship between trinucleotide repeat expansion and phenotypic variation in Huntington's disease. Nat Genet *4*, 393-397.

Sofroniew, M.V. (2009). Molecular dissection of reactive astrogliosis and glial scar formation. Trends Neurosci *32*, 638-647.

Solomon, A.C., Stout, J.C., Johnson, S.A., Langbehn, D.R., Aylward, E.H., Brandt, J., Ross, C.A., Beglinger, L., Hayden, M.R., Kieburtz, K.*, et al.* (2007). Verbal episodic memory declines prior to diagnosis in Huntington's disease. Neuropsychologia *45*, 1767-1776.

Steffan, J.S., Kazantsev, A., Spasic-Boskovic, O., Greenwald, M., Zhu, Y.Z., Gohler, H., Wanker, E.E., Bates, G.P., Housman, D.E., and Thompson, L.M. (2000). The Huntington's disease protein interacts with p53 and CREB-binding protein and represses transcription. Proc Natl Acad Sci U S A *97*, 6763-6768.

Storey, J.D., Tibshirani, R. (2003). Statistical significance for genomewide studies. Proc Natl Acad Sci U S A *100*, 9440-9445.

Strand, A.D., Baquet, Z.C., Aragaki, A.K., Holmans, P., Yang, L., Cleren, C., Beal, M.F., Jones, L., Kooperberg, C., Olson, J.M.*, et al.* (2007). Expression profiling of Huntington's disease models suggests that brain-derived neurotrophic factor depletion plays a major role in striatal degeneration. J Neurosci *27*, 11758-11768.

Strong, T.V., Tagle, D.A., Valdes, J.M., Elmer, L.W., Boehm, K., Swaroop, M., Kaatz, K.W., Collins, F.S., and Albin, R.L. (1993). Widespread expression of the human and rat Huntington's disease gene in brain and nonneural tissues. Nat Genet *5*, 259-265.

Subramanian, A., Tamayo, P., Mootha, V.K., Mukherjee, S., Ebert, B.L., Gillette, M.A., Paulovich, A., Pomeroy, S.L., Golub, T.R., Lander, E.S.*, et al.* (2005). Gene set enrichment analysis: a knowledge-based approach for interpreting genome-wide expression profiles. Proc Natl Acad Sci U S A *102*, 15545-15550.

Sugiaman-Trapman, D., Vitezic, M., Jouhilahti, E.M., Mathelier, A., Lauter, G., Misra, S., Daub, C.O., Kere, J., and Swoboda, P. (2018). Characterization of the human RFX transcription factor family by regulatory and target gene analysis. BMC Genomics *19*, 181.

Swiss, V.A., and Casaccia, P. (2010). Cell-context specific role of the E2F/Rb pathway in development and disease. Glia *58*, 377-390.

Szlachcic, W.J., Switonski, P.M., Krzyzosiak, W.J., Figlerowicz, M., and Figiel, M. (2015). Huntington disease iPSCs show early molecular changes in intracellular signaling, the expression of oxidative stress proteins and the p53 pathway. Dis Model Mech *8*, 1047-1057.

Tabrizi, S.J., Scahill, R.I., Owen, G., Durr, A., Leavitt, B.R., Roos, R.A., Borowsky, B., Landwehrmeyer, B., Frost, C., Johnson, H.*, et al.* (2013). Predictors of phenotypic progression and disease onset in premanifest and early-stage Huntington's disease in the TRACK-HD study: analysis of 36-month observational data. Lancet Neurol *12*, 637-649.

Thomas, E.A., Coppola, G., Desplats, P.A., Tang, B., Soragni, E., Burnett, R., Gao, F., Fitzgerald, K.M., Borok, J.F., Herman, D.*, et al.* (2008). The HDAC inhibitor 4b ameliorates the disease phenotype and transcriptional abnormalities in Huntington's disease transgenic mice. Proc Natl Acad Sci U S A *105*, 15564-15569.

Ting, J.H., Marks, D.R., Schleidt, S.S., Wu, J.N., Zyskind, J.W., Lindl, K.A., Blendy, J.A., Pierce, R.C., and Jordan-Sciutto, K.L. (2014). Targeted gene mutation of E2F1 evokes age-dependent synaptic disruption and behavioral deficits. J Neurochem *129*, 850-863.

Tong, X., Ao, Y., Faas, G.C., Nwaobi, S.E., Xu, J., Haustein, M.D., Anderson, M.A., Mody, I., Olsen, M.L., Sofroniew, M.V.*, et al.* (2014). Astrocyte Kir4.1 ion channel deficits contribute to neuronal dysfunction in Huntington's disease model mice. Nat Neurosci *17*, 694-703.

Trapnell, C., Roberts, A., Goff, L., Pertea, G., Kim, D., Kelley, D.R., Pimentel, H., Salzberg, S.L., Rinn, J.L., and Pachter, L. (2012). Differential gene and transcript expression analysis of RNA-seq experiments with TopHat and Cufflinks. Nat Protoc *7*, 562-578.

Valenza, M., Leoni, V., Karasinska, J.M., Petricca, L., Fan, J., Carroll, J., Pouladi, M.A., Fossale, E., Nguyen, H.P., Riess, O.*, et al.* (2010). Cholesterol defect is marked across multiple rodent models of Huntington's disease and is manifest in astrocytes. J Neurosci *30*, 10844-10850.

Valor, L.M. (2015). Transcription, epigenetics and ameliorative strategies in Huntington's Disease: a genome-wide perspective. Mol Neurobiol *51*, 406-423.

Valor, L.M., Viosca, J., Lopez-Atalaya, J.P., and Barco, A. (2013). Lysine acetyltransferases CBP and p300 as therapeutic targets in cognitive and neurodegenerative disorders. Curr Pharm Des *19*, 5051-5064.

van der Burg, J.M., Bjorkqvist, M., and Brundin, P. (2009). Beyond the brain: widespread pathology in Huntington's disease. Lancet Neurol *8*, 765-774.

van Hagen, M., Piebes, D.G.E., de Leeuw, W.C., Vuist, I.M., van Roon-Mom, W.M.C., Moerland, P.D., and Verschure, P.J. (2017). The dynamics of early-state transcriptional changes and aggregate formation in a Huntington's disease cell model. BMC Genomics *18*, 373.

Vaseva, A.V., and Moll, U.M. (2009). The mitochondrial p53 pathway. Biochim Biophys Acta *1787*, 414-420.

Vashishtha, M., Ng, C.W., Yildirim, F., Gipson, T.A., Kratter, I.H., Bodai, L., Song, W., Lau, A., Labadorf, A., Vogel-Ciernia, A.*, et al.* (2013). Targeting H3K4 trimethylation in Huntington disease. Proc Natl Acad Sci U S A *110*, E3027-3036.

Vermunt, M.W., Tan, S.C., Castelijns, B., Geeven, G., Reinink, P., de Bruijn, E., Kondova, I., Persengiev, S., Netherlands Brain, B., Bontrop, R.*, et al.* (2016). Epigenomic annotation of gene regulatory alterations during evolution of the primate brain. Nat Neurosci *19*, 494-503.

Volterra, A., and Meldolesi, J. (2005). Astrocytes, from brain glue to communication elements: the revolution continues. Nat Rev Neurosci *6*, 626-640.

von Schimmelmann, M., Feinberg, P.A., Sullivan, J.M., Ku, S.M., Badimon, A., Duff, M.K., Wang, Z., Lachmann, A., Dewell, S., Ma'ayan, A.*, et al.* (2016). Polycomb repressive complex 2 (PRC2) silences genes responsible for neurodegeneration. Nat Neurosci *19*, 1321-1330.

Vonsattel, J.P., Myers, R.H., Stevens, T.J., Ferrante, R.J., Bird, E.D., and Richardson, E.P., Jr. (1985). Neuropathological classification of Huntington's disease. J Neuropathol Exp Neurol *44*, 559-577.

Waldvogel, H.J., Kim, E.H., Tippett, L.J., Vonsattel, J.P., and Faull, R.L. (2015). The Neuropathology of Huntington's Disease. Curr Top Behav Neurosci *22*, 33-80.

Wang, F., Yang, Y., Lin, X., Wang, J.Q., Wu, Y.S., Xie, W., Wang, D., Zhu, S., Liao, Y.Q., Sun, Q.*, et al.* (2013). Genome-wide loss of 5-hmC is a novel epigenetic feature of Huntington's disease. Hum Mol Genet *22*, 3641-3653.

Wang, L., Lin, F., Wang, J., Wu, J., Han, R., Zhu, L., Zhang, G., DiFiglia, M., and Qin, Z. (2012). Truncated N-terminal huntingtin fragment with expanded-polyglutamine (htt552-100Q) suppresses brain-derived neurotrophic factor transcription in astrocytes. Acta Biochim Biophys Sin (Shanghai) *44*, 249-258.

Watts, J.K., and Corey, D.R. (2012). Silencing disease genes in the laboratory and the clinic. J Pathol *226*, 365-379.

West, K.L., Castellini, M.A., Duncan, M.K., and Bustin, M. (2004). Chromosomal proteins HMGN3a and HMGN3b regulate the expression of glycine transporter 1. Mol Cell Biol *24*, 3747-3756.

Wexler NS, Y.A., Tanzi RE, Travers H, Starosta-Rubinstein S, Penney JB, Snodgrass SR, Shoulson I, Gomez F, Ramos Arroyo MA, et al. (1987). Homozygotes for Huntington's disease. Nature *326*, 194-197.

White, J.K., Auerbach, W., Duyao, M.P., Vonsattel, J.P., Gusella, J.F., Joyner, A.L., and MacDonald, M.E. (1997). Huntingtin is required for neurogenesis and is not impaired by the Huntington's disease CAG expansion. Nat Genet *17*, 404-410.

Wiatr, K., Szlachcic, W.J., Trzeciak, M., Figlerowicz, M., and Figiel, M. (2018). Huntington Disease as a Neurodevelopmental Disorder and Early Signs of the Disease in Stem Cells. Mol Neurobiol *55*, 3351-3371.

Wild, E.J., and Tabrizi, S.J. (2008). Biomarkers for Huntington's disease. Expert Opin Med Diagn *2*, 47-62.

Wu, D., Faria, A.V., Younes, L., Mori, S., Brown, T., Johnson, H., Paulsen, J.S., Ross, C.A., Miller, M.I., Investigators, P.-H.*, et al.* (2017). Mapping the order and pattern of brain structural MRI changes using change-point analysis in premanifest Huntington's disease. Hum Brain Mapp *38*, 5035-5050.

Wu, J., Sabirzhanov, B., Stoica, B.A., Lipinski, M.M., Zhao, Z., Zhao, S., Ward, N., Yang, D., and Faden, A.I. (2015). Ablation of the transcription factors E2F1-2 limits neuroinflammation and associated neurological deficits after contusive spinal cord injury. Cell Cycle *14*, 3698-3712.

Wu, Y., Hu, X., Li, Z., Wang, M., Li, S., Wang, X., Lin, X., Liao, S., Zhang, Z., Feng, X.*, et al.* (2016). Transcription Factor RFX2 Is a Key Regulator of Mouse Spermiogenesis. Sci Rep *6*, 20435.

Xie, Y., Hayden, M.R., and Xu, B. (2010). BDNF overexpression in the forebrain rescues Huntington's disease phenotypes in YAC128 mice. J Neurosci *30*, 14708-14718.

Yang, S.H., Cheng, P.H., Banta, H., Piotrowska-Nitsche, K., Yang, J.J., Cheng, E.C., Snyder, B., Larkin, K., Liu, J., Orkin, J.*, et al.* (2008). Towards a transgenic model of Huntington's disease in a non-human primate. Nature *453*, 921-924.

Yu, D., Pendergraff, H., Liu, J., Kordasiewicz, H.B., Cleveland, D.W., Swayze, E.E., Lima, W.F., Crooke, S.T., Prakash, T.P., and Corey, D.R. (2012). Single-stranded RNAs use RNAi to potently and allele-selectively inhibit mutant huntingtin expression. Cell *150*, 895-908.

Yu, M.S., and Tanese, N. (2017). Huntingtin Is Required for Neural But Not Cardiac/Pancreatic Progenitor Differentiation of Mouse Embryonic Stem Cells In vitro. Front Cell Neurosci *11*, 33.

Zeitlin, S., Liu, J.P., Chapman, D.L., Papaioannou, V.E., and Efstratiadis, A. (1995). Increased apoptosis and early embryonic lethality in mice nullizygous for the Huntington's disease gene homologue. Nat Genet *11*, 155-163.

Zeron, M.M., Hansson, O., Chen, N., Wellington, C.L., Leavitt, B.R., Brundin, P., Hayden, M.R., and Raymond, L.A. (2002). Increased sensitivity to N-methyl-D-aspartate receptor-mediated excitotoxicity in a mouse model of Huntington's disease. Neuron *33*, 849-860.

Zhang, D., Stumpo, D.J., Graves, J.P., DeGraff, L.M., Grissom, S.F., Collins, J.B., Li, L., Zeldin, D.C., and Blackshear, P.J. (2006). Identification of potential target genes for RFX4_v3, a transcription factor critical for brain development. J Neurochem *98*, 860-875.

Zhang, J., Gao, Q., Li, P., Liu, X., Jia, Y., Wu, W., Li, J., Dong, S., Koseki, H., and Wong, J. (2011). S phase-dependent interaction with DNMT1 dictates the role of UHRF1 but not UHRF2 in DNA methylation maintenance. Cell Res *21*, 1723-1739.

Zhang, Y., Liu, T., Meyer, C.A., Eeckhoute, J., Johnson, D.S., Bernstein, B.E., Nusbaum, C., Myers, R.M., Brown, M., Li, W.*, et al.* (2008). Model-based analysis of ChIP-Seq (MACS). Genome Biol *9*, R137.

Zimin, A.V., Cornish, A.S., Maudhoo, M.D., Gibbs, R.M., Zhang, X., Pandey, S., Meehan, D.T., Wipfler, K., Bosinger, S.E., Johnson, Z.P.*, et al.* (2014). A new rhesus macaque assembly and annotation for next-generation sequencing analyses. Biol Direct *9*, 20.

Zuccato, C., and Cattaneo, E. (2007). Role of brain-derived neurotrophic factor in Huntington's disease. Prog Neurobiol *81*, 294-330.

Zuccato, C., and Cattaneo, E. (2009). Brain-derived neurotrophic factor in neurodegenerative diseases. Nat Rev Neurol *5*, 311-322.

Zuccato, C., Valenza, M., and Cattaneo, E. (2010). Molecular mechanisms and potential therapeutical targets in Huntington's disease. Physiol Rev *90*, 905-981.